USGS
science for a changing world

Prepared in cooperation with U.S. Environmental Protection Agency through Washington State Department of Fish and Wildlife

Prepared in collaboration with Whatcom County Flood Control Zone District, Nooksack Indian Tribe, and Lummi Tribe

# Compound Flood Model for the Lower Nooksack River and Delta, Western Washington—Assessment of Vulnerability and Nature-Based Adaptation Opportunities to Mitigate Higher Sea Level and Stream Flooding

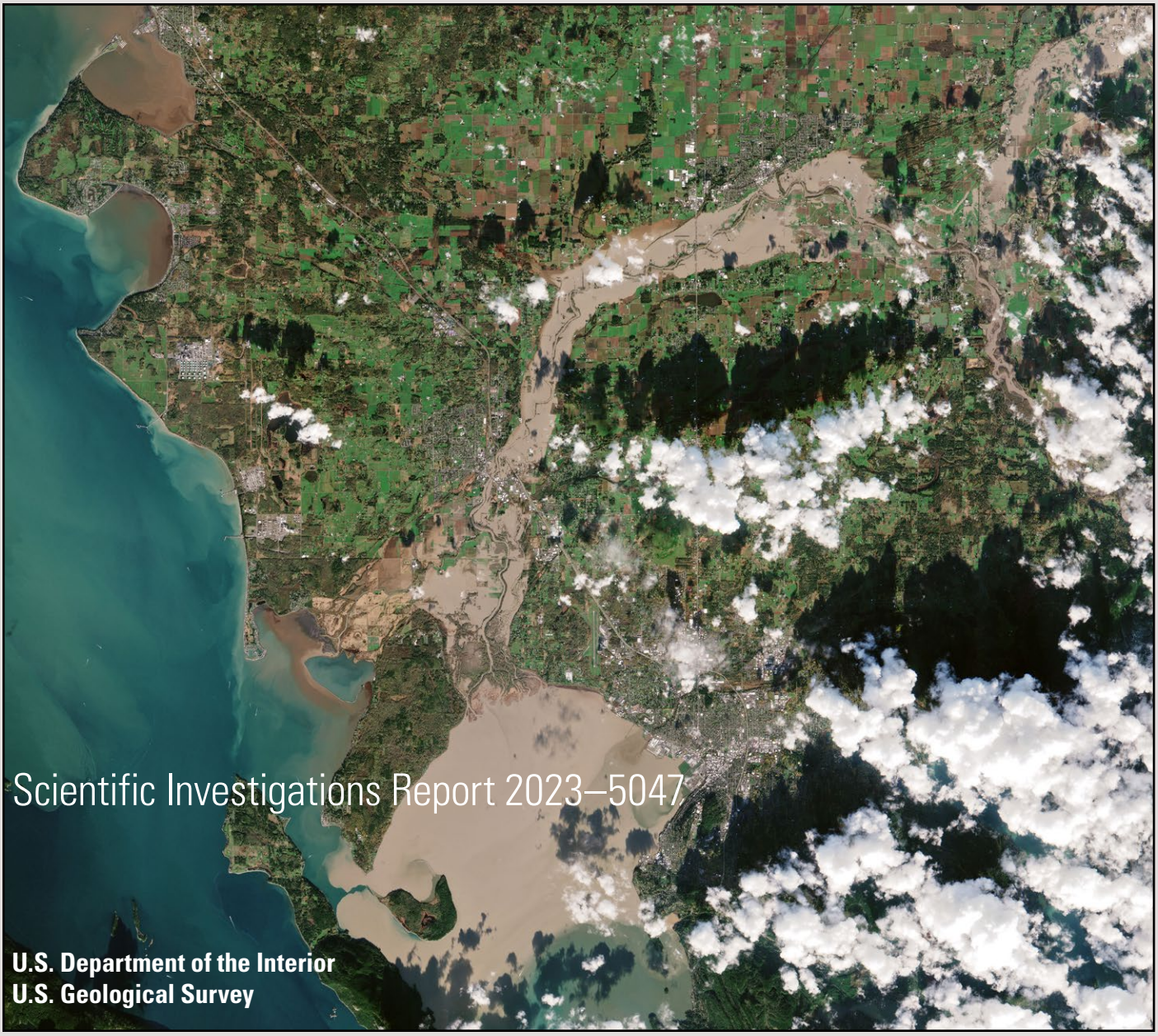

Scientific Investigations Report 2023–5047

U.S. Department of the Interior
U.S. Geological Survey

**Cover.** Satellite image showing flooding in lower Nooksack River during November 16, 2021, flood event. Image courtesy of National Aeronautics and Space Administration.

# Compound Flood Model for the Lower Nooksack River and Delta, Western Washington—Assessment of Vulnerability and Nature-Based Adaptation Opportunities to Mitigate Higher Sea Level and Stream Flooding

By Eric E. Grossman, Nathan R. vanArendonk, and Kees Nederhoff

Prepared in cooperation with U.S. Environmental Protection Agency through Washington State Department of Fish and Wildlife

Prepared in collaboration with Whatcom County Flood Control Zone District, Nooksack Indian Tribe, and Lummi Tribe

Scientific Investigations Report 2023–5047

**U.S. Department of the Interior**
**U.S. Geological Survey**

U.S. Geological Survey, Reston, Virginia: 2023



Suggested citation:
Grossman, E.E., vanArendonk, N.R., and Nederhoff, K., 2023, Compound flood model for the lower Nooksack River and delta, western Washington—Assessment of vulnerability and nature-based adaptation opportunities to mitigate higher sea level and stream flooding: U.S. Geological Survey Scientific Investigations Report 2023–5047, 49 p., https://doi.org/10.3133/sir20235047.

Associated data for this publication:
Grossman, E.E., vanArendonk, N.R., Nederhoff, K., and Parker, K.A., 2023, Model input and projections of compound floodwater depths for the lower Nooksack River and delta, western Washington State: U.S. Geological Survey data release, https://doi.org/10.5066/P9DJM7X2.

ISSN 2328-0328 (online)

# Acknowledgments

This work was supported by a grant from the U.S. Environmental Protection Agency through Washington State Department of Fish and Wildlife and the U.S. Geological Survey (USGS), from USGS' projects Coastal Habitats in Puget Sound and Integrated Climate Driven Coastal Hazards.

We thank Paula Harris-Cooper, John Thompson, and Deborah Johnson of Whatcom County Flood Zone Control District for collaborating on flood-response mapping, stakeholder engagement and coordination, and access to important historical validation data.

The study benefitted from numerous discussions with and insight of Michael Maudlin and Ned Currence of the Nooksack Indian Tribe and Merle Jefferson, Leroy Deardorff, and Kara Kuhlman of the Lummi Tribe regarding historical changes in the Nooksack River, as well as granting access to sites to measure and map flood effects.

We are grateful for the comprehensive peer review and efforts of the two anonymous reviewers who improved the clarity of the narrative.

# Contents

## Figures

## Tables

# Conversion Factors

U.S. customary units to International System of Units

| Multiply | By | To obtain |
|---|---|---|
| | Length | |
| inch (in.) | 2.54 | centimeter (cm) |
| inch (in.) | 25.4 | millimeter (mm) |
| foot (ft) | 0.3048 | meter (m) |
| mile (mi) | 1.609 | kilometer (km) |
| | Area | |
| square mile ($mi^2$) | 2.590 | square kilometer ($km^2$) |
| | Flow rate | |
| cubic foot per second ($ft^3/s$) | 0.02832 | cubic meter per second ($m^3/s$) |

International System of Units to U.S. customary units

| Multiply | By | To obtain |
|---|---|---|
| | Length | |
| centimeter (cm) | 0.3937 | inch (in.) |
| millimeter (mm) | 0.03937 | inch (in.) |
| meter (m) | 3.281 | foot (ft) |
| kilometer (km) | 0.6214 | mile (mi) |
| | Area | |
| square kilometer ($km^2$) | 0.3861 | square mile ($mi^2$) |
| | Flow rate | |
| cubic meter per second ($m^3/s$) | 35.31 | cubic foot per second ($ft^3/s$) |
| | Mass | |
| metric ton (t) | 1.102 | ton, short [2,000 lb] |

# Datum

Elevations are relative to North American Vertical Datum of 1988 (NAVD 88)

# Abbreviations

| | |
|---|---|
| 1D | one dimensional |
| 2DH | two dimensional horizontal |
| AEP | annual exceedance probability |
| CFHMP | Comprehensive Flood Hazard Management Plan |
| CoNED | USGS coastal national elevation database |
| Delft3D FM | Delft3D Flexible Mesh |
| DEM | digital elevation model |
| E-H | Engelund-Hansen |
| FLIP | Floodplain Integrated Planning |
| GPS | global positioning system |
| Hz | hertz |
| I–5 | Interstate Highway 5 |
| IPCC | Intergovernmental Panel on Climate Change |
| K1 | diurnal lunar tidal constituent |
| LNRP | Lower Nooksack River Project |
| M2 | semidiurnal lunar tidal constituent |
| MAE | mean absolute error (bias removed) |
| MLLW | mean lower low water |
| NAIP | National Agricultural Imagery Program |
| NAVD 88 | North American Vertical Datum of 1988 |
| NLCD | National Land Cover Database |
| NOAA | National Oceanic and Atmospheric Administration |
| RCP | Representative [Carbon] Concentration Pathway |
| RMSE | root mean square error (bias removed) |
| RTK-GPS | real-time-kinematic global positioning system |
| SBF | Super Bowl flood |
| SWL | still-water level |
| *uMAE* | mean absolute error accounting for bias |
| *uRMSE* | root mean square error accounting for bias |
| USGS | U.S. Geological Survey |
| WSE | water-surface elevation |

# Compound Flood Model for the Lower Nooksack River and Delta, Western Washington—Assessment of Vulnerability and Nature-Based Adaptation Opportunities to Mitigate Higher Sea Level and Stream Flooding

By Eric E. Grossman,[1] Nathan R. vanArendonk,[1] and Kees Nederhoff[2]

## Abstract

Higher sea level and stream runoff associated with climate change is expected to lead to greater lowland flooding across the Pacific Northwest. Increases in stream runoff that range from 20 to 32 percent by the 2040s and from 52 to 72 percent by the 2080s is expected to steadily increase flood risk. Flood risk is also expected to increase in response to the landward shift in high tides and storm surge, which will retard downstream conveyance. The combination of higher stream runoff, which is expected to drive greater fluvial sediment delivery to the coast, and more frequent, higher coastal waters relative to present-day (2023) levels, which will retard streamflow, is projected to cause more sedimentation across coastal and estuarine systems, exacerbating the flood risk. In the Nooksack River delta of western Washington, as in many Puget Sound deltas, resilient adaptation planning to mitigate impacts to community assets and infrastructure, nationally essential agricultural areas, and valued habitats and restoration investments that support endangered and threatened salmon recovery are underway but are in need of more informed projections of compound flood hazards.

A Delft3D Flexible Mesh hydrodynamic model was constructed and used to assess changes in the extent, frequency, and timing of flood exposure associated with higher sea level and stream runoff projected to occur in the 2040s and 2080s. The model was also used to evaluate the change in and potential mitigating effects to flood exposure associated with individual and cumulative salmon-habitat-restoration strategies. Model simulations also evaluated the sensitivity of sedimentation to the individual and cumulative effects of higher fluvial delivery, trapping by sea-level rise, and changes in hydrodynamics associated with the rerouting of flows by proposed restoration strategies. The model performed well, having mean absolute errors for water levels below 1 foot (0.3 meters) when tested during a 2-year period for two recent flood events of record, the February 2, 2020, "Super Bowl flood" and the January 8, 2009, stream flood, both of which caused substantial flooding and damage across the study area. Fluvial discharge was found to dominate flood hazard at higher elevations in the study area, whereas near the coast, sea-level rise is computed to turn a less extreme 2-year (50 percent annual exceedance probability [AEP]) bankfull streamflow, which, at present (2023), causes nuisance flooding, into a more extreme 5-year (20 percent AEP) and 10 percent AEP stream-flood event by the 2050s and 2100, respectively.

The February 2020 Super Bowl flood was calculated to be a 10-year or 10 percent AEP peak-flow event, and the January 2009 flood was calculated to be a 25-year (4 percent AEP) peak-flow event. Extreme events such as the February 2020 Super Bowl flood and the January 2009 flood caused extensive damage across the Nooksack River floodplain, and model computations predict these magnitudes of events would have notably greater effect in the 2040s and 2080s in response to higher projected sea level and stream runoff. The modeled January 2009 flood is predicted to transform into a flood event, causing flood exposure that is comparable to the 100-year or 1 percent AEP flood by the 2040s. The modeled January 2009 flood is also predicted to exceed the flood exposure of the recent November 16, 2021, flood, which caused substantial damage in the lower Nooksack River floodplain and restricted access for emergency-management efforts on important arterial roadways in the area; the measured peak discharge during the November 16, 2021, flood exceeded that of the January 2009 flood.

Two of several identified alternative strategies that reroute floodwaters to restore salmon habitat were projected to reduce exposure to the increasingly impactful 10 and 4 percent AEP stream-flood events through the 2080s. The effects of the suggested alternatives, however, were found to reduce flow velocities, promote additional sedimentation, and reduce flow conveyance in the main-stem Nooksack River, a concern to flood-management efforts, navigation, and fishing. The model also suggests that main-stem channel sedimentation is likely, given projected climate change. Higher stream runoff that increases fluvial-sediment delivery

[1]U.S. Geological Survey.

[2]Deltares USA.

and higher sea levels that retard downstream flow are expected to lead to greater sedimentation. Lastly, the model was used to assess the sensitivity of flood exposure to the individual and cumulative effects of climate changes, alternative strategies, and sedimentation, including recently observed decadal-scale aggradation patterns. These results indicate that sediment is likely to continue to be a challenge to flood-management efforts and that nature-based alternatives that benefit ecosystem restoration may also mitigate flood exposure for several decades.

# Introduction

## Problem

Low-lying coastal environments are expected to experience increasing flooding and ecosystem disruptions in the coming decades in response to climate change, namely the interaction of sea-level rise and associated land-use effects (Barnosky and others, 2012). In the Pacific Northwest, regional sea-level rise is projected to accelerate, reaching 0.5 to 1.0 meters (m) above present-day (2023) levels by the 2080s (Miller and others, 2018). Coastal flooding is expected to be exacerbated by increased (and more frequent) stream runoff (Mauger and others, 2015; Lee and others, 2016) in response to regional warming and a shift of precipitation from snow to rain in autumn and winter (Mauger and others, 2015). Peak streamflows draining the high Cascade Range are expected to increase by 20 to 32 percent by the 2040s and by 52 to 72 percent by the 2080s, and coupled with more intense lowland rainfall, storms are expected to generate more rapid runoff across the Puget Lowland (Mauger and others, 2015). Increased sediment delivery by higher streamflows (Curran and others, 2016; Lee and others, 2016), accompanied by sediment accumulation in the region's estuaries as sea-level rise reduces downstream flow conveyance, are considered positive feedbacks to the growing coastal flood risk (Grossman and others, 2020). Increased groundwater flooding and prolonged groundwater drainage, which are important to flood risk, agriculture, and ecosystem functions, are anticipated in response to higher sea-level rise, greater lowland rainfall, and increased coastal sedimentation (Grossman and others, 2020).

Extensive amounts of land, resources, and community infrastructure are at risk in coastal settings, especially in places in the Pacific Northwest where steep, narrow watersheds that have high rainfall and sediment runoff meet low-lying coastal plains. In the Nooksack River and delta, located between Puget Sound and the Strait of Georgia in northwestern Washington State, substantial flood disturbances can affect Tribal and local communities and infrastructure and the agricultural lands that are critical to the Nation's vegetable and fruit supply, as well as investments that are being planned to recover endangered salmon habitats (fig. 1). The Whatcom County [Washington] Department of Public Works, on behalf of the Whatcom County Flood Control Zone District, and in collaboration with other Federal, State, and local agencies, is updating the Lower Nooksack River Comprehensive Flood Hazard Management Plan (CFHMP) (Whatcom County Department of Public Works, 1999). The Whatcom County Department of Public Works is using the Nooksack River Floodplain Integrated Planning (FLIP), a stakeholder consortium of land and resource managers from the Nooksack River watershed, to update the CFHMP.

The FLIP and the CFHMP identified that predictive hydrodynamic-sediment-transport modeling, capable of assessing cumulative effects of sea-level rise, climate change, sediment dynamics, and adaptation strategies, was needed to evaluate potential tipping points[3] that may affect the economy and culture of the area, as well as the opportunity to evaluate and enhance resilience. Through the FLIP, several floodplain-modification alternatives that have potential to alleviate flooding have been identified; these alternatives are formulated around removing or setting back levees, reconnecting historical distributary channels, and raising roads or elevating them on bridges. Questions remain, however, including whether the alternatives may also benefit how the ecosystem functions (for example, for salmon) and also the extent to which, and length of time into the future that, the alternatives would provide flood-mitigation benefits, given the projections of climate change and the complex responses of sedimentation and geomorphology.

This report summarizes the development and implementation of a new numerical hydrodynamic flood model to evaluate projected changes in compound flood exposure owing to the individual and cumulative effects of anticipated climate changes, which include higher sea level and increased stream flooding, along with identified restoration strategies and their influences on sedimentation. After quantifying model performance for a range of flow conditions that include two historical floods of record, we present model simulations that show how flood exposure associated with recently observed, extreme stream-flood events are expected to change in response to the projected effects of sea-level rise, tides, and storm surge in the 2040s and 2080s, which are periods of interest for near- and long-term planning by FLIP and CFHMP.

When referring to the evaluated stream floods, we use nomenclature that characterizes their probabilities of occurrence in any given year. For example, a 10-year flood is the 10 percent-annual-chance stream flood, and it is herein referred to as the 10 percent annual exceedance probability (AEP) stream flood. Similarly, a 25-year stream flood is the 4 percent AEP stream flood. Next, several restoration alternative strategies for routing streamflow that have been identified to improve fish habitat are evaluated for existing floods and for those projected to be larger in the 2040s and 2080s, providing insight into their capacity to mitigate flood exposure. The model was also used to assess how observations of stream-channel sedimentation, which reduces flow conveyance, may affect future flood exposure, as well as

[3]Tipping point (as used herein) is defined as a "threshold in one or more external drivers or controlling variables within the system that when breached causes a major change in the system's structure, function, or dynamics" (Moore, 2018).

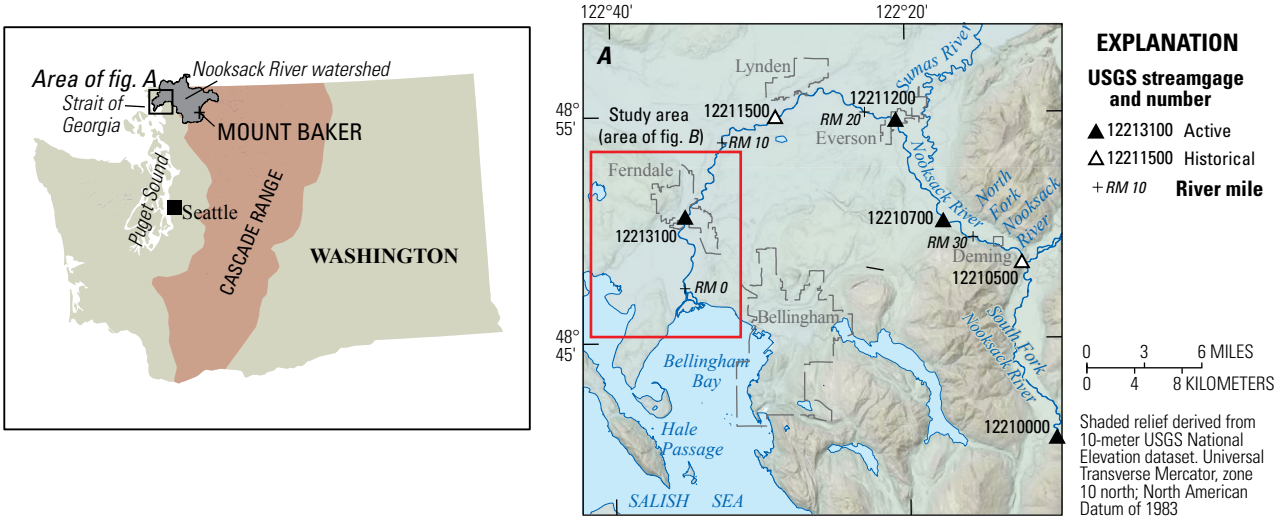


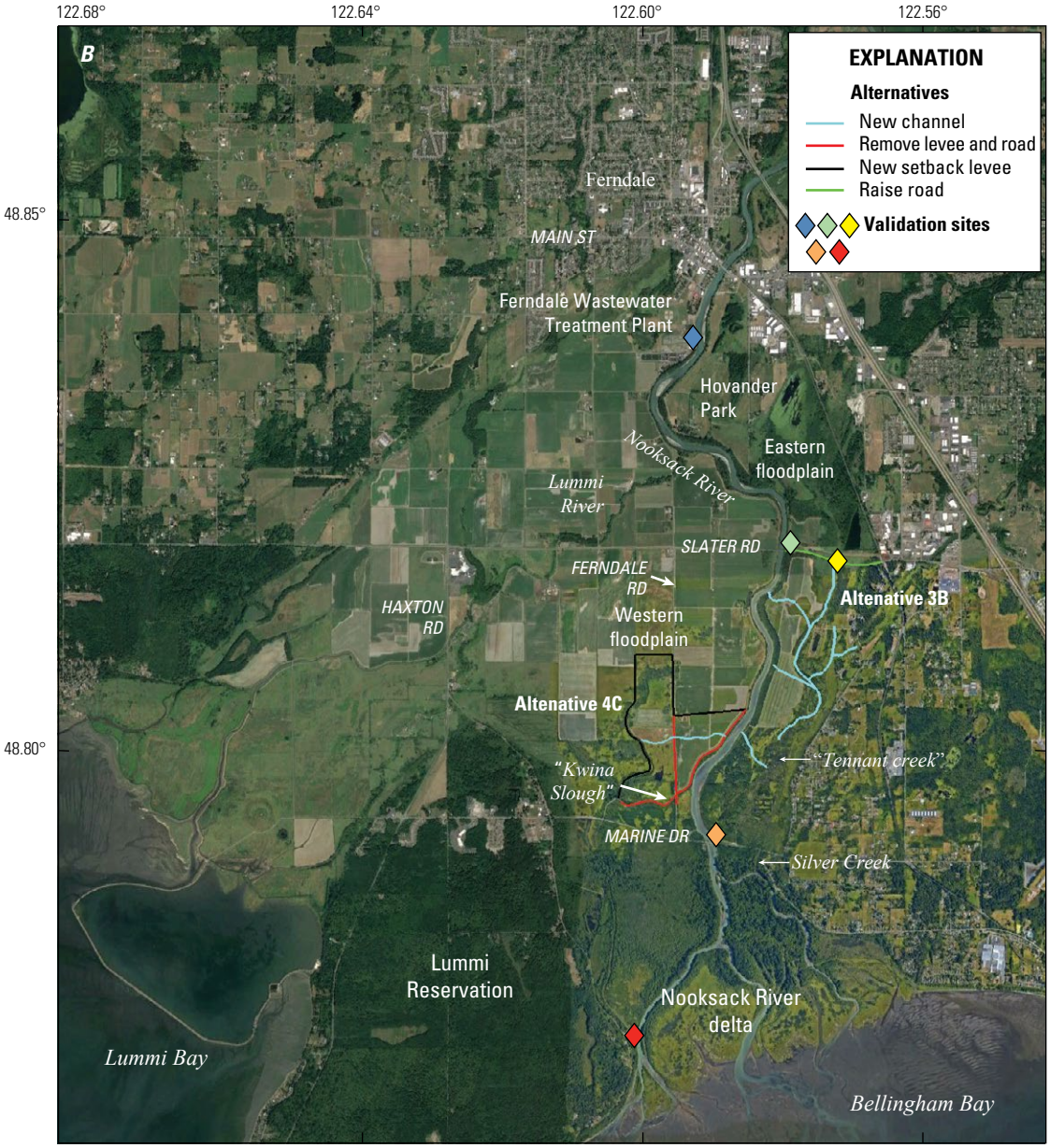


**Figure 1.** Shaded-relief map (*A*) and National Agricultural Imagery Program (NAIP) composite image (*B*) of study area (red outline in *A*) within Nooksack River Basin, showing locations of proposed restoration and flood-mitigation alternatives, model validation sites within Reach 1 of Nooksack River, streamgages, and geographic features mentioned in text. Colored diamonds show validation sites: blue, Ferndale Wastewater Treatment Plant; green, Slater Road; yellow, "Slater Road East"; orange, Marine Drive; red, Nooksack River delta. NAIP image from U.S. Department of Agriculture National Agricultural Imagery Program.

how the proposed restoration and flood-mitigation alternatives, in turn, may alter sedimentation that can affect flood risk, wildlife habitats, and access to fisheries important to Tribal nations in the area. These assessments are fundamental to flood management and ecosystem-restoration planning, as sedimentation patterns that affect flow conveyance and habitat suitability are expected to change in complex ways in response to climate and land-use change. Lastly, the individual contributions of sea-level rise and streamflow changes are isolated to help inform where in the lower Nooksack River floodplain sea-level rise by itself will transform today's (2023) low to moderate floods into extreme flood events that cause extensive disturbance, as well as when, in the coming decades, it will occur. The relative influences of expected sea-level rise, climate changes, flood-mitigation alternatives, and sediment responses provide important information to evaluate pending climate-driven flood exposure, as well as opportunities to mitigate their effects by making informed decisions in a risk-based framework.

## Setting

The focus of this flood-modeling study is the Nooksack River, between Ferndale, located at River Mile 6.4, and the Nooksack River delta in Bellingham Bay. The Nooksack River drainage basin extends across approximately 2,046 square kilometers ($km^2$) (790 square miles [$mi^2$]), including the partly glaciated flanks of the northern Cascade Range and Mount Baker (fig. 1). The North Fork Nooksack and Middle Fork Nooksack Rivers drain the high elevations that have glaciers and significant winter snowpack, whereas the South Fork Nooksack River, which represents about 33 percent of the watershed, drains the rain-dominated lower elevation terrain. Near Deming, these three steep tributaries flow into one main-stem braided-channel network that extends downstream to River Mile 22 near Everson. Downstream from Everson, the channel is confined by levees through most of its length to Marine Drive (see fig. 1 for location), at the head of the river delta. The Nooksack River floodplain downstream from River Mile 22 has a slope of 0.02 to 0.07 percent, which is an order of magnitude lower than that of the river upstream from it; for example, between Everson and the town of Glacier, located at River Mile 51, about 21 kilometers (km) east-northeast of Deming, the slope is 0.5 percent. As a result, the lower Nooksack River and floodplain are sensitive and vulnerable to flooding, as well as to changes in fluvial-sediment input and accumulation.

The Nooksack River has the highest sediment yield of all the watersheds that drain into Puget Sound (Czuba and others, 2011). The sediment load at the U.S. Geological Survey (USGS) streamgage at Ferndale (station 12213100; U.S. Geological Survey [USGS], 2022) ranged from 0.78 to 1.17 million metric tons per year and averaged 0.97 million metric tons per year for water years 2012–17 (Anderson and others, 2019). The sediment load consisted of about 93 percent suspended sediment and about 7 percent bedload. The suspended load consisted of 53 percent fines (silt and clay) and 47 percent sand or larger sediment (Anderson and others, 2019). Anderson and others (2019) also showed that between 0.5 and 1.0 m of sedimentation has occurred across the lower river since 2006 and that waves of coarse bed aggradation that reach 1 m high and are 1 to 4 km long migrate downstream on decadal time scales in response to climate cycles such as the Pacific Decadal Oscillation, changing channel conveyance.

A network of flood-protection levees along the west bank (on the right side when traveling downstream) of the Nooksack River downstream from Ferndale have protected the western floodplain from 10-year (10 percent AEP) stream floods. Levees along the east bank (on the left side when traveling downstream) are lower and only accommodate flooding during less extreme flows (Whatcom County, 2017). The lower Nooksack River and delta are located in a mesotidal environment; they have a mean tidal range of 8.2 feet (ft) (2.5 m) and a great diurnal range of 9.8 ft (3.0 m). As a result, tidal propagation reaches from about 4.5 miles (mi) (7.5 km) upstream from the delta to just upstream from the confluence with the Lummi River, which has been disconnected from Nooksack River flow by levees since the late 1800s. The river delta is subject to high winds and waves in Bellingham Bay, which create an annual storm surge of 1 to 2 ft (0.3–0.6 m) that can reach as high as about 3 ft (0.8–1.0 m) during extreme weather conditions.

## Historical Flooding in the Lower Nooksack River

The Nooksack River watershed has a long history of extensive flooding. Historical floods that caused damage across the watershed include the floods of 1909, 1932, 1935, 1951, 2008, 2020, and 2021 (fig. 2). The 1932 flood (similar to the November 2021 flood) sent floodwater over the banks at Everson, through the Everson overflow and to Sumas, about 11 km north-northeast of Everson (KCM, Inc., 1995; Boyd and others 2019). During the November 2021 flood, Interstate Highway 5 (I–5) near Ferndale was temporarily closed for the duration of the high tides, an acknowledgment of the growing concern for sea-level rise compounding flood exposure.

Early accounts and mapping of the Nooksack River downstream from the town of Deming showed that the lower Nooksack River and Reach 1 were shallow and braided, a complex network of meandering channels (Collins and others, 2003). In addition, extensive areas of wetted channels, bars, islands, and channel-bank features contained abundant large, woody debris, sourced from natural dense forests in response to active erosion processes, particularly after logging and clear-cutting activities began in the mid-1800s (Collins and others, 2002). The shallow, complex ancestral river and its floodplains were swamps and forested wetlands, indicating frequent hydrologic connectivity by means of regular flooding of the main-stem river across extensive areas (Collins and others, 2003). Beginning in the late 1800s, settlers removed log jams, straightened the river, and dredged bed sediment to reduce flooding and enhance navigational capacity.

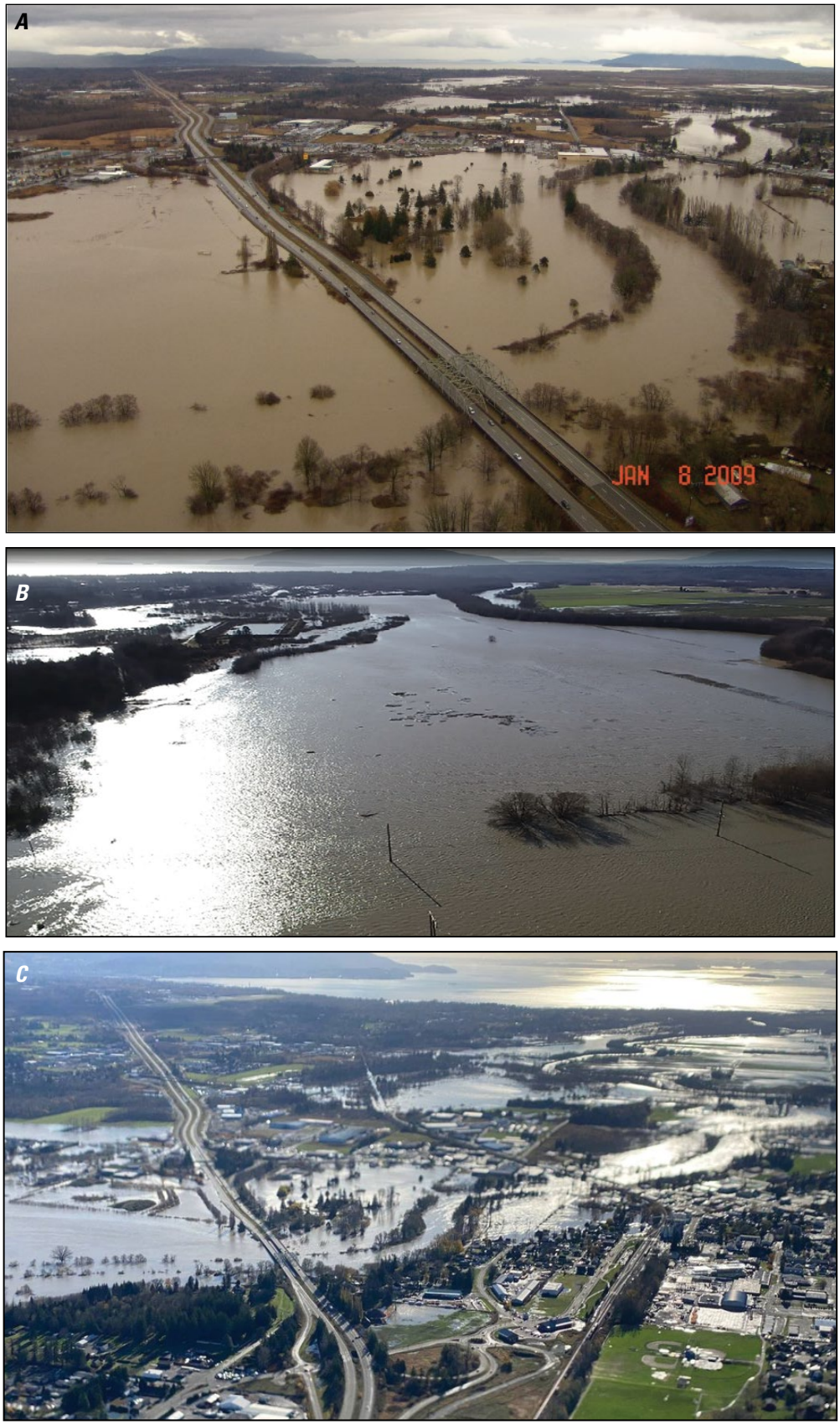


**Figure 2.** Oblique aerial photographs showing flooding in lower Nooksack River. *A*, View to south-southeast of flooding near Ferndale, taken January 8, 2009. Photograph courtesy of Washington Department of Transportation, used with permission. *B*, View to south-southwest of flooding across submerged Slater Road (marked by line of trees in lower right quadrant of image), taken February 2, 2020 (during Super Bowl flood). Photograph courtesy of Jesse Allen, Whatcom County, used with permission. *C*, View to south-southeast of flooding near Ferndale, taken November 16, 2021. Photograph courtesy of Larry McCarter, used with permission.

## Compound Flood Models

The utility of compound flood modeling has grown with the recognition of diverse coastal-flood hazards associated with accelerated sea-level rise and the influence of climate changes on watershed hydrology, storm surges, and coastal processes (Santiago-Collazo and others, 2019; Wang and others, 2021). Compound coastal flooding may occur in response to the interaction of tides, storm surge, river discharge, groundwater movement, and localized overland flow in areas where precipitation exceeds infiltration (Wahl and others, 2015). Additional processes contributing to changing flood hazards include sedimentation, vertical land motion, and changes in land cover. Computational power has generally limited coastal-flood assessments to simulations of extreme coastal- or riverine-flood phenomena, either separately or as scenarios having one or more static model boundaries (for example, 1 percent AEP stream-flood hydrograph with a higher "tidal" boundary; Hamman and others, 2016). In the last decade (that is, from about 2013 to 2023), increased computational power has enabled the calculation of hydrodynamics for multiple processes simultaneously and for longer periods of time than was previously possible. For example, a new San Francisco Bay and Sacramento-San Joaquin Delta still-water level (SWL) model reconstructed a 70-year hindcast[4] SWL to perform reliable extreme-value analysis across the estuary via a one-dimensional (1D)–two-dimensional horizontal (2DH), depth-averaged Delft3D Flexible Mesh model (Nederhoff and others, 2021). The 1D–2DH model schematization allowed for efficient yet accurate computation of water levels driven by coastal and riverine processes across the bay, its local tributaries, and its delta channels.

# Methods

To evaluate projected changes in flood exposure associated with higher sea levels and streamflows and with and without restoration and flood-mitigation alternatives, a compound flood model that couples river discharge with coastal processes (for example, tides, storm surge, and sea-level rise) was constructed for the lower Nooksack River and delta. The model was validated using time-series and point measurements of water levels in the main-stem river and across the floodplain for recent floods of record between Ferndale and Marine Drive (see figs. 1, 3 for location), in addition to aerial photographs and still images extracted from video footage of flood extents. Identified flood-mitigation alternatives were simulated to examine the extent to which each scenario may reduce flood exposure under existing and projected climate changes. The model was also used to isolate the sources of flooding to estimate where in the Nooksack River Reach 1 flooding will occur, as well as when in the future sea-level rise will contribute to flood exposure, relative to estimated climate-change-driven runoff and anticipated sedimentation. The models also deconstructed the relative contributions of the drivers to flooding, allowing for estimates of when the alternatives would be likely to mitigate flooding and also when the thresholds of disturbance will be reached.

[4]"Hindcast" refers to the forecasting of past events using prior data as a way of testing a model. Known inputs for past events are entered into the model to see how well the output matches the known results.

## Model Configuration and Set-Up

A hydrodynamic numerical model was constructed for Reach 1 of the lower Nooksack River between Ferndale (at River Mile 6.4) and the delta, and it was extended offshore to include Lummi Bay and part of Bellingham Bay, which are connected through Hale Passage (figs. 1, 3). The model, which was built with the numerical-modeling software Delft3D Flexible Mesh (Delft3D FM; Kernkamp and others, 2011), solves equations for shallow-water environments, under Boussinesq assumptions that mean flow is modulated by dissipation related to turbulence, using a finite-volume method on variably sized, unstructured grids in 1D and 2DH schematizations. The 1D and 2DH grid cells are solved in the same system of equations to ensure a smooth 1D–2DH coupling, which conserves momentum and is computationally efficient. A network of 2D cells was implemented across the nearshore embayment and the floodplain, and a 1D array of cross-channel profiles was implemented within the 1D grid throughout the main-stem Nooksack River and distributary channels and then connected to the 2DH domain (fig. 4). The principal difference between the 1D and 2DH formulations is that in 2D, the grid area is based on X-, Y-, and Z-coordinates of the network, whereas in 1D, these values are based on profile definitions, interpolated in between the user-defined cross-sectional profile. Model resolution in the 2DH domain varied from 100 m in the offshore to as fine as 25 m in areas of interest on the floodplain, whereas the 1D grid had a base resolution of 100 m, which was refined to 20 to 30 m spacing along tidal channels and inflections and meanders in the river to best capture the thalweg.

### Inputs and Boundary Conditions

Elevations in the model were prescribed using the USGS Coastal National Elevation Database (CoNED) 1-m-resolution topographic-bathymetric dataset of Puget Sound (Tyler and others, 2020), which includes 2015 bathymetry of the lower Nooksack River wetted channel from Anderson and Grossman (2017). The high-resolution CoNED digital elevation model (DEM) values were averaged at the center of each model cell, resulting in a smoothed DEM at the spatial resolution of the model. In the main stem of the Nooksack River and its distributary channels lower in the system (for example, Silver Creek), transects that cover the entire channel width at each 1D-grid node were generated, and they were used to sample the CoNED DEM data, generating a profile at each location. The 1D profiles were then downsampled to a

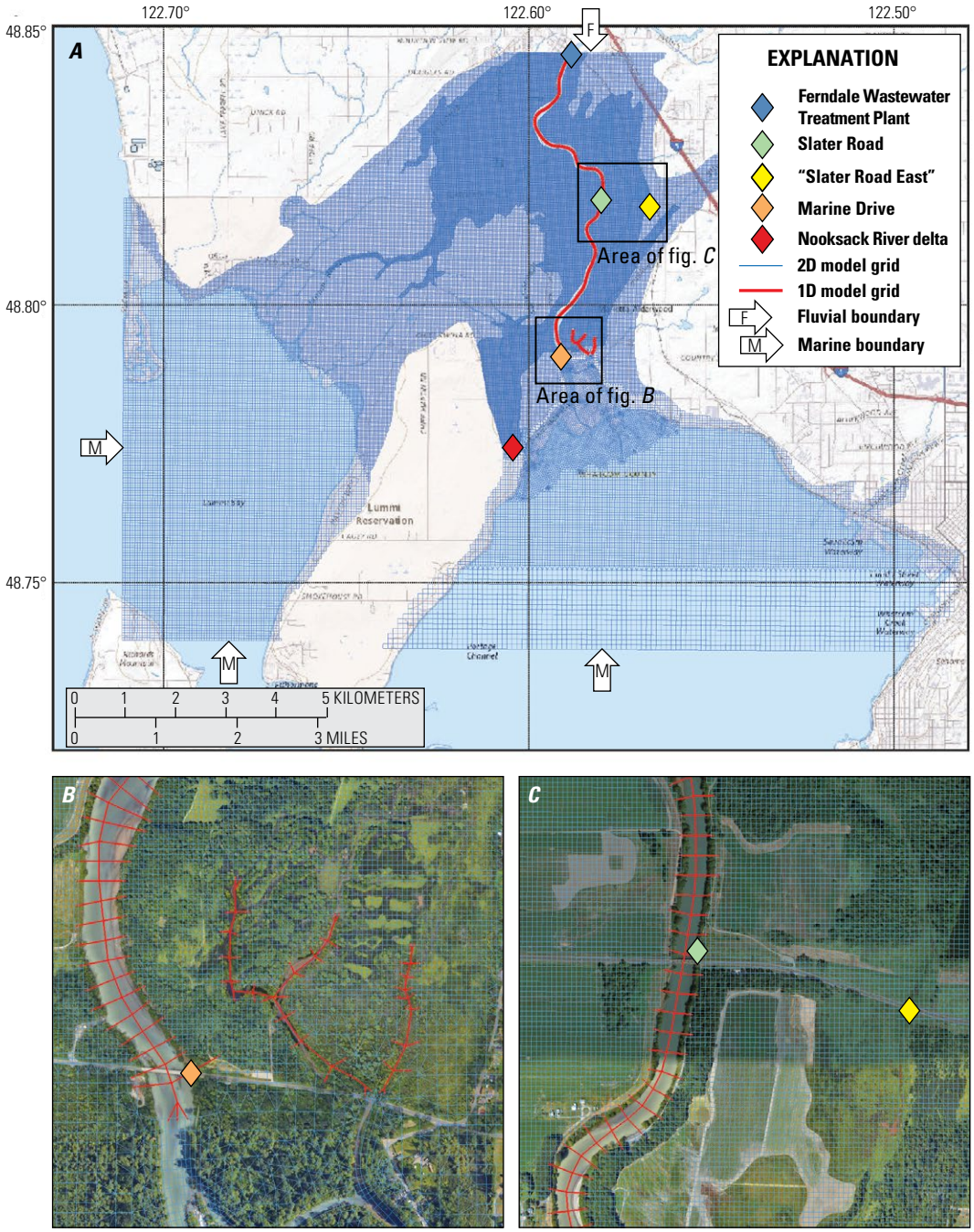


**Figure 3.** Map (*A*) and National Agricultural Imagery Program (NAIP) composite images (*B*, *C*) of study area, showing model domains and model-validation sites across Nooksack River Reach 1. In *A*, open arrows show locations of boundaries (F, freshwater discharge; M, marine) of two-dimensional model grid. In *B*, red cross-hachures show locations of cross-channel profiles used in modeling (see example profiles shown in figure 4). NAIP images from U.S. Department of Agriculture National Agricultural Imagery Program.

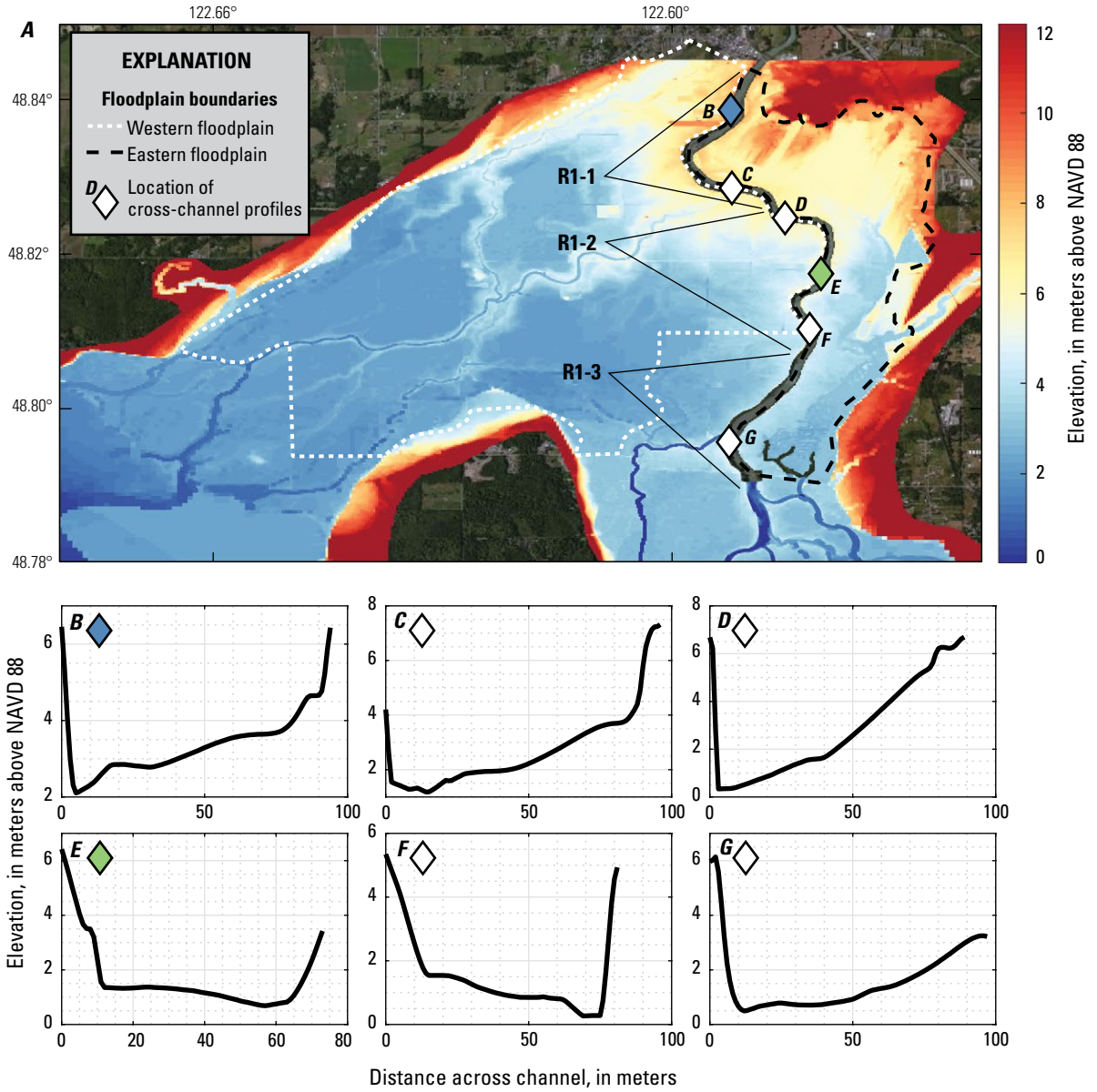


**Figure 4.** *A*, National Agricultural Imagery Program (NAIP) composite image showing model elevations, boundaries of western (dashed white line) and eastern (dashed black line) floodplains, and extents of Nooksack River subreaches R1-1, R1-2, and R1-3 (used for flood calculations); subreach R1-4 (not shown) spans subreaches R1-1, R1-2, and R1-3. Also shown are locations of representative cross-channel profiles (diamonds) shown in *B–G,* that span Nooksack River Reach 1. NAIP image from U.S. Department of Agriculture National Agricultural Imagery Program. *B–G* Cross-channel profiles, used to simulate bed-aggradation effects and for all calculations of flow, river stage, flooding, and sediment flux; note horizontal exaggeration of profiles. NAVD 88, North American Vertical Datum of 1988.

spatial resolution that affords computational efficiency while resolving the hydrodynamics.

The cross-channel profiles of the downsampled CoNED transect dataset were reviewed for quality and continuity and then exported into the required format for Delft3D FM. In some cases, the profile data were smoothed across the channel to eliminate abrupt morphological inflection points while preserving the overall widths, minimum and maximum depths, locations, and levels of conveyance. This method has been proven to accurately simulate river stage in a similar compound-flood study in San Francisco Bay and Sacramento-San Joaquin Delta while being computationally efficient (Nederhoff and others, 2021).

Discharge recorded at the USGS streamgage at Ferndale (station 12213100; USGS, 2022) was prescribed as the riverine forcing at the upstream boundary of the model for simulations of historical and existing conditions. The marine boundary (denoted by arrows and an ‘M’ in figure 3) was forced with tidal harmonics and nontidal residual values (anomalies) derived from the 27-year observational record

at the National Oceanic and Atmospheric Administration (NOAA) Cherry Point tide gage (station 9449424). Nontidal water levels were determined by subtracting observed water levels from the NOAA tidal predictions.

A spatially varying roughness coefficient (Manning's *n*) was generated from the USGS National Land Cover Database (NLCD), which characterizes land cover (for example, vegetated forest, wetlands, and so on) at 30-m resolution across the continental United States. The NLCD data were transformed into roughness coefficients using a look-up-table approach, sourcing U.S. Army Corps of Engineers conversion factors (Mattocks and Forbes, 2008; Brunner, 2021). Manning's *n* coefficient values that reproduced water levels best within the main-stem channel and on the floodplain over a range of flows, including the February 2020 Super Bowl flood event, were averaged inside of each grid cell.

Open-source geospatial datasets of engineered structures that influence overland flow such as roads, levees, and bridges were acquired from the Washington Geospatial Open Data Portal (https://geo.wa.gov) to help identify flow-control structures such as dikes, berms, and sea walls that are too small to be represented by the model grid. The location and height of these structures were used to query and evaluate the nearest CoNED DEM elevation point, then they were prescribed in the model as subgrid features (1D weirs) where necessary to accurately represent their elevation and ensure representative flow routing. Engineering properties of structures such as roughness and hydrodynamic effects from detailed geometry of levees, bridge abutments or piers, and culverts were not included in the subgrid features and so were not evaluated in the model. Model configuration and boundary-condition files for the February 2020 Super Bowl flood event for existing conditions and the 2080s mean-change scenario are provided in Grossman and others (2023).

## Model Validation

Model performance was determined through comparison of modeled and observed time series of water levels at sites in the lower main-stem Nooksack River and Bellingham Bay. Water-level data were also used to test model sensitivity and calibrate the model for roughness. Water-level observations recorded during the period from 2015 to 2017 from atmospheric-calibrated pressure sensors at Ferndale, Slater Road, and Marine Drive (see fig. 3 for locations) from Anderson and others (2019) provided information to assess model skill in the main-stem Nooksack River between I–5 and the Nooksack River delta (fig. 4). The 2015–2017 dataset helped to characterize the variable influence of tides, storm surge, and streamflow on water levels. A second source of water-level data were provided by Whatcom County Flood Control Zone District: a dataset of time-series measurements on the east edge of the floodplain near Slater Road and an unnamed creek (informally referred to herein as "Tennant creek"; see fig. 1 for location), and a dataset of high-water marks at select floodplain sites set during the January 2009 flood. Water-level observations provided validation of marine water levels in Bellingham Bay; these data were derived from laser-rangefinder measurements of the water-surface elevation at 10 hertz (Hz) and georeferenced to the North American Vertical Datum of 1988 through real-time-kinematic global positioning system (RTK-GPS) and tape-down surveys.

Model skill for water levels was evaluated by computing the following three parameters:
(1) model bias (eq. 1),

$$bias = \frac{1}{n}\sum_{i=1}^{n}(y_i - x_i), \quad (1)$$

where

$bias$ = model bias,
$n$ = number of observations,
$i$ = individual observation number,
$y_i$ = modeled water level, and
$x_i$ = observed water level;

(2) bias-removed mean absolute error (MAE) (eq. 2),

$$uMAE = \frac{\sum_{i=1}^{n}|y_i - x_i|}{n} - bias, \quad (2)$$

where

$uMAE$ = mean absolute error accounting for bias,
$n$ = number of observations,
$i$ = individual observation number,
$y_i$ = modeled water level,
$x_i$ = observed water level, and
$bias$ = computed model bias from equation 1;

and (3) bias-removed root mean square error (RMSE) (eq. 3),

$$uRMSE = \sqrt{\frac{\sum_{i=1}^{n}(y_i - x_i)^2}{n}} - bias, \quad (3)$$

where

$uRMSE$ = root mean square error accounting for bias,
$n$ = number of observations,
$i$ = individual observation number,
$y_i$ = modeled water level,
$x_i$ = observed water level, and
$bias$ = computed model bias from equation 1.

Airborne video surveys during and after the February 2020 Super Bowl flood, provided by Whatcom County, were used to evaluate spatial patterns of flooding and to adjust subgrid features to improve model performance. Flow-control structures were evaluated for their ability to influence the conveyance of floodwaters across the floodplain, on the basis of historical imagery of flooding; photographs were analyzed for specific spatial flood patterns that could be easily discernable in the model output. In situations where the model predicted dissimilar flood footprints, elevations of the 1D weirs were compared to the CoNED data and adjusted to the DEM value if found in error.

## Model Calibration

The model was calibrated by adjusting bed roughness in the Nooksack River and its distributary channels to minimize MAE at available observation locations. Manning's

*n* roughness coefficient values, which ranged from 0.032 to 0.036 for the main-stem Nooksack River and its distributaries, respectively, were found to maximize model skill across all sites (fig. 5). These values are characteristic of temperate rivers and estuaries where Manning's *n* coefficient values of 0.02 to 0.04 have been found to represent the system well (Chow, 1959). It is important to note that roughness is uncertain, as it may vary considerably in space and time owing primarily to changing river morphology and bed composition and also to other important processes that affect discharge. The application of a Manning's *n* roughness coefficient value of 0.032 along the main-stem Nooksack River in the model was based on an analytically derived best fit to the extreme discharges and the water levels that spanned the model domain that were of interest to the study.

## Model Simulations and Vulnerability

### Sea-Level Rise and Tidal Propagation

The effects of tides and sea-level rise, including the extent of tidal propagation in the lower Nooksack River, were modeled by simulating a 1-month period centered on a king tide of early to mid-January 2003, which had 66 dominant tidal-harmonic constituents, derived from the regional

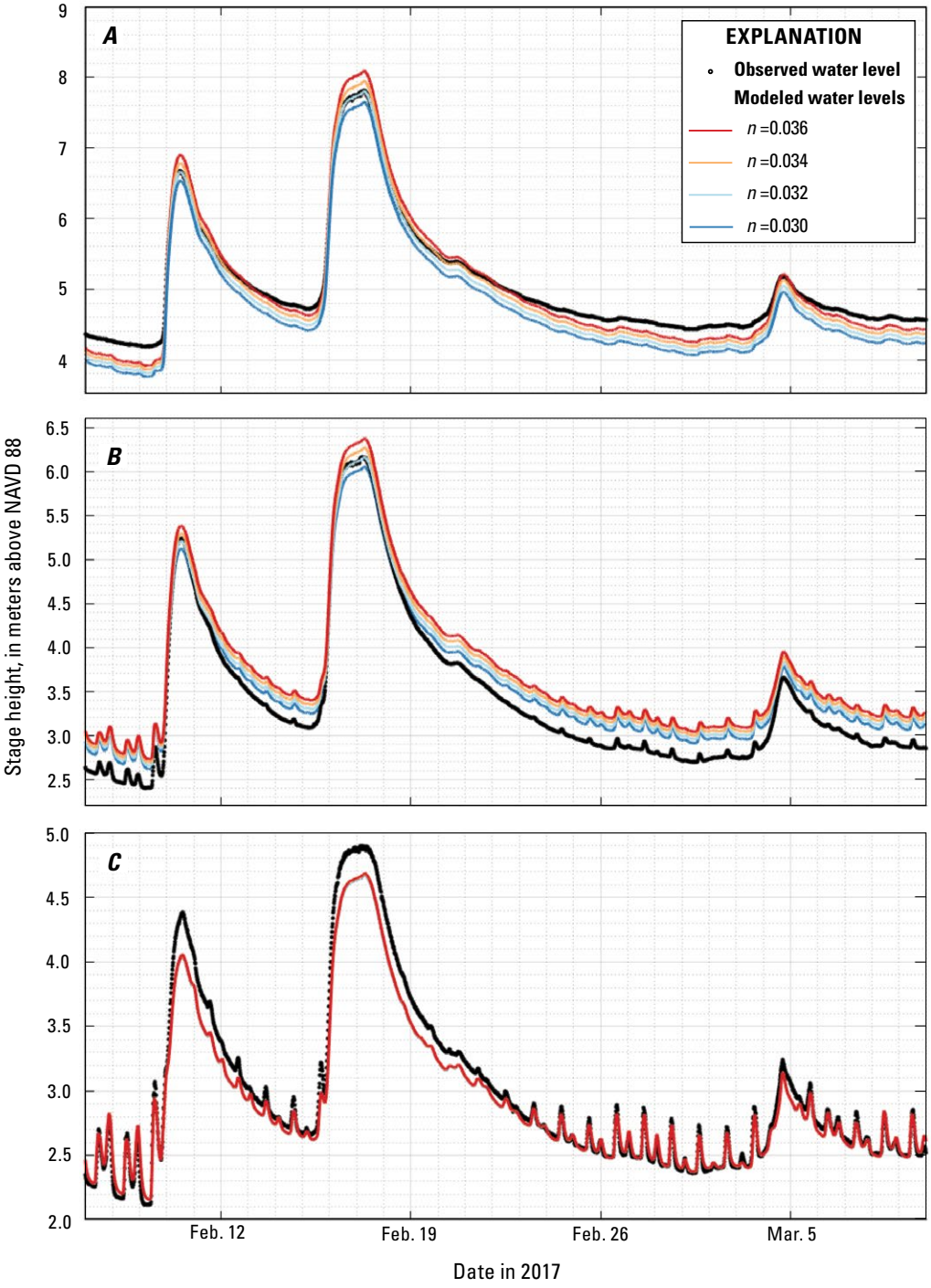


**Figure 5.** Plots showing sensitivity of modeled water levels to range of Manning's *n* roughness coefficients versus observed water levels for main stem of lower Nooksack River. Black line showing observed water level is made up of discrete 15-minute observations. *A*, Plot showing modeled and observed water levels at Ferndale validation site. *B*, Plot showing modeled and observed water levels at Slater Road validation site. *C*, Plot showing modeled and observed water levels at Marine Drive validation site; note that in *C*, modeled water levels for other values of *n* are not visible beneath red line (*n* =0.036) because all values plot on same line. NAVD 88, North American Vertical Datum of 1988.

Delft3D FM model, that contributed about 90 percent of the tidal amplitude. These simulations were conducted using a steady discharge value of 3,860 cubic feet per second ($ft^3/s$) (109.30 cubic meters per second [$m^3/s$]), which represents mean annual flow at USGS streamgage Nooksack River at Ferndale (station 12213100; USGS, 2022). In addition to the mean annual flow, the 2-year (50 percent AEP) bankfull flow (25,500 $ft^3/s$) (722 $m^3/s$), the 10 percent AEP stream flood (40,601 $ft^3/s$) (1,149 $m^3/s$), and the 4 percent AEP stream flood (48,801 $ft^3/s$) (1,382 $m^3/s$) were simulated to evaluate the relative influence of stream discharge on tidal propagation and vice versa across the lower Nooksack River (values are based on USGS streamgage measurements, from https://streamstats.usgs.gov/ss/; see also, USGS, 2022). The time frame chosen for the tidal-propagation simulation also included an about 1.5-ft tidal anomaly to capture the effects of a common winter storm surge.

Simulations of the effects of sea-level rise on water levels throughout Nooksack River Reach 1 were made by adjusting the sea-level positions at the marine boundary in 3.9-inch (in.) (10-centimeter [cm]) increments to 6.5 ft (+2 m) for discrete amounts expected in the 2040s and 2080s. The range of 0 to 6.5 ft (0–2 m) of potential sea-level rise represents plausible amounts of sea-level rise to the year 2150 (Miller and others, 2018). Discrete amounts of sea-level rise that are based on the 50 and 1 percent probabilities of relative sea-level rise for the Nooksack River delta by Miller and others (2018) were also prescribed for the mean- and high-change scenarios for the 2040s and 2080s, respectively. For the 2040s, the mean-change scenario included +0.4 ft (0.15 m) of sea-level rise, whereas the high-change scenario included +0.9 ft (0.27 m) (table 1). Similarly, the mean-change scenario for the 2080s included +1.3 ft (0.40 m) of sea-level rise, and the high-change scenario included +3.1 ft (0.94 m) (table 1). Both sets of sea-level-rise estimates reflect the moderate to high Intergovernmental Panel on Climate Change (IPCC) Representative [Carbon] Concentration Pathway[5] (RCP) 8.5 to provide a greater level of risk assessment. Miller and others (2018) integrated estimates of sea-level trends and land movements from tide gages, measurements from regional-leveling and continuous global positioning system (GPS) surveys, and tectonic-model data, along with probabilistic forecasts of global sea-level responses to climate change, to provide downscaled spatial and temporal predictions of sea-level rise relative to Washington's complex coastline. The probabilistic sea-level-rise estimates of Miller and others (2018) were also used to qualify the timing of modeled 10-cm-incremental sea-level-rise effects. The estimates of Miller and others (2018) were corroborated by those of Sweet and others (2022), which showed greater confidence and a narrower range of global sea-level-rise estimates for 2050 than were previously reported and that were within the uncertainty associated with regional vertical land motion and interannual climate variability.

[5]Representative Concentration Pathway (RCP) is a greenhouse-gas-concentration (not emissions) trajectory adopted by the IPCC.

## Historical Floods

For this study, two historical floods on the Nooksack River were simulated: the February 2020 Super Bowl flood (SBF), representing a 10 percent AEP stream flood, and the January 2009 flood, representing a 4 percent AEP stream flood. The hydrographs measured by the USGS at the USGS streamgage at Ferndale (USGS, 2022) were fed directly into the model at the upstream discharge boundary. Prior to simulating the January 2009 event, flow routing and flood footprints from the modeled February 2020 SBF were qualitatively validated from drone imagery and photographs of the event and also compared to observed water depths on the floodplain near Slater Road (see fig. 3 for location). Hydrographs from the February 2020 SBF and the January 2009 flood were also simulated for each 10-cm increment of sea-level rise from 0 to 2 m to evaluate the effects of sea-level rise on patterns of observed flooding. The February 2020 SBF event included moderately high tides that peaked prior to the flood at 8.8 ft (mean lower low water [MLLW]), as well as a storm surge of 0.95 ft, as measured at the NOAA Cherry Point tide gage (station 9449424). The January 2009 event included tides that reached 9.2 ft (MLLW) and a storm surge of 0.88 ft, as measured at Cherry Point tide gage. Annual tides reach 10.0 to 10.5 ft (MLLW), and winter storm surges average 1.0 to 2.0 ft and periodically reach almost 3.0 ft at the Cherry Point tide gage. Lastly, the 1 percent AEP was simulated on the basis of idealized hydrographs from Northwest Hydraulic Consultants (Northwest Hydraulic Consultants, 2015).

**Table 1.** Change scenarios for projected sea-level rise and higher fluvial discharge amounts in the modeled time periods of the 2040s and 2080s.

[ft, feet; m. meter]

| Change scenario | Time period | Sea-level-rise probability, in percent | Sea-level rise, in ft (m) | Discharge change, in percent |
|---|---|---|---|---|
| 2040s mean change | 2040s | 50 | 0.4 ft (0.15 m) | 20 |
| 2040s high change | 2040s | 1 | 0.9 ft (0.27 m) | 32 |
| 2080s mean change | 2080s | 50 | 1.3 ft (0.40 m) | 52 |
| 2080s high change | 2080s | 1 | 3.1 ft (0.94 m) | 72 |

## Future Floods

Similar to sea-level rise, extreme runoff and stream floods in the Pacific Northwest are expected to progressively increase by (and throughout) the 2040s and 2080s (Hamlet and others, 2013) in response to climate change (fig. 6). Hamlet and other (2013) generated estimates of expected changes in streamflow owing to rising temperatures, more precipitation falling as rain rather than snow, and more intense lowland rainfall in the 2040s and 2080s relative to present day (2023), on the basis of 10 global climate models, as part of the Columbia Basin Climate Change Scenarios Project. Hamlet and others (2013) also developed a regional hydrologic model of the Pacific Northwest using the variable infiltration capacity model that computed a variety of hydrologic outputs (for example, precipitation, potential evapotranspiration, streamflow) at 297 locations across the domain for the historical time period of 1916–2006 and the three future time frames of the 2020s, 2040s, and 2080s. The moderate- and low-greenhouse-gas-emissions scenarios A1B and B1, respectively, as defined by the IPCC Fourth Assessment Report, were used as boundary conditions. Mean and high estimates of potential increases in stream discharge were developed using the delta hybrid method, a statistical downscaling technique (Hamlet and others, 2013). The mean- and high-discharge-change estimates were used to adjust the 10 percent AEP February 2020 SBF and the 4 percent AEP January 2009 flood hydrographs for the mean- and high-change scenarios defined in this study (table 1).

The mean- and high-change scenarios for the combined effects of sea-level rise and stream discharge provide a framework for assessing the potential exposure and risk to flood hazards that span a range of probabilities. Model outputs that are based on discrete amounts of change in sea level and stream discharge are designed to have a long shelf life, as the timing of their occurrences can be revised as new projections

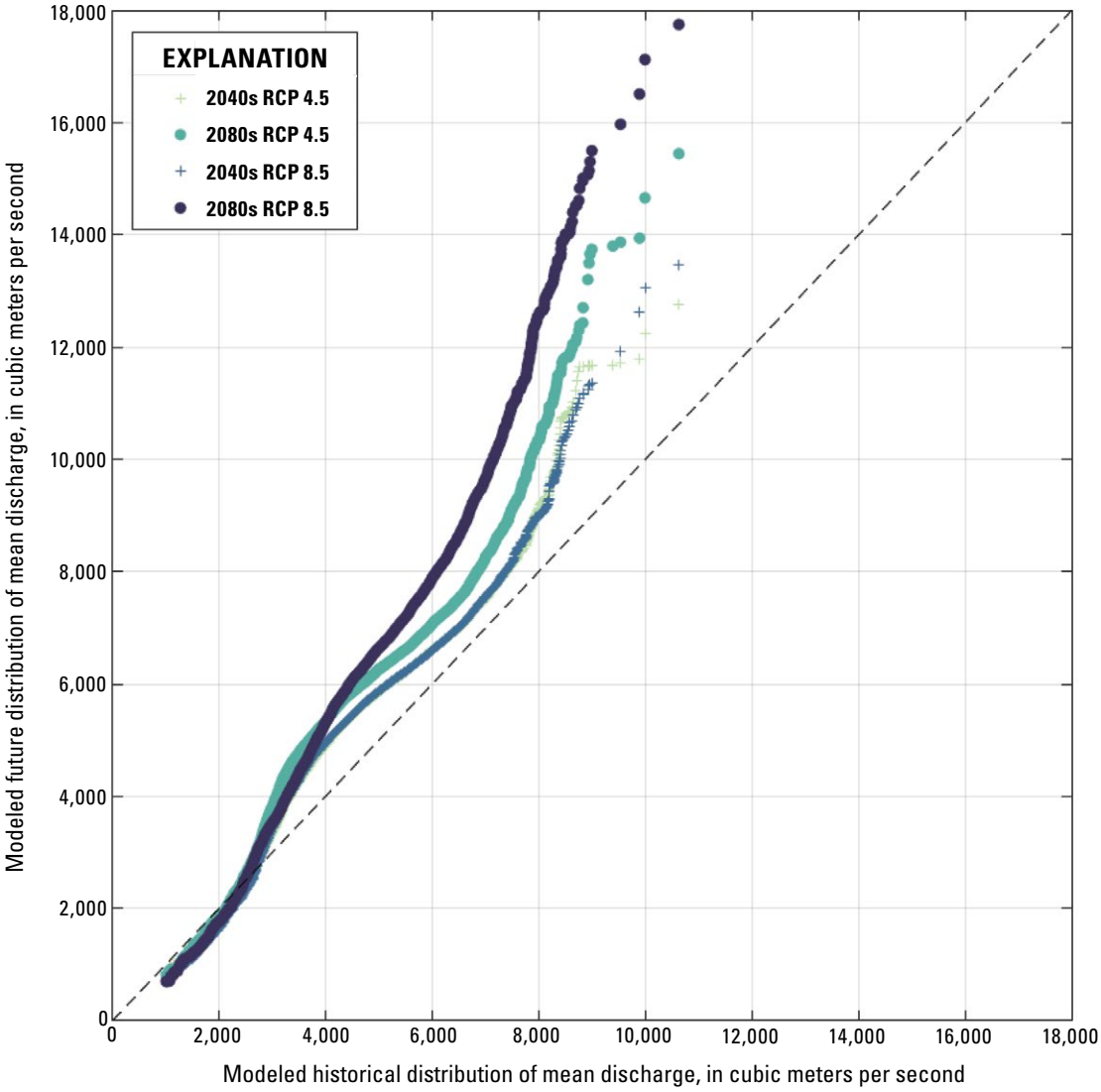


**Figure 6.** Plot showing projected change in Nooksack River mean-discharge distributions for modeled future distributions (that is, set of models available) of 2040s (plusses) and 2080s (dots) for Representative Concentration Pathways (RCP) 4.5 and RCP 8.5 scenarios (Hamlet and others 2013) relative to modeled historical distributions. Dashed black line shows one-to-one relation if future distributions were equal to historical distributions.

of the rates of change in sea-level rise and fluvial discharge are published. Notably, although the high-change scenario has a low probability of occurrence, it is not necessarily the most severe scenario possible, as larger floods that may occur can be estimated. We also note that extreme events such as the 10 percent AEP and 4 percent AEP stream floods are defined on the basis of their historical recurrence and (or) their probabilities of occurrence, which are often based on relatively short observational records that limit their derivation and representativeness. As a result, the magnitudes and recurrence frequencies of extreme events are continuously being revised as new floods occur, and they are projected to change in complex ways with accelerating sea-level rise and climate change.

## Alternatives Analyses

Proposed adaptive-management alternatives, including modifications to roads, levees, and surrounding wetlands along the Nooksack River downstream from Ferndale, were implemented in the model to examine the extent to which they may affect the flow of water and sediment and, thus, potentially mitigate flood exposure. Design specifics were added to the model of existing conditions that were based on the following lower Nooksack River Project (LNRP) alternatives 3B and 4C (Northwest Hydraulic Consultants, 2015). The proposed alternatives are summarized below:

*Alternative 3B.*—This proposed alternative would lower the levee along the left bank of the Nooksack River, in two pilot areas between Slater Road and Marine Drive, to reconnect streamflow between the main-stem Nooksack River and the floodplain in the area of "Tennant creek"; it would also raise the roadway of Slater Road along parts of the eastern floodplain (see fig. 1 for locations).

*Alternative 4C.*—This proposed alternative would add to alternative 3B by (1) removing the southern part of the existing right-bank levee downstream from the informally named "Kwina slough" and Ferndale Road, (2) setting back the levee along the right bank of "Kwina slough" and along Ferndale Road, and (3) adding a trainer channel into the restored floodplain area (see fig. 1 for locations).

Prior to simulating the suite of different flood scenarios using the floodplain alterations, the sensitivity of river stage upstream from Slater Road to the width of the bridge opening associated with elevating Slater Road was evaluated (no other design alterations were considered during these sensitivity tests). An iterative approach was undertaken by increasing the bridge-opening widths in 100-m increments to determine the width of opening needed to maintain less than a 1-ft river-stage increase upstream from Slater Road that would potentially be associated with any roadway modifications under the 4 and 1 percent AEP stream floods. Following this analysis, the 10 percent, 4 percent, and 1 percent AEP stream floods were simulated using alternatives 3B and 4C under contemporary conditions and under the 2040s and 2080s mean- and high-change scenarios.

## Sediment Transport

An offline sediment-transport model was coupled to the 1D–2DH hydrodynamic numerical model to provide a first-order estimate of the potential for sedimentation and erosion in the Nooksack River for the various flood scenarios modeled. The empirical Engelund-Hansen (E-H) model (eq. 4) was used with the hydrodynamic-model outputs in the river to estimate the total sediment transport (bedload plus suspended load) at each time step:

$$S = (0.05\alpha q^5)/(\sqrt{g}\, C^3\, \Delta^2\, D_{50}), \quad (4)$$

where

$S$ = sediment flux ($m^3/s$),
$\alpha$ = calibration parameter (dimensionless),
$q$ = discharge ($m^3/s$),
$g$ = gravity (meters per second squared [$m/s^2$]),
$C$ = Chezy roughness (dimensionless),
$\Delta$ = normalized sediment density (dimensionless), and
$D_{50}$ = median grain size (m).

Although the E-H model can be used with a calibration parameter ($\alpha$), here we have prescribed $\alpha = 1$, and, therefore, it does not affect our calculations. The E-H model is valuable to assess the relative differences in potential sediment transport that result from different forcing, assuming that sediment transport under existing conditions is generally in equilibrium with the system's hydrodynamic and geomorphic processes. Herein we use the model to evaluate the potential changes in sediment transport through, and retention within, the model domain associated with the projected mean- and high-change scenarios, mitigation alternatives, and recently observed bed changes.

Cross sections recorded river stage, velocity, bed level, surface area, and sediment flux every 50 m in the riverine part of the model, creating evenly spaced areas where the flux of potential sediment entering and leaving each cross section could be calculated and the total retained within reaches of interest could be estimated. Model outputs varying through time were provided to the E-H model, along with uniform estimates of bed roughness (Chezy value of 55) and the median diameter of sediment in the river ($D_{50}$ = 0.25 millimeters [mm]) that is assumed to be isotropic and unchanging. The sediment flux through each cross section was calculated throughout the entire simulation and then integrated, in order to provide estimates of the total volume either moved or retained in the river. Sediment transport was computed for all change scenarios and floodplain-restoration alternatives, providing an approximation of the potential for geomorphic change in the river that is due solely to climate change and to mitigation efforts. Comparison of the results of the E-H model to the estimated sediment flux through the lower Nooksack River for the year 2011 showed good model skill, varying within about 30 percent of the cumulative sediment transport that was estimated by Anderson and others (2019).

# Results

## Model Validation

Comparison of modeled and measured water levels across the lower Nooksack River and Bellingham Bay shows that the model has high skill (fig. 7). An *uRMSE* value of 0.11 ft (0.03 m) for water levels at the USGS streamgage at Ferndale (USGS, 2022) indicates that river stage–discharge relations that force the rest of the model are well represented and are within the desired uncertainty of 1 ft or less (fig. 7*A*; table 2). The *uRMSE* value for water levels at Slater Road and Marine Drive (fig. 3) of 0.03 and 0.25 ft, respectively, during the 3 months of the spring 2017 validation period, reveal the high skill of the model across a wide range of streamflow- and marine-forcing conditions (figs. 7*B*, 7*C*). Modeled water levels in Bellingham Bay showed an *uRMSE* value of 0.27 ft (0.08 m) during the model-validation period (fig. 7*D*).

## Model Performance of Historical Floods

Model simulation of the February 2020 SBF showed the complex interaction of streamflow, tides, and storm surge (fig. 8). After typical tidal flooding of the Silver Creek and "Tennant creek" areas at high tide on January 31, 2020 (fig. 8*A*), modest flooding of the area was computed during the

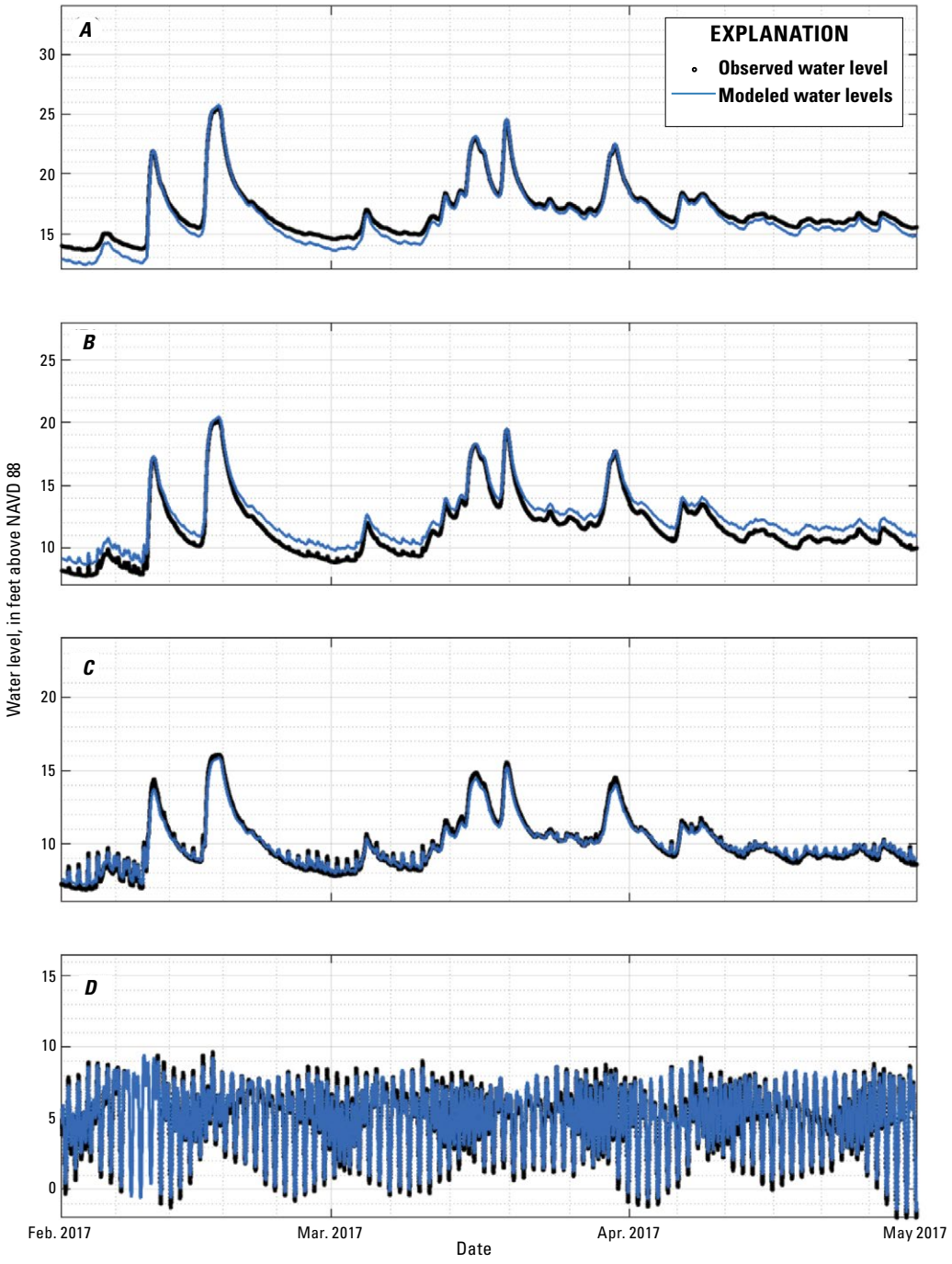


**Figure 7.** Plots showing modeled and observed water levels at (*A*) Ferndale Wastewater Treatment Plant, (*B*) Slater Road, (*C*) Marine Drive, and (*D*) Nooksack River delta sites. Black line showing observed water level is composed of discrete 15-minute observations. NAVD 88, North American Vertical Datum of 1988.

**Table 2.** Model error and bias values at Ferndale Wastewater Treatment Plant, Slater Road, Marine Drive, and Nooksack River delta validation sites.

[See figure 3 for locations. ft, feet; m, meter]

| Error statistic | Site | | | |
|---|---|---|---|---|
| | Ferndale Wastewater Treatment Plant | Slater Road | Marine Drive | Nooksack River delta |
| Bias | −0.48 ft (0.15 m) | 0.79 ft (0.24 m) | 0.02 ft (0.006 m) | 0.09 ft (0.03 m) |
| Unbiased mean average error | 0.03 ft (0.009 m) | 0.01 ft (0.003 m) | 0.20 ft (0.06 m) | 0.19 ft (0.06 m) |
| Unbiased root mean square error | 0.11 ft (0.03 m) | 0.03 ft (0.009 m) | 0.25 ft (0.07 m) | 0.27 ft (0.08 m) |

next low tide on February 1, 2020, as river discharge increased and river stage rose above 24 ft at the USGS streamgage at Ferndale (fig. 8*B*) (USGS, 2022). The model predicted overtopping of the left bank at Hovander Park in Ferndale when river stage at Ferndale reached 26 ft (fig. 8*C*). Note that storm surge in Bellingham Bay signified as nontidal residual raised coastal water levels between January 30 and February 2 (2020), reaching a maximum of about 1.5 ft on February 1, just before the peak of the stream flood (fig. 8*C*). By the peak of the stream flood on February 2, the entire eastern floodplain was computed to be flooded; the western floodplain was not predicted to experience flooding (fig. 8*D*).

Where surveyed water-level, flood-extent, and high-water-mark data exist, they show that the model has high skill for the February 2020 SBF and the January 2009 flood. Modeled flood extents and maximum water depths associated with the February 2020 SBF show extensive flooding across the east bank (left side when traveling downstream) of the Nooksack River downstream from Ferndale and the lower Nooksack River floodplain downstream from Marine Drive (fig. 9*A*). Modeled maximum water depths ranged from 1 to 2 ft (0.3–0.6 m) across Hovander Park upstream from Slater Road and 4 to 5 ft (1.3–1.6 m) between Slater Road and Marine Drive (fig. 9*A*). Modeled maximum water levels during the February 2020 SBF were within 1 ft of measured values on the floodplain at Slater Road (fig. 9*B*). The model reproduced the general timing of flooding and drainage at the site well (fig. 9*B*), despite not directly accounting for rainfall or groundwater, which are suspected to have influenced the early onset of flooding and postflood drainage, respectively.

Computed flood extents and maximum water levels of the 4 percent AEP January 2009 flood show moderate flooding of the west bank (right side when traveling downstream) floodplain between Slater Road and Marine Drive (fig. 10*A*). Modeled maximum water depths of the January 2009 flood ranged from 2 to 4 ft (0.6–1.3 m) upstream from Slater Road, 4 to 6 ft (1.3–2.0 m) along the eastern floodplain downstream from Slater Road, and 0.5 to 2.5 ft (0.1–0.8 m) across the western floodplain (fig. 10*A*). Comparison of computed maximum water levels to 28 measurements of high-water marks across the domain were used to estimate the MAE of 0.5 ft for the model (fig. 10*B*).

## Tidal Propagation

The high skill of the model enables the contributions of tides, storm surge, and stream discharge to water levels across Nooksack River Reach 1 to be resolved. The model indicates that tidal propagation associated with the two dominant tidal constituents, principal lunar semidiurnal (M2) and diurnal (K1), affects water levels in the Nooksack River about 4.5 mi (7.5 km) upstream from the delta, depending on discharge (figs. 11*A*, 11*B*). Under mean daily stream discharge of 3,840 $ft^3/s$ (109 $m^3/s$), tides raise and lower water levels 0.5 to 1.0 ft near Marine Drive, and the influence decreases markedly upstream. The projected increase in sea level of 3.3 ft (1.0 m) by 2080 (Miller and others, 2018) is predicted to double the upstream area that is affected by tides under existing daily mean-streamflow conditions, creating tidal oscillations of 0.5 to 1.0 ft near the main-stem confluence with the Lummi River (figs. 11*C*, 11*D*, 11*E*). Whereas simulations of the January 2003 period (see discussion in the "Model Simulations and Vulnerability" section above) contained an observed time-varying storm surge that had a maximum of 2.3 ft (0.7 m), actual storm surge can reach as much as 3.3 ft (1.0 m) at any time, adding additional water level and flood potential. Storm surge also can propagate upstream on top of the tides in complex ways, especially depending on the duration of the storm (Herdman and others, 2018; Santiago-Collazo and others, 2019). Therefore, these results may underestimate the effect of coastal water levels on flood exposure across Reach 1.

## Growing Exposure to Higher Sea Level and Stream Flooding

The lower Nooksack River and its floodplain are expected to become increasingly influenced by compound flooding associated with the combination of higher sea levels and larger peak stream floods. Flood extent, depth over land, and the duration of flood events are projected to be primarily driven by the higher peak-stream discharges that are expected in the coming decades. The modeling in this study, which showed the sensitivity of flooding to tides during the February 2020 SBF upstream from Slater Road (fig. 8), indicates that extreme water levels that cause flooding will steadily expand upstream through time with sea-level rise.

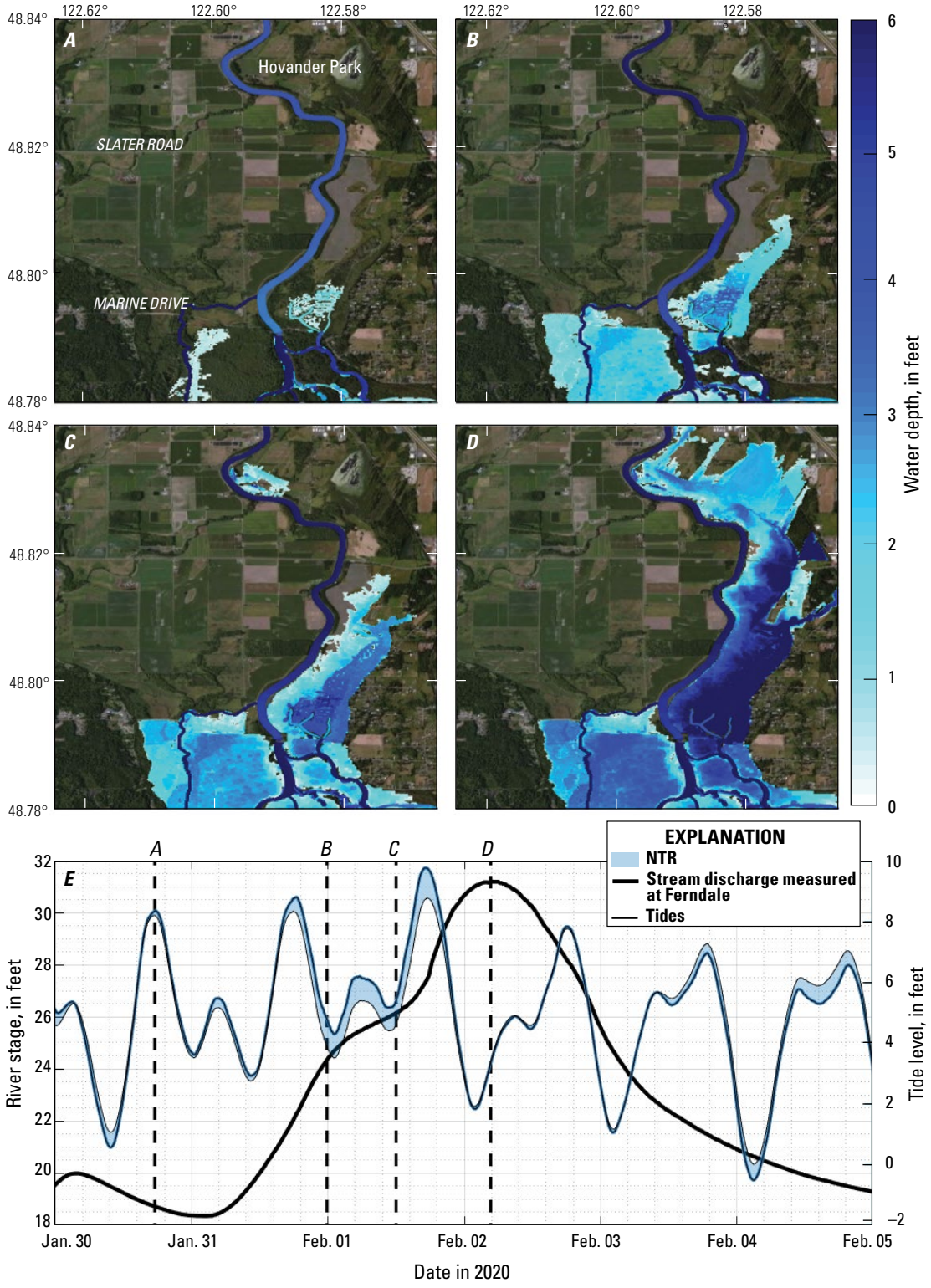


**Figure 8.** *A–D*, National Agricultural Imagery Program (NAIP) composite images showing modeled progression of flooding during February 2020 Super Bowl flood. *E*, Plot showing flood response to stream discharge (thick black line) measured at U.S. Geological Survey (USGS) streamgage at Ferndale (USGS, 2022) interacting with tides (thin black line) and nontidal-residual (NTR) processes (blue shading). Dashed black lines show timing of modeled progressions of flooding shown in *A–D*. River stages and tide levels measured relative to North American Vertical Datum of 1988. NAIP images from U.S. Department of Agriculture National Agricultural Imagery Program.

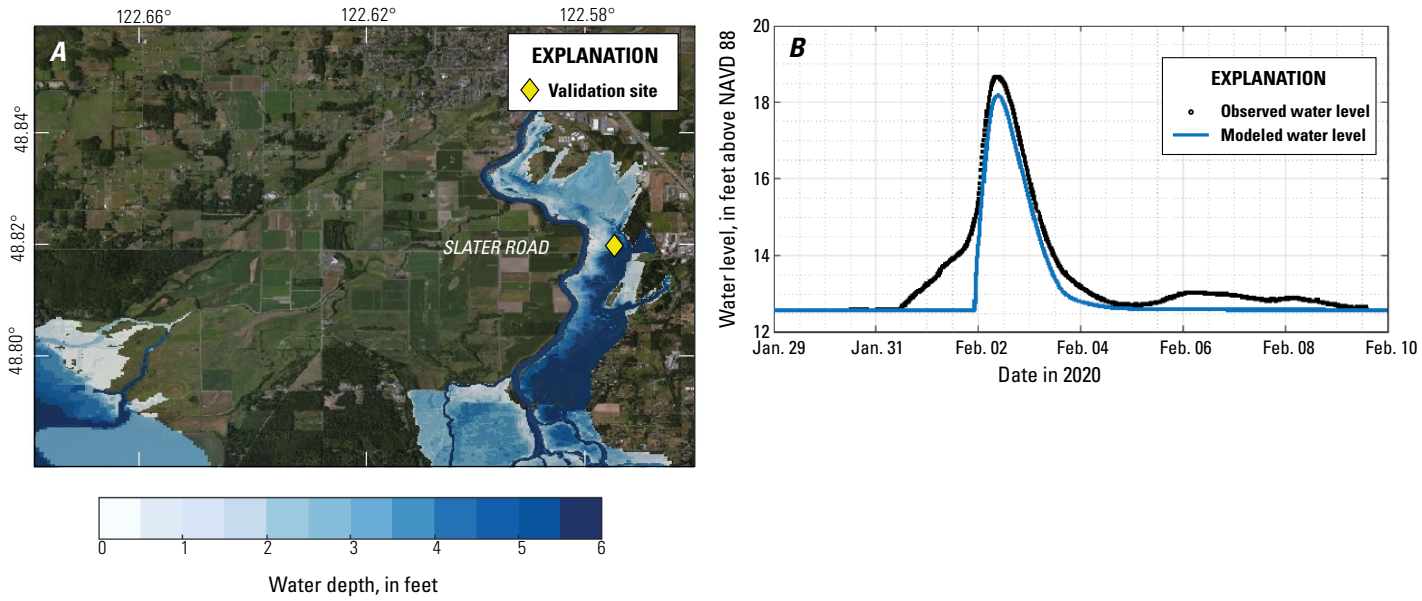


**Figure 9.** *A*, National Agricultural Imagery Program (NAIP) composite image showing computed maximum flood extent and water depth across Nooksack River floodplain during 10 percent annual exceedance probability (AEP) February 2020 Super Bowl flood. *B*, Plot of modeled water levels compared to recorded water levels at Slater Road validation site (see fig. 3 for location). NAIP image from U.S. Department of Agriculture National Agricultural Imagery Program. NAVD 88, North American Vertical Datum of 1988.

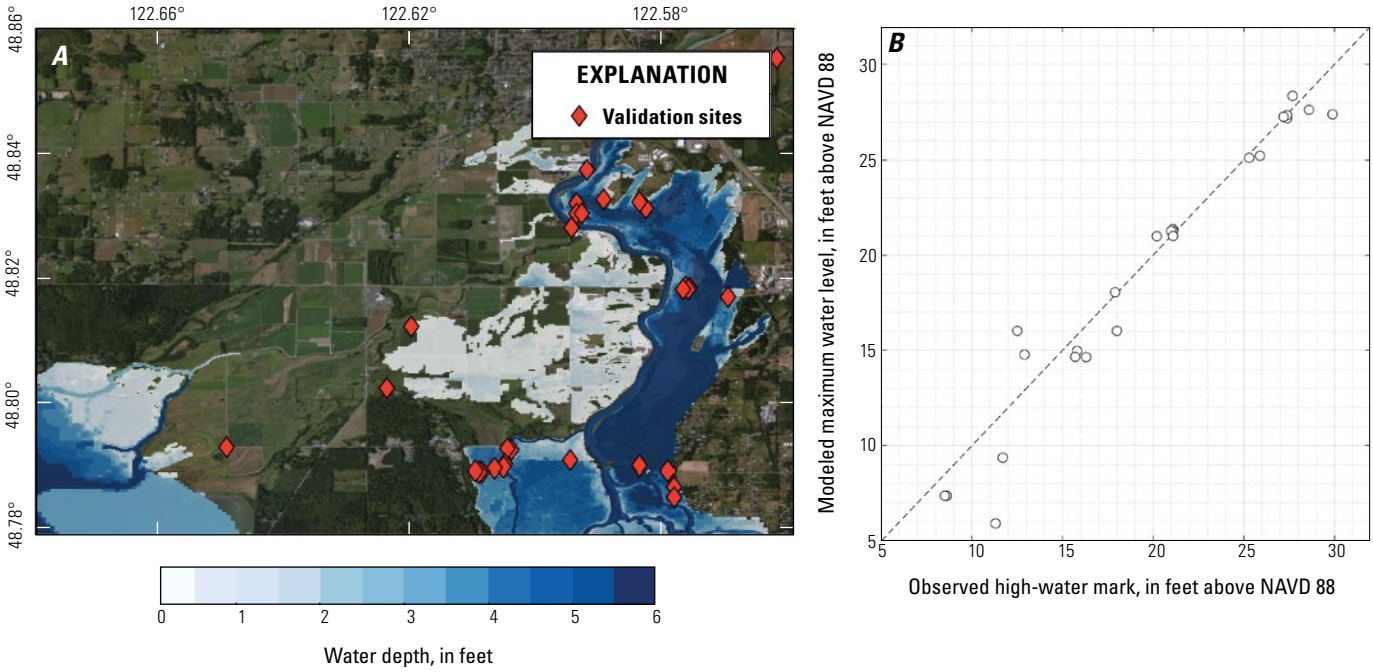


**Figure 10.** *A*, National Agricultural Imagery Program (NAIP) composite image showing computed maximum flood extent and water depth across Nooksack River floodplain during 4 percent annual exceedance probability (AEP) January 2009 flood. Note that validation sites (red diamonds) in this figure are not same as validation sites shown in other figures (see, for example, figs. 1, 3, 9, 19, 20, 29). NAIP image from U.S. Department of Agriculture National Agricultural Imagery Program. *B*, Plot of modeled maximum water levels (circles) versus measured high-water marks at various validation sites. NAVD 88, North American Vertical Datum of 1988.

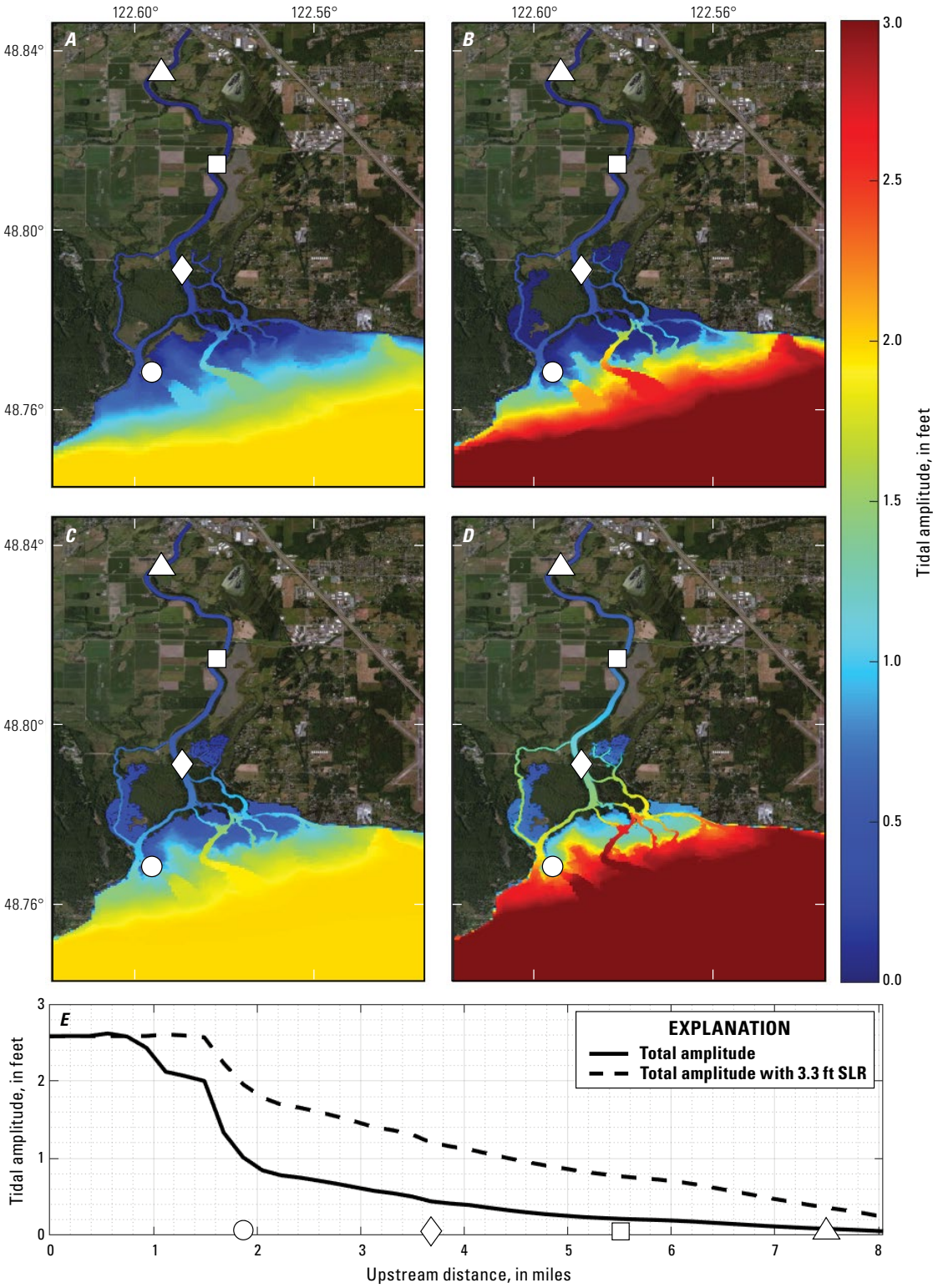


**Figure 11.** National Agricultural Imagery Program (NAIP) composite images showing modeled amplitudes of two dominant tidal constituents, principal lunar semidiurnal and diurnal ([M2 and K1, respectively]), during mean daily discharge under existing conditions (*A* and *B*, respectively) and with 3.3 feet (ft) (1.0 meter [m]) of sea-level rise (*C* and *D*, respectively). Markers show locations of observation sites (in thalweg), listed in downstream order: triangle, Ferndale Wastewater Treatment Plant; square, Slater Road; diamond, Marine Drive; circle, Nooksack River delta. NAIP images from U.S. Department of Agriculture National Agricultural Imagery Program. *E*, Plot of changes in tidal amplitude associated with all tidal constituents versus distance upstream from Nooksack River delta: solid black line, amplitudes under existing conditions; dashed black line, amplitudes with 3.3 ft (1.0 m) of sea-level rise (SLR). Markers showing observation sites in *A*–*D* plotted for reference. Tidal amplitudes relative to North American Vertical Datum of 1988.

## 2040s

The combined influence of 0.4 to 0.9 ft of sea-level rise and between 20 and 32 percent higher peak stream discharges by the 2040s is computed to have extensive effects within Nooksack River Reach 1. Whereas the 2040s mean-change scenario (for example, a 50 percent likelihood of sea-level rise and a mean increase in streamflow of 20 percent) is not projected to increase flood exposure of the western floodplain during a 10 percent AEP stream-flood event (fig. 12*B*), the 2040s high-change scenario is computed to lead to flooding across 33 percent of the western floodplain (figs. 12*C*, 13). The area projected to be the most affected is between Slater Road and Marine Drive (fig. 12*C*). A difference in water depth between the projected 10 percent AEP stream flood under the 2040s high-change scenario relative to present day (2023) across the western floodplain ranges from 0.5 to 1.5 ft (fig. 12*E*). Flood extent across the eastern floodplain, which already sustains extensive flooding during a 10 percent AEP stream flood such as was observed in February 2020, is not projected to increase substantially; however, water depths during such an event are estimated to increase about 1 ft in the 2040s for the mean-change scenario (figs. 12*D*, 13) and as much as 2 to 3 ft for the high-change scenario (figs. 12*E*, 13).

The combined influences of sea-level rise and higher peak-stream discharges for a 4 percent AEP stream flood, such as what was observed in January 2009 flood, by the 2040s is computed to have substantially greater effects across Reach 1 of the Nooksack River. Both the mean- and high-change scenarios of the 2040s are predicted to cause the 4 percent AEP event to more than double the area flooded across the western floodplain (figs. 14*A*, 14*B*). Whereas about 23 percent of the western floodplain was affected by the January 2009 event, 50 percent (and as much as 94 percent) of the western floodplain is computed to experience flooding under the 2040s mean- and high-change scenarios, respectively (figures 14*B* and 14*C*, respectively; see also, appendix 1). The differences in water depth owing to higher levels of runoff and sea-level rise in the 2040s that are associated with projected changes to the 4 percent AEP stream flood range from 1 to 3 ft for the 2040s mean-change scenario (fig. 14*D*), and they reach as much as 5 to 6 ft for the 2040s high-change scenario (fig. 14*E*).

The expected changes to peak stream discharge and flood extents by the 2040s are projected to be comparable to, or more extreme than, the November 2021 flood on the Nooksack River. Whereas the 10 percent AEP February 2020 SBF is estimated to become as severe as the November 2021 flood under the 2040s high-change scenario (fig. 12*C*), flooding associated with the 4 percent AEP January 2009 flood event is expected to exceed that of the November 2021 event under both the 2040s mean- and high-change scenarios (fig. 14*B*; table 3). Under the 2040s high-change scenario, flood extent across the western floodplain during a 10 percent AEP stream flood is estimated to become nearly equal to (that is, 99 percent) the November 2021 flood. Flood exposure across the western floodplain in the 2040s during a 4 percent AEP stream flood such as the January 2009 event is projected to be more severe than the November 2021 flood by 10 percent under the 2040s mean-change scenario and by 40 percent under the 2040s high-change scenario.

## 2080s

The combined influence of 1.3 to 3.1 ft of sea-level rise and between 52 and 72 percent increase in peak stream discharges by the 2080s (Hamlet and others, 2013; Mauger and others 2015) is computed to further expose Nooksack River Reach 1 to extreme flooding. A 10 percent AEP stream-flood event similar to that observed in February 2020 is projected to affect 32 percent of the western floodplain under the 2080s mean-change scenario (fig. 15*B*) and cause flooding across 58 percent of the western floodplain under the 2080s high-change scenario (fig. 15*C*; see also, appendix 1). Projected changes in water depth during a 10 percent AEP stream flood in the 2080s range from 1 to 3 ft on the western floodplain and as much as 5 ft on the eastern floodplain relative to flooding in February 2020 (figs. 15*D*, 15*E*). Flood extent across the western floodplain under the 2080s mean-change scenario for today's (2023) 10 percent AEP stream-flood event is projected to be nearly comparable to that in the November 2021 flood, but it will lead to a 112 percent increase in flood area relative to the November 2021 flood under the 2080s high-change scenario (table 3).

Flood extent during a 4 percent AEP stream flood similar to the January 2009 event is projected to become severe by the 2080s and will affect most of the western floodplain of Reach 1. Whereas a modest 23 percent of the western floodplain was affected in January 2009, the combined

**Table 3.** Discharge comparisons relative to the November 2021 flood at U.S. Geological Survey streamgage at Ferndale (station 12213100).

[Data for U.S. Geological Survey (USGS) streamgage at Ferndale (station 12213100) from USGS (2022). --, not determined; Feb., February; ft³/s, cubic feet per second; high, high-change scenario; Jan., January; mean, mean-change scenario; Nov., November; SBF, Super Bowl flood]

| Event | Discharge (ft³/s) | Projected discharge (ft³/s) | | | | Ratio of projected flow to that of Nov. 2021 flood | | | |
|---|---|---|---|---|---|---|---|---|---|
| | | 2040s mean | 2040s high | 2080s mean | 2080s high | 2040s mean | 2040s high | 2080s mean | 2080s high |
| Nov. 2021 | 56,300 | 67,560 | 85,576 | 74,316 | 96,836 | -- | -- | -- | -- |
| Feb. 2020 SBF | 36,600 | 43,920 | 55,632 | 48,312 | 62,952 | 0.78 | 0.99 | 0.86 | 1.12 |
| Jan. 2009 | 51,700 | 62,040 | 78,584 | 68,244 | 88,924 | 1.10 | 1.40 | 1.21 | 1.58 |

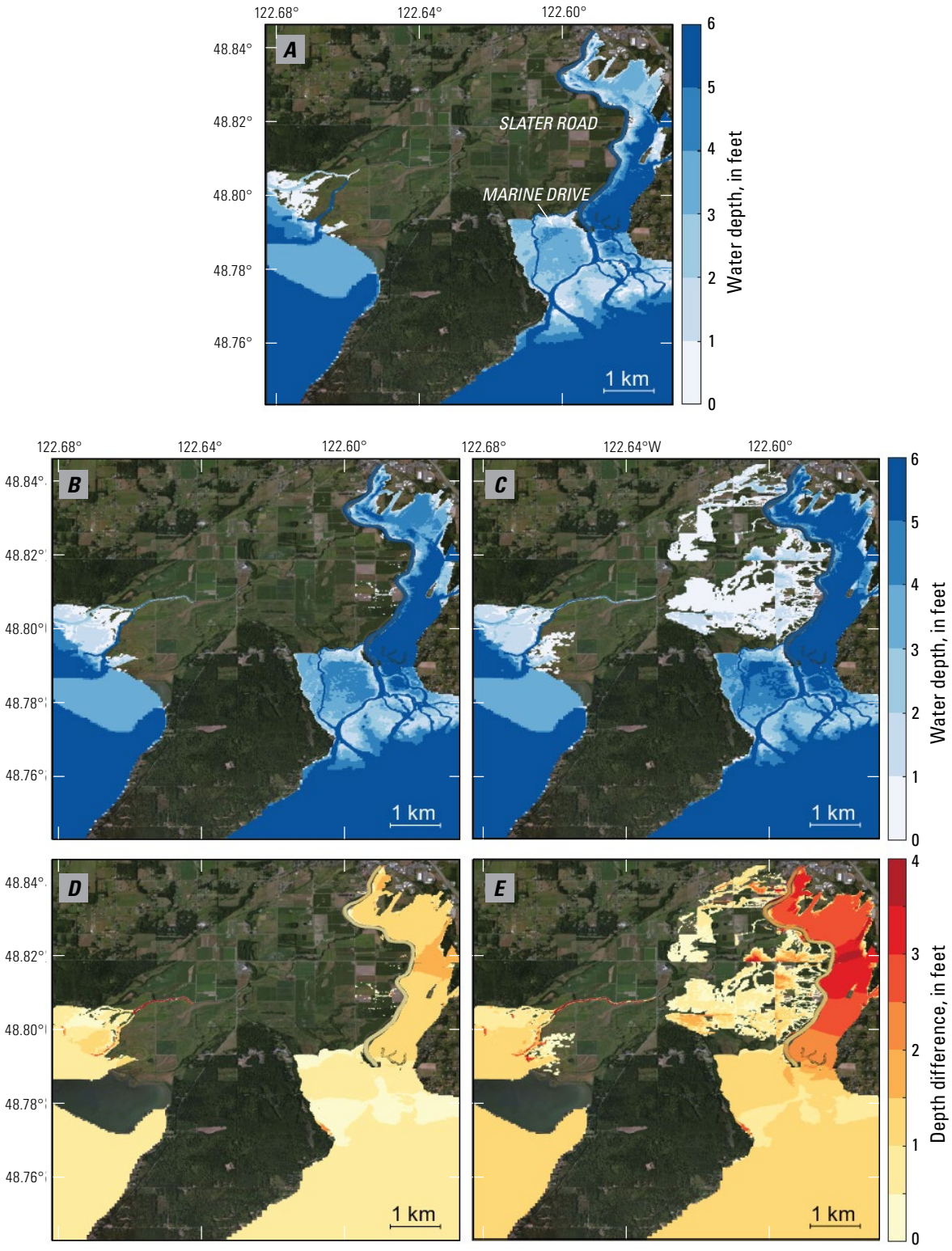


**Figure 12.** National Agricultural Imagery Program (NAIP) composite images showing modeled maximum flood depths and depth differences for 10 percent annual exceedance probability (AEP) stream-flood events. *A*, Existing water depths. *B*, Combined effect on water depths of modeled increases in stream discharge and sea-level rise for 2040s mean-change scenario. *C*, Combined effect on water depths of modeled increases in stream discharge and sea-level rise for 2040s high-change scenario. *D*, Differences in water depths shown in *B* relative to present day (2023). *E*, Differences in water depths shown in *C* relative to present day (2023). NAIP images from U.S. Department of Agriculture National Agricultural Imagery Program.

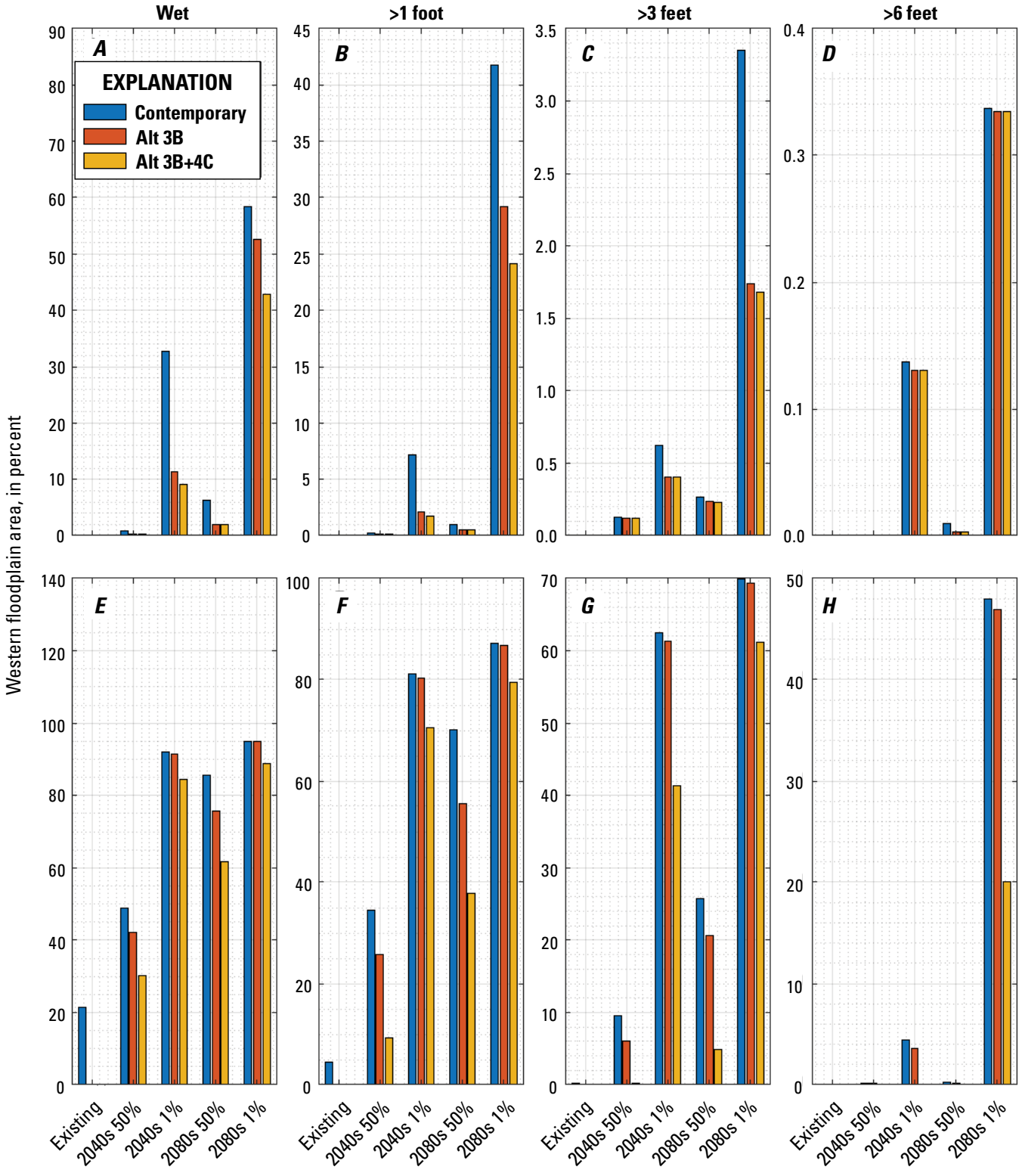


**Figure 13.** Bar plots showing percentages of area in western floodplain under 10 percent annual exceedance probability (AEP) stream flood (*A*–*D*) and 4 percent AEP stream flood (*E*–*H*), computed to experience flooding of (*A*, *E*) about 1 inch (wet), (*B*, *F*) >1 foot (ft), (*C*, *G*) >3 ft, and (*D*, *H*) >6 ft, after no action (contemporary; blue bars) compared to after alternatives 3B (alt 3B; red bars) and 3B and 4C combined (alt 3B+4C; gold bars), under existing conditions and under 2040s and 2080s mean- and high-change scenarios (50 and 1 percent probabilities, respectively).

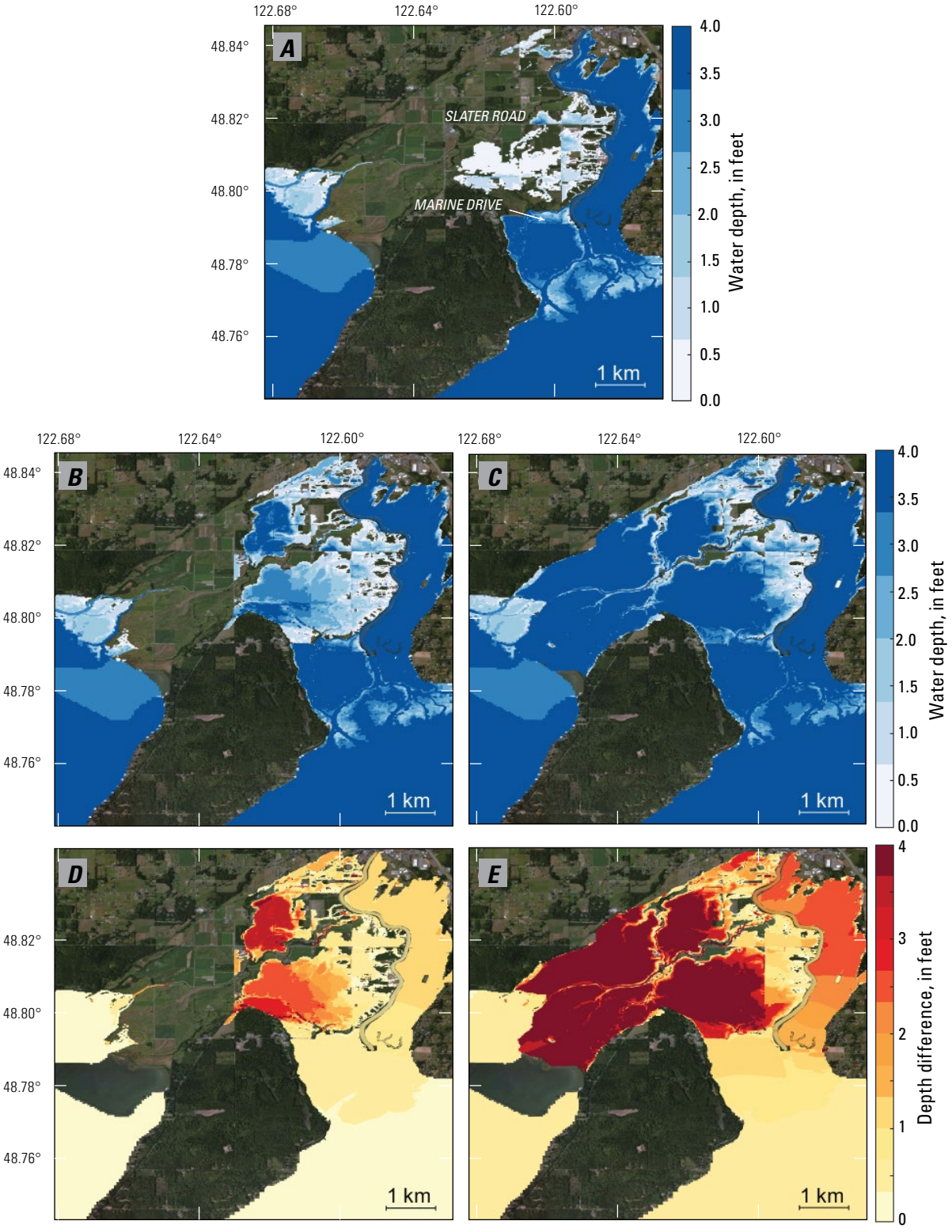


**Figure 14.** National Agricultural Imagery Program (NAIP) composite images showing modeled maximum flood depths and depth differences for 4 percent annual exceedance probability (AEP) stream-flood events. *A*, Existing water depths. *B*, Combined effect on water depths of modeled increases in stream discharge and sea-level rise for 2040s mean-change scenario. *C*, Combined effect on water depths of modeled increases in stream discharge and sea-level rise for 2040s high-change scenario. *D*, Differences in water depths shown in *B* relative to present day (2023). *E*, Differences in water depths shown in *C* relative to present day (2023). NAIP image from U.S. Department of Agriculture National Agricultural Imagery Program.

influences of higher sea level and higher stream discharges by the 2080s on a 4 percent AEP stream flood is computed to lead to flooding of 84 and 91 percent of the western floodplain under the 2080s mean- and high-change scenarios, respectively (figs. 16*B*, 16*C*; see also, appendix 1). These projected changes in today's (2023) 4 percent AEP stream flood are equivalent to a 121 percent greater flood extent under the 2080s mean-change scenario, as well as a 158 percent greater flood extent under the 2080s high-change scenario, than that of the November 2021 event (table 3). The corresponding change in flood depth over land also reveals a shift toward greater flood depths over the western floodplain than over the eastern foodplain (figs. 16*D*, 16*E*) where lower land elevations are more vulnerable to flooding. Projected flooding every 10 years of 58 percent (fig. 15*B*), and every 25 years of 84 to 91 percent (figs. 16*B*, 16*C*), of the western floodplain in the 2080s would represent substantial disruption to the area's economy and cultural ways of life and would likely be a tipping point, given the extensive damages observed in recent floods, including the 2009, 2020, and 2021 flood events.

## Assessment of Flood-Mitigation Alternatives

### Reduced Flood Exposure

The model indicates that the Lower Nooksack River Project alternatives 3B and 4C (fig. 1) have potential beneficial effects in reducing the extent and water depths associated with flooding across the western floodplain under current (2023) and future conditions (fig. 17). The reconnection of historical side channels with alternative 3B was estimated to redirect about 30 percent of a 10 percent AEP streamflow out of the main-stem river and along the eastern floodplain. As a result, the eastern floodplain in the 2040s and 2080s is projected to experience greater flood depths but little change in extent because it already is inundated by flows of 10 percent AEP stream-flood magnitude or higher (figs. 12*A*, 17). An exception is across Hovander Park, where alternative 3 is projected to reduce flood depths by about 0.5 ft (0.15 m) (figs. 17*B*, 17*D*, 17*F*, 17*H*).

Flood extents and depths across the western floodplain in the 2040s and 2080s are computed to be generally lower with alternative 3B, which, by design, routes floodwaters toward the east (fig. 17). The benefit to reduced flooding of the western floodplain by alternative 3B is also generally greater for larger floods such as the 4 percent AEP stream-flood event than the 10 percent AEP stream flood and for high-change scenarios of the 10 percent AEP stream-flood event in the 2040s and 2080s (fig. 13; see also, appendix 1). Alternative 3B is projected to reduce the area of the western floodplain that is exposed to flooding by just 1 percent for the 2040s mean-change scenario (figs. 17*A*, 17*B*) and from 33 percent without the project to 13 percent with the alternative under the 2040s high-change scenario (figs. 13*A*, 17*C*, 17*D*). Perhaps more importantly, flood depths are estimated to be 0.5 to 1.5 ft (0.15–0.45 m) lower in areas of Hovander Park and the western floodplain with alternative 3B (figs. 17*B*, 17*D*). Alternative 3B is projected to reduce the area of the western floodplain that is exposed to flooding under the 2080s mean-change scenario from 7 to 3 percent (figs. 13*A*, 17*E*, 17*F*) and, under the 2080s high-change scenario, from 59 to 52 percent (figs. 13*A*, 17*G*, 17*H*). Substantial areas exposed to flooding in the 2080s are computed to be 1 to 2 ft (0.3–0.6 m) shallower with alternative 3B than without it (figs. 13*A*, 17*F*, 17*H*). In terms of the severity of flooding, a greater benefit is computed with a 4 percent decrease in area of flood depth (>1 ft [0.3 m]) under the 2040s high-change scenario and a 13 percent reduction under the 2080s high-change scenario (fig. 13*A*; see also, appendix 1).

The additional influence of alternative 4C, which reconnects the lower western floodplain to the main-stem river, in combination with alternative 3B was computed to further reduce exposure of the western floodplain to the 10 percent AEP stream flood for the 2040s and 2080s high-change scenarios (figs. 13, 18). A benefit is also projected across the eastern floodplain upstream from Slater Road for a 10 percent AEP stream-flood event. The cumulative effects of alternatives 3B and 4C is projected to reduce flood area across the western floodplain from 33 percent without any projects to 8 percent for the 10 percent AEP flood under the 2040s high-change scenario (figs. 13*A*, 18*C*, 18*D*; see also, appendix 1). The associated decrease in computed flood depths range from 0.5 to 1.5 ft. The cumulative effects of alternatives 3B and 4C for the 10 percent AEP stream flood under the 2080s high-change scenario is estimated to reduce flood area across the western floodplain from 58 percent without any projects to 43 percent (figs. 18*G*, 18*H*). The western floodplain area, projected to sustain greater than 1 ft of flooding under the 2080s high-change scenario, is reduced from 42 to 24 percent by the cumulative effects of alternatives 3B and 4C (appendix 1).

The cumulative effects of alternatives 3B and 4C are computed to have additional benefits to reduce flood exposure of the western floodplain during 4 percent AEP stream floods (fig. 13; see also, appendix 1). Whereas this is, in part, associated with more flooding during the larger flows, alternatives 3B and 4C together are predicted to reduce the total area of flooding by 20 percent under existing conditions and 13 to 19 percent for projected changes in the 2040s and 2080s (fig. 13*E*; see also, appendix 1). The cumulative effects of alternatives 3B and 4C also are computed to reduce the area that is vulnerable to flooding with water depths of (1) more than 1 ft (0.3 m), by 27 percent under the 2080s mean-change scenario, (2) more than 3 ft (1.0 m), by 20 percent under both the 2040s high-change and 2080s mean-change scenarios, and (3) more than 6 ft (2.0 m), by 28 percent under the 2080s high-change scenario, thresholds that may be of particular concern for planning (appendix 1).

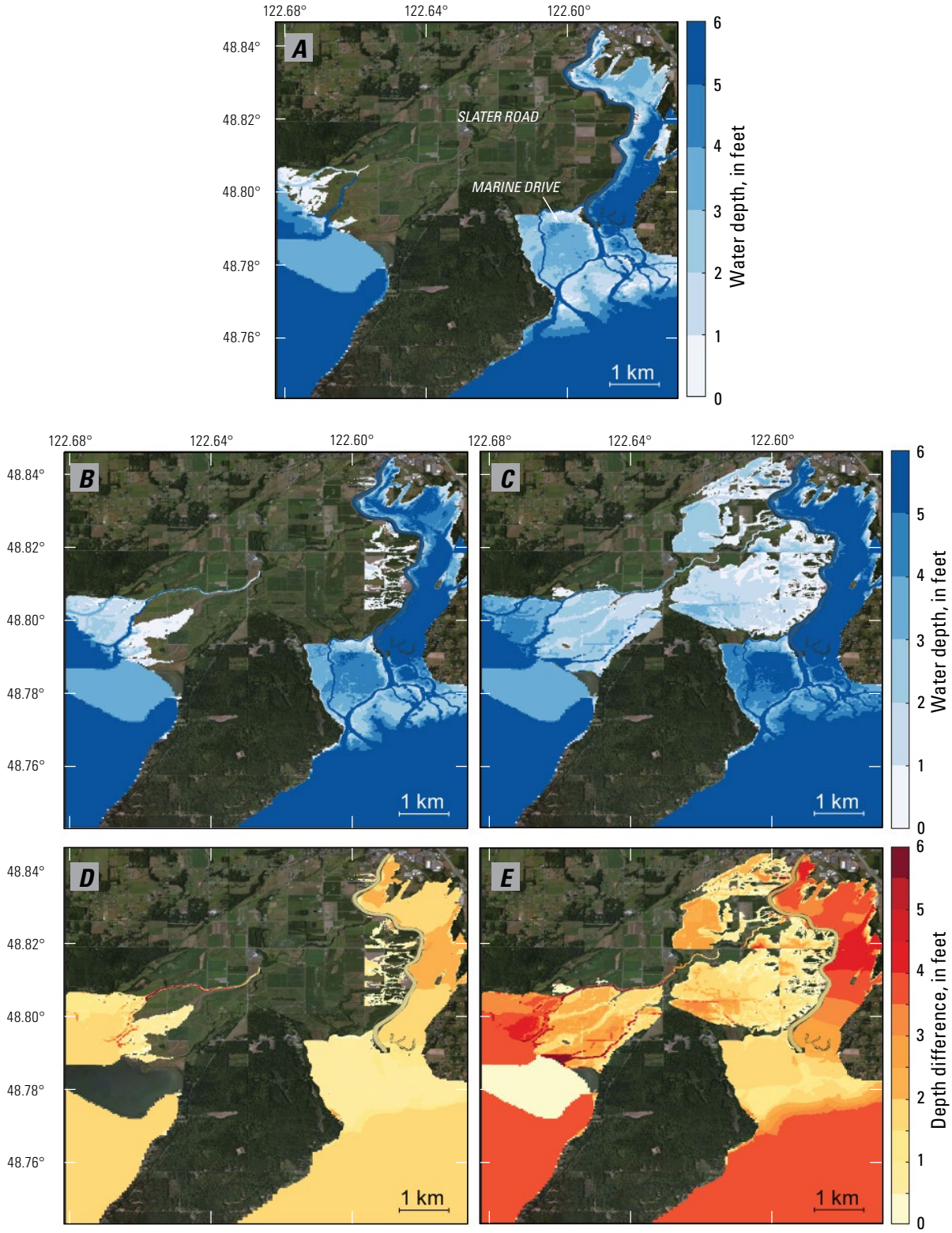


**Figure 15.** National Agricultural Imagery Program (NAIP) composite images showing modeled maximum flood depths and depth differences for 10 percent annual exceedance probability (AEP) stream-flood events. *A*, Existing water depths. *B*, Combined effect on water depths of modeled increases in stream discharge and sea-level rise for 2080s mean-change scenario. *C*, Combined effect on water depths of modeled increases in stream discharge and sea-level rise for 2080s high-change scenario. *D*, Differences in water depths shown in *B* relative to present day (2023). *E*, Differences in water depths shown in *C* relative to present day (2023). NAIP images from U.S. Department of Agriculture National Agricultural Imagery Program.

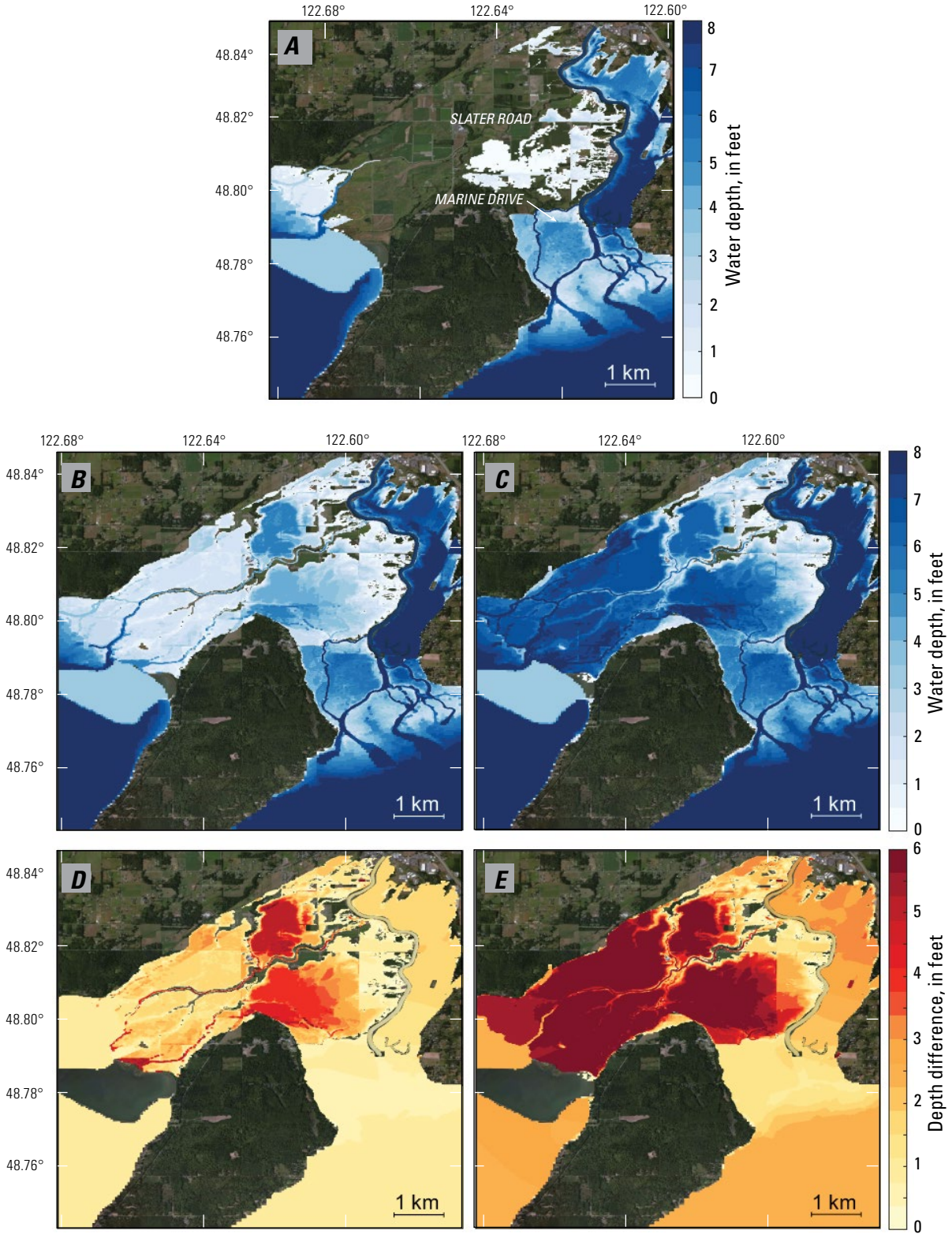


**Figure 16.** National Agricultural Imagery Program (NAIP) composite images showing modeled maximum flood depths and depth differences for 4 percent annual exceedance probability (AEP) stream-flood events. *A*, Existing water depths. *B*, Combined on water depths of modeled increases in stream discharge and sea-level rise for 2080s mean-change scenario. *C*, Combined effect on water depths of modeled increases in stream discharge and sea-level rise for 2080s high-change scenario. *D*, Differences in water depths shown in *B* relative to present day (2023). *E*, Differences in water depths shown in *C* relative to present day (2023). NAIP images from U.S. Department of Agriculture National Agricultural Imagery Program.

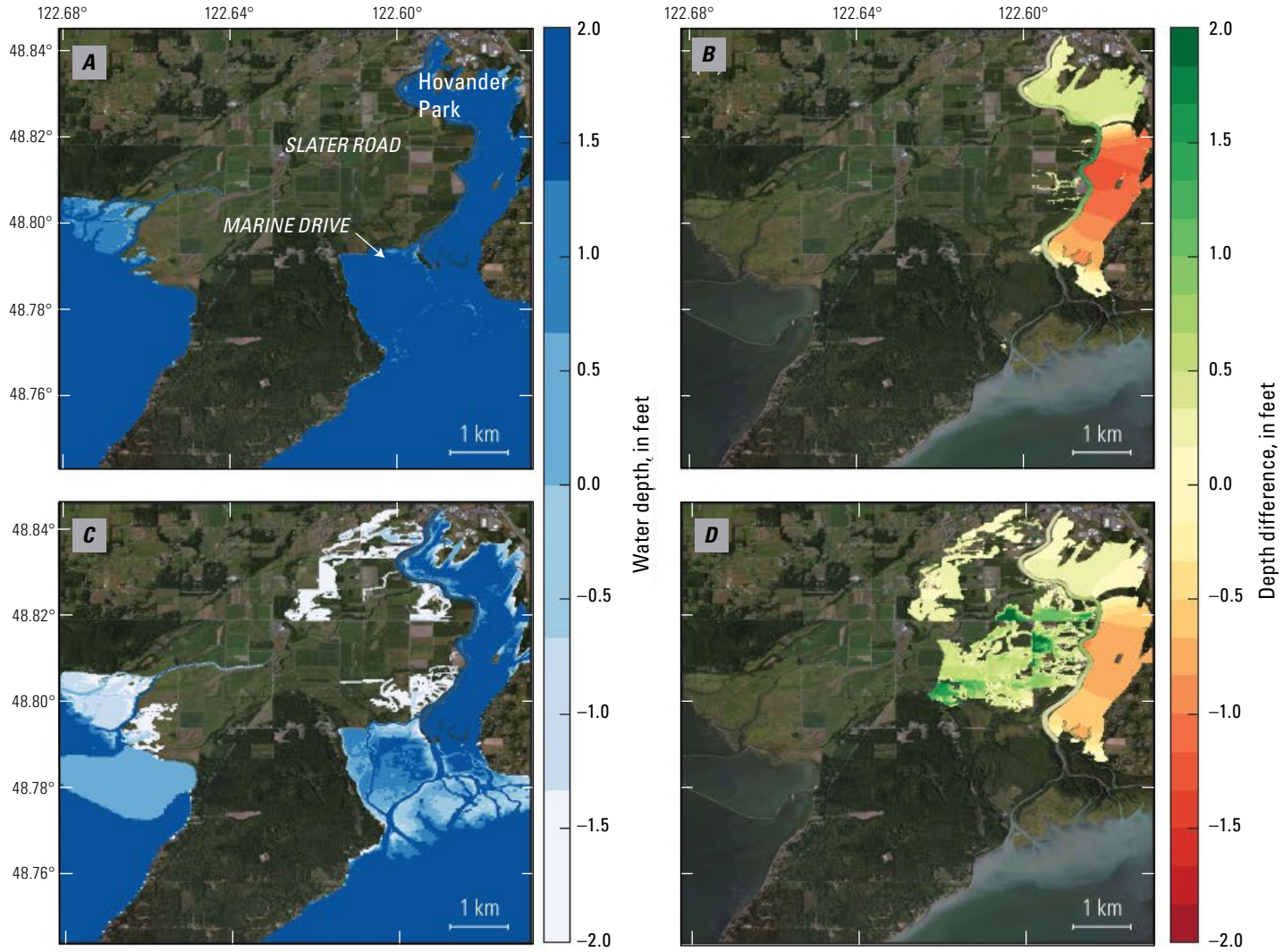


**Figure 17 (pages 26–27).** National Agricultural Imagery Program (NAIP) composite images showing modeled influences of alternative 3B on flood extents (as water depths) across lower Nooksack River during 10 percent annual exceedance probability (AEP) stream flood and differences in water depths from existing conditions. *A*, *B*, Flood extents (as water depths) and differences in water depths, respectively, for 2040s mean-change scenario. *C*, *D*, Flood extents (as water depths) and differences in water depths, respectively, for 2040s high-change scenario. *E*, *F*, Flood extents (as water depths) and differences in water depths, respectively, for 2080s mean-change scenario. *G*, *H*, Flood extents (as water depths) and differences in water depths, respectively, for 2080s high-change scenario. Note that green colors indicate benefit in reducing flood exposure. NAIP images from U.S. Department of Agriculture National Agricultural Imagery Program.

## Reduction in River Stage

The model indicates that the Lower Nooksack River Project alternatives 3B and 4C have beneficial effects in reducing the water-surface elevation (WSE) or river stage in the main-stem Nooksack River Reach 1 under current and future conditions. The model shows that rerouting flow through alternative 3B would reduce the WSE in the main-stem river during a 10 percent AEP stream flood (similar to the SBF) by as much as 1.9 ft (0.6 m) (figs. 19*A*, 19*B*). The greatest benefit to reducing flooding of the right-bank levee, which protects the western floodplain, is estimated across the middle of Reach 1 centered on the area about 500 ft (152 m) downstream from Slater Road (fig. 19*B*). Benefits of alternative 3B to reducing WSE extend as far upstream as the Ferndale Wastewater Treatment Plant and downstream past Marine Drive. The WSE during a 10 percent AEP stream flood is also projected to be lower and to reduce flood exposure in the 2040s and 2080s in response to alternative 3B. This benefit decreases steadily through time and is lower for the more extreme change scenarios; under the 2040s high-change scenario and both of the 2080s change scenarios, WSE exceeds the west-bank-levee elevations in several locations (figs. 19*C*–19*F*).

The model indicates that the addition of Lower Nooksack River Project alternative 4C in combination with 3B further

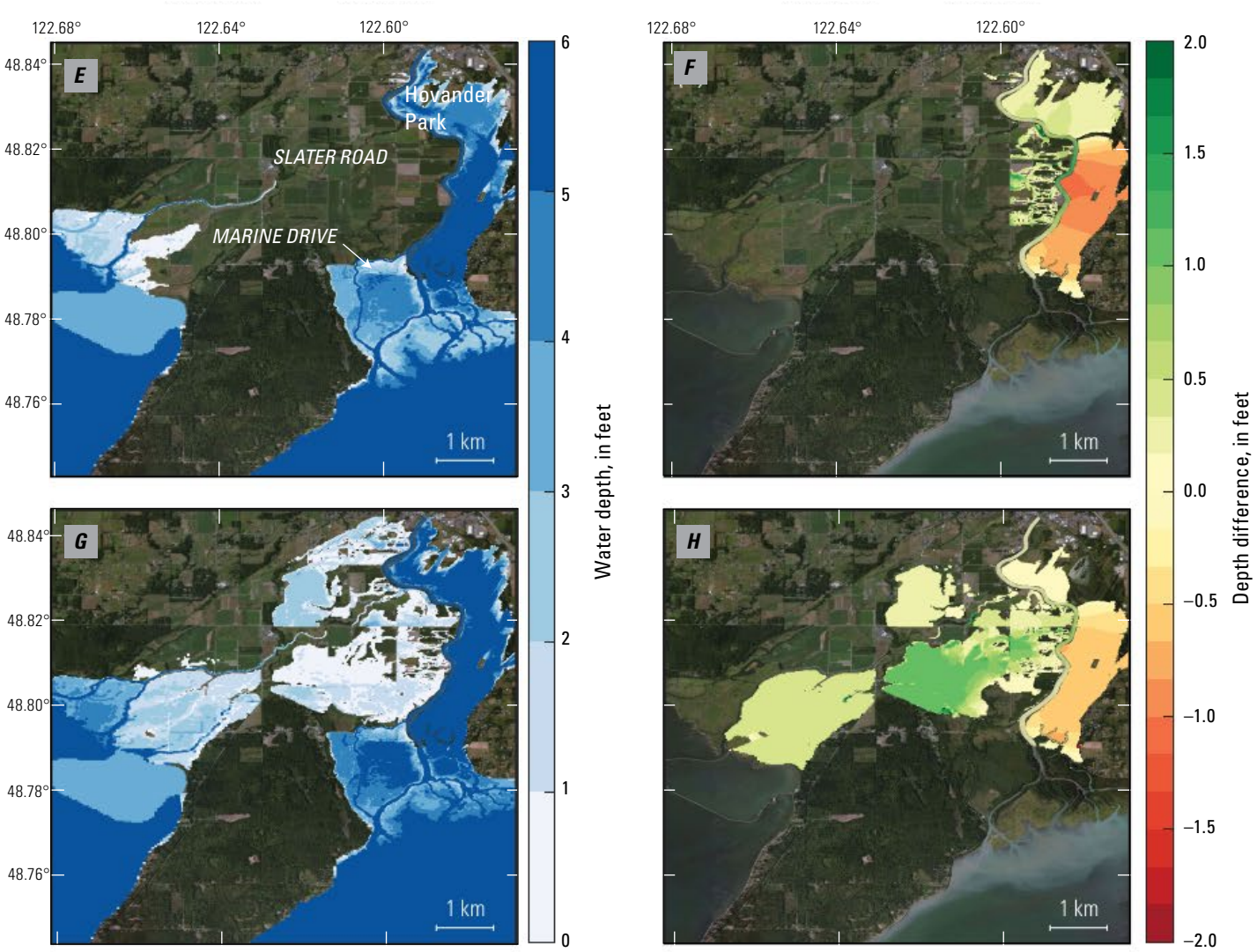


**Figure 17 (pages 26–27).**—Continued

reduces river stage in the main-stem Nooksack River Reach 1 during a 10 percent AEP stream-flood event under current and future conditions (figs. 20*A*, 20*B*). The cumulative benefits of both alternatives 3B and 4C are modeled to further reduce WSE during a 10 percent AEP flood such as the February 2020 SBF and, importantly, lower the flood stage both upstream to the Lummi River confluence and downstream beyond Marine Drive (fig. 20*B*). In this reach, alternative 4C is estimated to reduce WSE in the main-stem river an additional 0.5 to 1.0 ft beyond the benefits seen from alternative 3B. The cumulative benefits of alternatives 3B and 4C also extend into the 2040s and 2080s to reduce water levels projected under higher streamflows and sea level (figs. 20*C*–20*F*). Despite the fact that the west-bank levee is predicted to overtop under the 2040s mean-change scenario and both of the 2080s change scenarios, these model results indicate the potential that a set of additional alternatives may have positive cumulative effects in reducing flood stage and exposure more broadly across Reach 1.

## Changes in Sedimentation

Changes in potential sediment transport and accumulation in Nooksack River Reach 1 in response to modified hydrodynamics associated with projected climate change and the alternatives were assessed. A marked increase in sediment flux during a 10 percent AEP stream flood such as

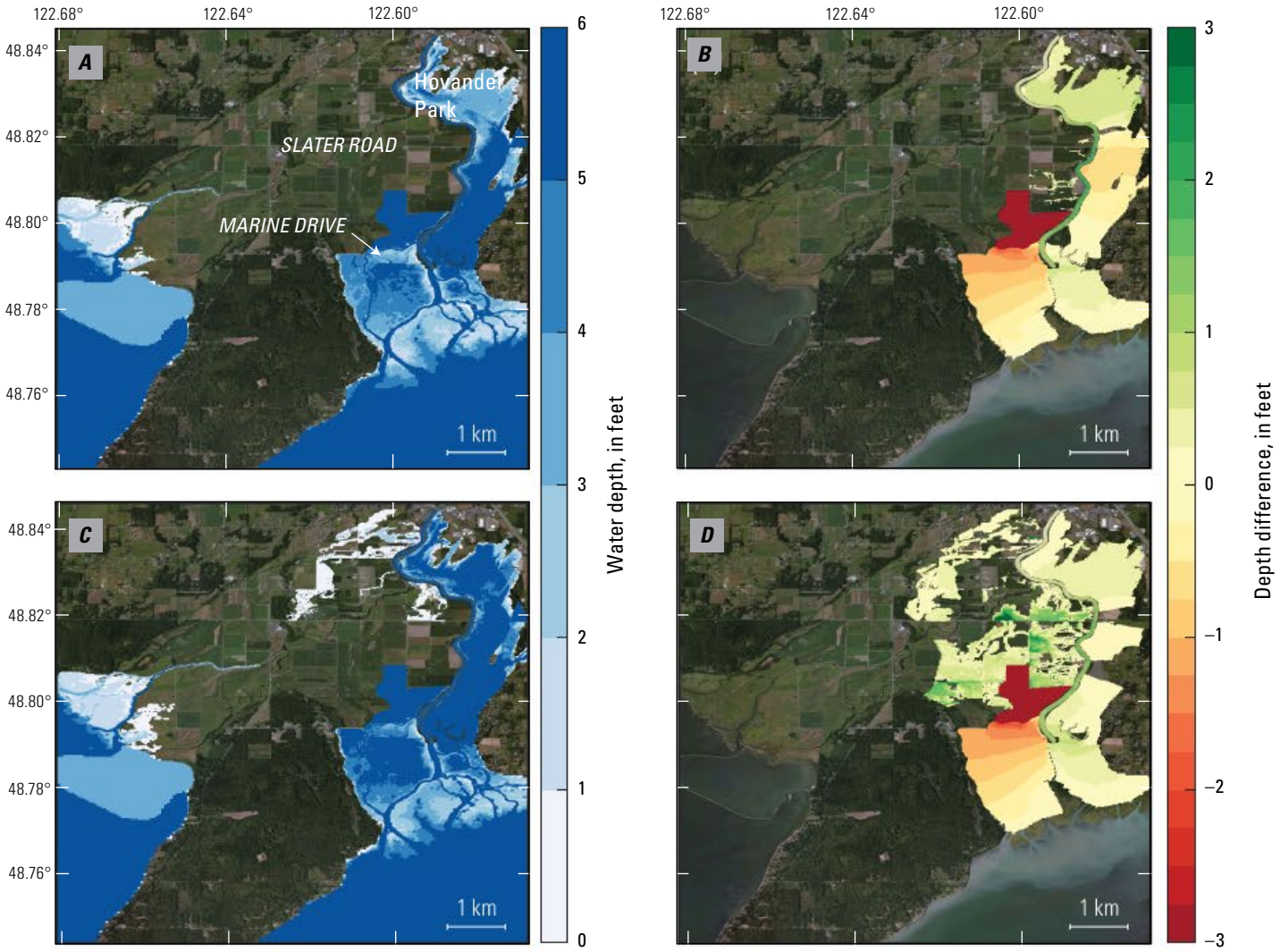


**Figure 18 (pages 28–29).** National Agricultural Imagery Program (NAIP) composite images showing modeled cumulative influences of combined alternatives 3B and 4C on flood extents (as water depths) across lower Nooksack River during 10 percent annual exceedance probability (AEP) stream flood and differences in water depths from existing conditions. *A*, *B*, Flood extents (as water depths) and differences in water depths, respectively, for 2040s mean-change scenario. *C*, *D*, Flood extents (as water depths) and differences in water depths, respectively, for 2040s high-change scenario. *E*, *F*, Flood extents (as water depths) and differences in water depths, respectively, for 2080s mean-change scenario. *G*, *H*, Flood extents (as water depths) and differences in water depths, respectively, for 2080s high-change scenario. Note that green colors indicate benefit in reducing flood exposure. NAIP images from U.S. Department of Agriculture National Agricultural Imagery Program.

the February 2020 SBF (fig. 21*A*) is computed for the 2040s (fig. 21*B*) and 2080s (fig. 21*C*) change scenarios; the increase is, in large part, due to the higher discharge that leads to systematically greater fluvial sediment transport (Curran and others, 2016). An increase in sediment flux across most of Reach 1 of 150 to 200 percent in the 2040s and 150 to 250 percent in the 2080s is consistent with the greater sediment delivery and transport expected with higher stream discharge driven by more precipitation as rain than snow and more intense rainfall (Mauger and others, 2015; Lee and others, 2016). Higher sea level in the 2040s and 2080s is expected to increasingly retard discharge and sediment flux through Reach 1. The extent of fluvial sediment that will be attenuated in Reach 1 is uncertain and remains a priority for resource- and flood-management decisions.

A general decrease in sediment flux during a 10 percent AEP stream flood such as the 2020 SBF (fig. 22*A*) was estimated downstream from alternative 3B in response to the individual effect of alternative 3B (fig. 22*B*) and the combined effects of alternatives 3B and 4C (fig. 22*C*). The decrease in

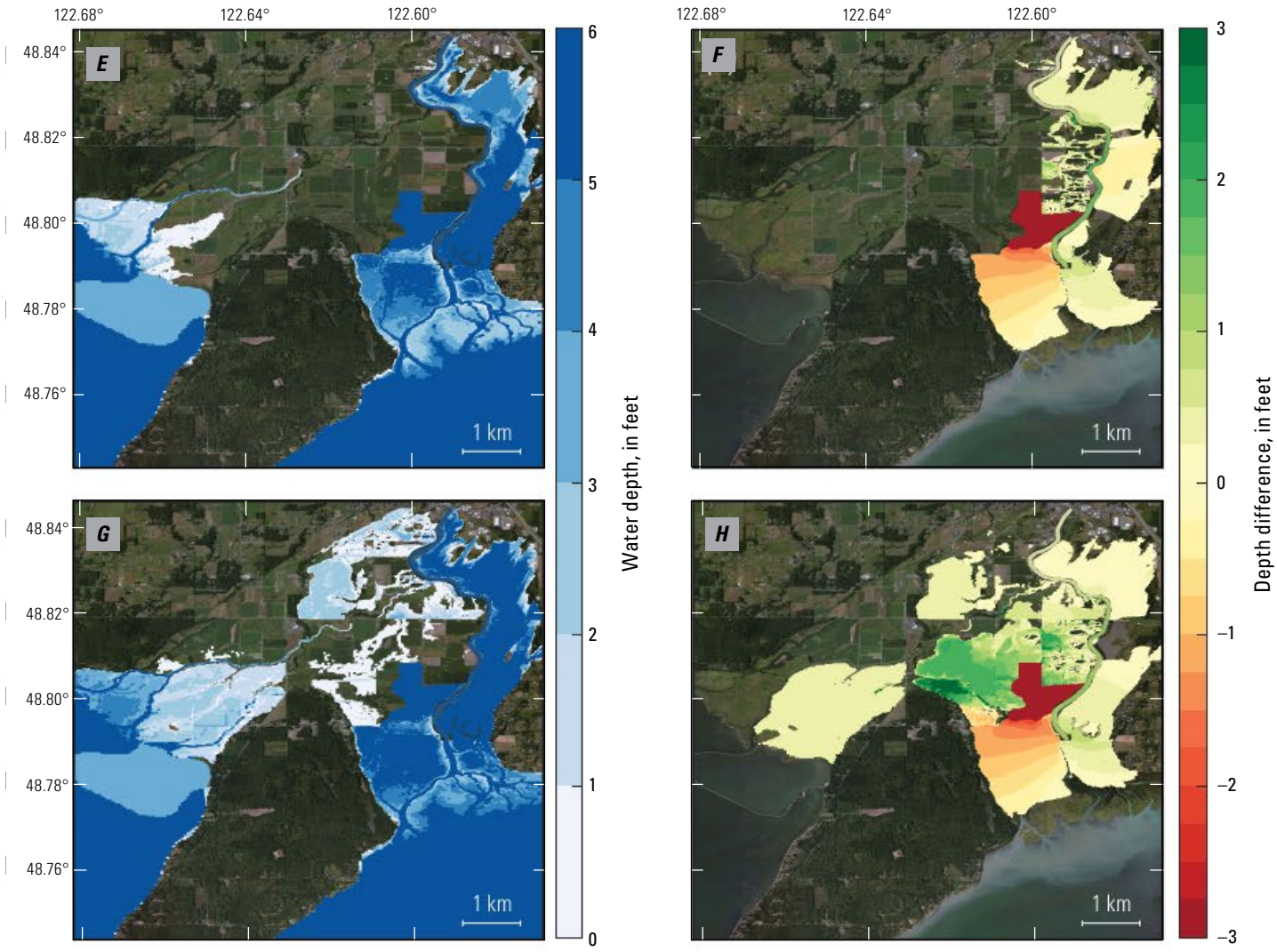


**Figure 18 (pages 28–29).**—Continued

sediment flux in the main-stem Nooksack River is consistent with reduced current velocities associated with the rerouting of floodwaters through alternatives 3B (fig. 22*B*) and 3B+4C (fig. 22*C*). The most pronounced reduction in sediment flux is computed immediately downstream from the Slater Road crossing and alternative 3B connection to the main stem (white arrows in figures 22*B* and 22*C*). Areas where the gradient in sediment flux decreases strongly and (or) abruptly, owing to reduced hydrodynamic forcing, are susceptible to sedimentation. Modeled changes in sediment flux for the 10 percent AEP stream flood under projected 2040s and 2080s change scenarios with alternatives 3B and 4C (not shown) reveal the same pattern as in figure 22 and simply scale with higher sediment delivery to, and flux through, the Nooksack River Reach 1, and they indicate the potential for attenuation owing to higher streamflow and sea level shown in figure 21. We caution that these simulations account only for the expected influence of changes in hydrodynamics on the total sediment flux and not for time-varying changes in sediment delivery or morphological responses of the bed.

The approach used here to estimate potential changes in sediment flux and sedimentation, assuming existing conditions of sediment conveyance through Reach 1, is generally in equilibrium with the channelized hydrodynamics and helps inform how the system will respond to perturbations in conveyance associated with each change scenario. The approach was employed here to identify if sedimentation should be a concern for the future and for restoration outcomes and, if so, where to focus additional sediment-transport-modeling efforts. The relatively high potential for sedimentation in Reach 1 suggests that a sediment-transport model capable of simulating morphologic adjustment (which

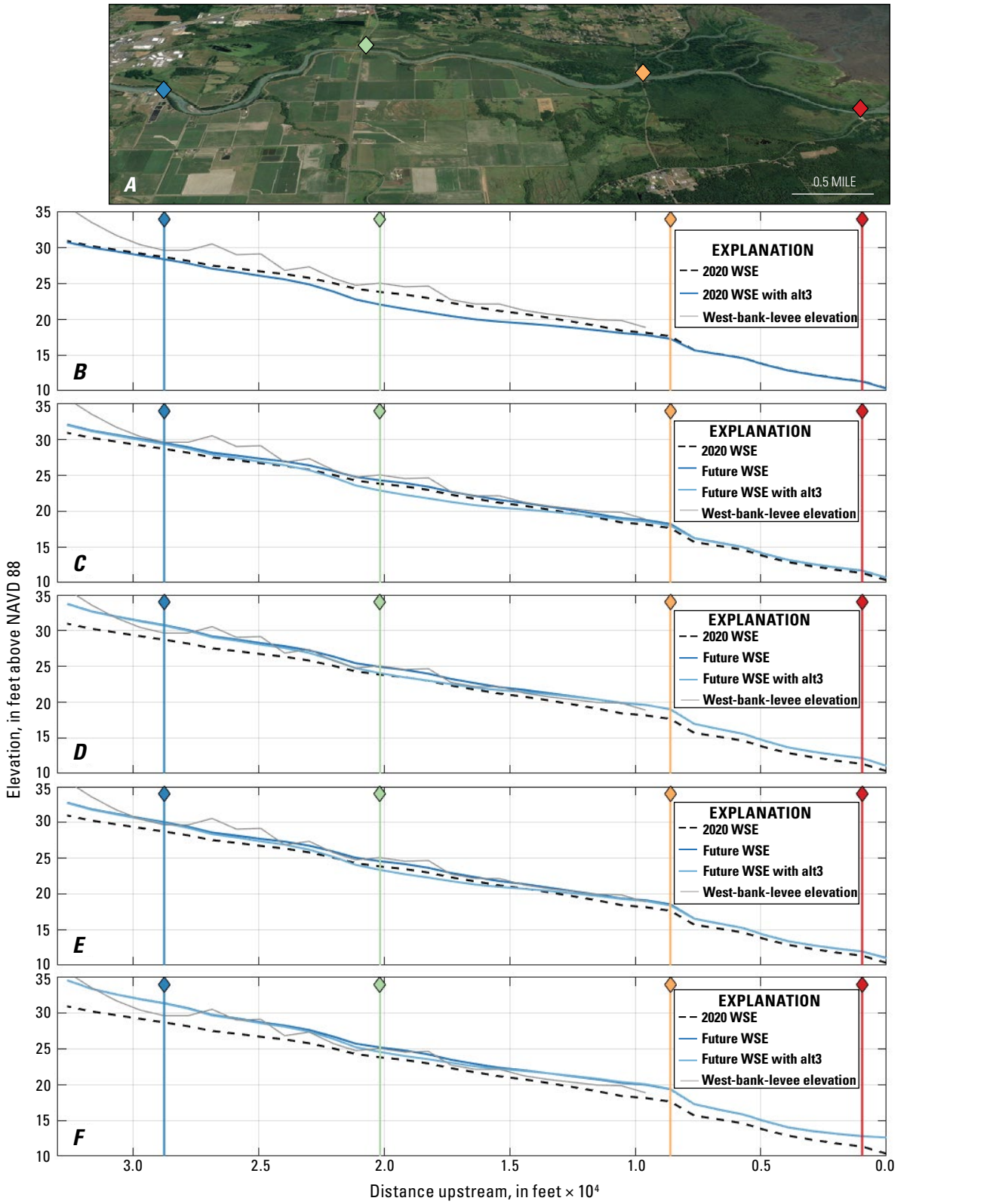


**Figure 19.** *A*, Oblique-view National Agricultural Imagery Program (NAIP) composite image showing locations of validation sites (colored diamonds): blue, Ferndale Wastewater Treatment Plant; green, Slater Road; orange, Marine Drive; red, Nooksack River delta. NAIP image from U.S. Department of Agriculture National Agricultural Imagery Program. *B*–*F*, Plots showing 2020 maximum water-surface elevation (WSE) (dashed black line) across Nooksack River Reach 1 and influence of alternative 3B (alt3B) on WSE with respect to west-bank-levee elevation (gray line) during 10 percent annual exceedance probability (AEP) stream flood, under (*B*) existing conditions and under future (*C*) 2040s mean-change, (*D*) 2040s high-change, (*E*) 2080s mean-change, (*F*) and 2080s high-change scenarios. Colored diamonds showing validation sites plotted for reference. NAVD 88, North American Vertical Datum of 1988.

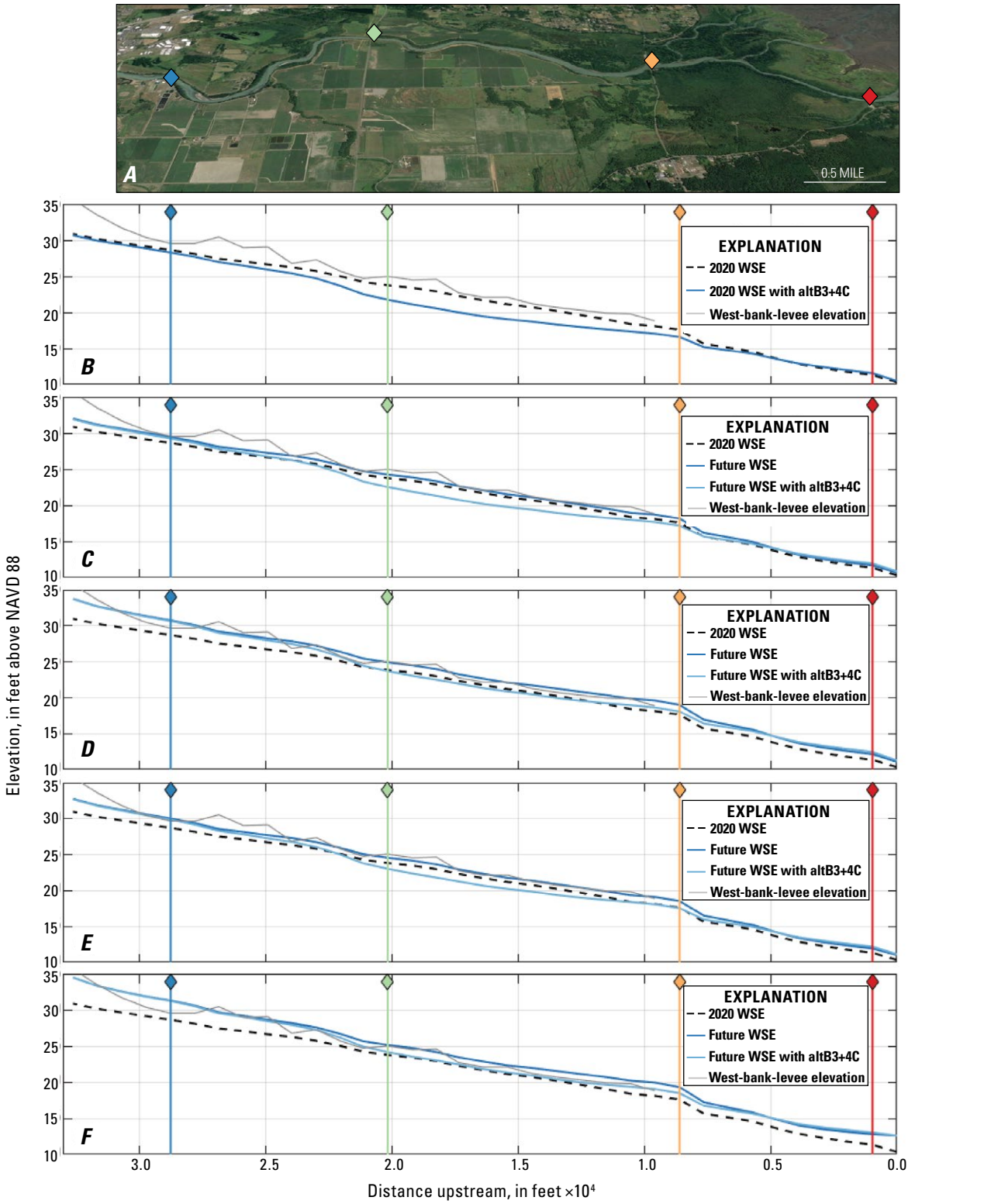


**Figure 20.** *A*, Oblique-view National Agricultural Imagery Program (NAIP) composite image showing locations of validation sites (colored diamonds): blue, Ferndale Wastewater Treatment Plant; green, Slater Road; orange, Marine Drive; red, Nooksack River delta. NAIP image from U.S. Department of Agriculture National Agricultural Imagery Program. *B*–*F*, Plots showing 2020 maximum water-surface elevation (WSE) (dashed black line) across Nooksack River Reach 1 and combined influences of alternatives 3B and 4C (alt3B+4C) on WSE with respect to west-bank-levee elevation (gray line) during 10 percent annual exceedance probability (AEP) stream flood, under (*B*) existing conditions, (*C*) 2040s mean-change, (*D*) 2040s high-change, (*E*) 2080s mean-change, and (*F*) 2080s high-change scenarios. Colored diamonds showing validation sites are plotted for reference. NAVD 88, North American Vertical Datum of 1988.

is outside the scope of this study) would further inform the expected cumulative changes in the absolute amount of transport, sedimentation, and bed changes with future flow conditions and identified mitigation alternatives. Such a model should account for the range of annual fluvial and estuarine sediment transport processes that occur and the particle sizes and transport properties of sediment in the system (see, for example, Grossman and others, 2022).

## Concerns with Long-Term Bed Aggradation

### Flood Extent

The potential effects of widespread, decadal-scale channel sedimentation (Anderson and others, 2019) to flood exposure were evaluated for the existing and future change scenarios, with and without the identified restoration

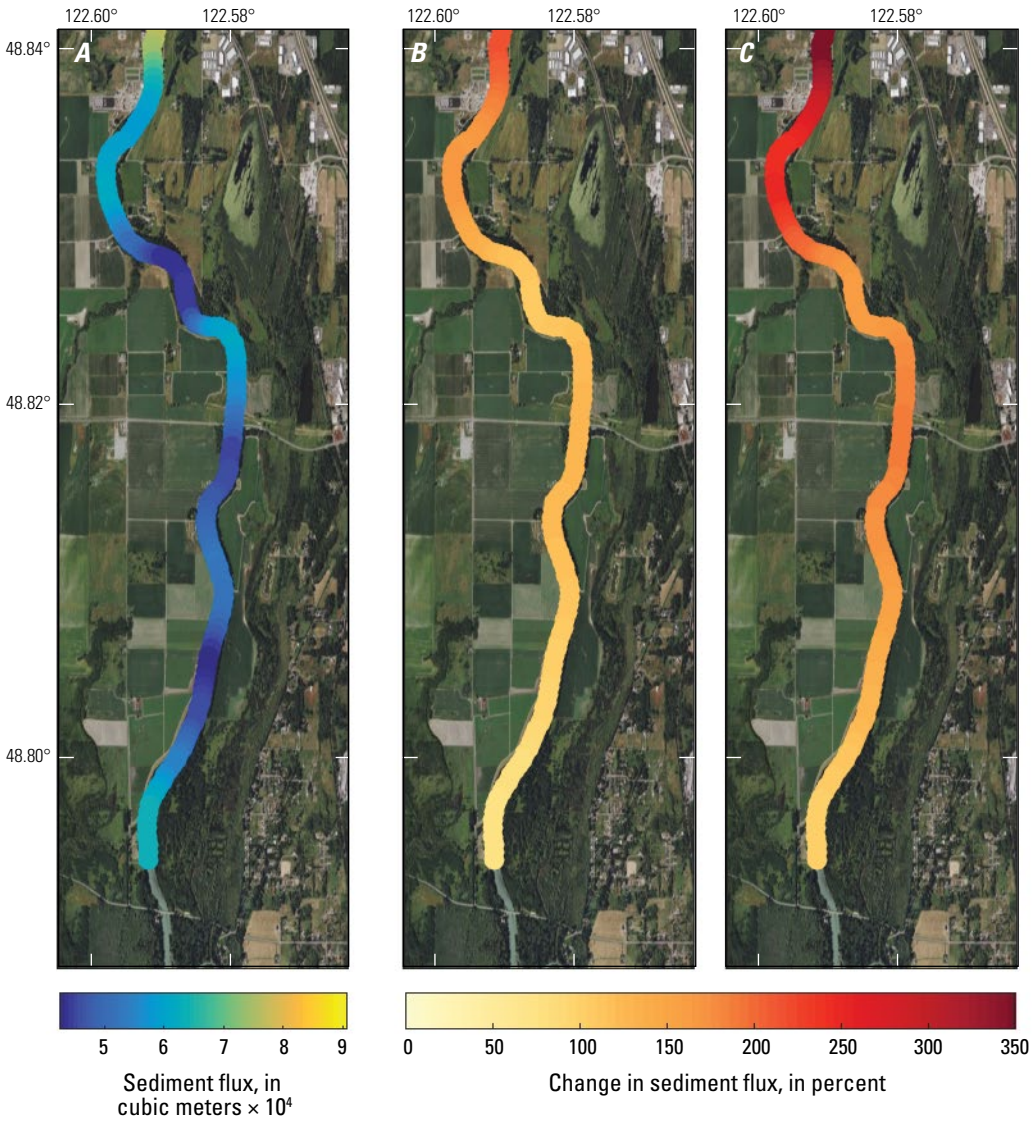


**Figure 21.** National Agricultural Imagery Program (NAIP) composite images showing (*A*) modeled sediment flux across Nooksack River Reach 1 during 10 percent annual exceedance probability (AEP) February 2020 Super Bowl flood and (*B*, *C*) computed change in sediment flux associated with (*B*) 2040s and (*C*) 2080s high-change scenarios, indicating potential for higher sediment delivery to, and flux through, study area. NAIP images from U.S. Department of Agriculture National Agricultural Imagery Program.

alternatives. Generally, the model indicates that a 3.3 ft (1.0 m) elevated bed in modeled subreaches R1-1 and R1-2 between Ferndale and Slater Road would have little effect on the 10 percent AEP stream flood (figs. 23*B*, 23*C*). However, a similar amount of aggradation in subreach R1-3 (between Slater Road and Marine Drive) and across subreach R1-4, which spans the entire main-stem Nooksack River Reach 1, is computed to cause greater flooding, including in the western floodplain (figs. 23*D*, 23*E*). A lower amount of western floodplain exposure and greater modeled flood depths over the eastern floodplain, with sedimentation in the upper rather than the lower part of Reach 1, is consistent with reduced flow conveyance near Ferndale, routing more floodwater across Hovander Park and the eastern floodplain. These areas are designed to accommodate floodwaters to reduce flood stage lower in the main-stem river. The fact that the model indicates greater flooding of the western floodplain, with aggradation of the bed in the lower subreach R1-3 (fig. 23*D*) rather than across the entire Reach 1 (fig. 23*E*), is consistent with a greater relative role of a 3.3 ft (1.0 m) bed shallowing on river flow conveyance where river flow is constrained by tides and sea-level position. More importantly, aggradation of subreach

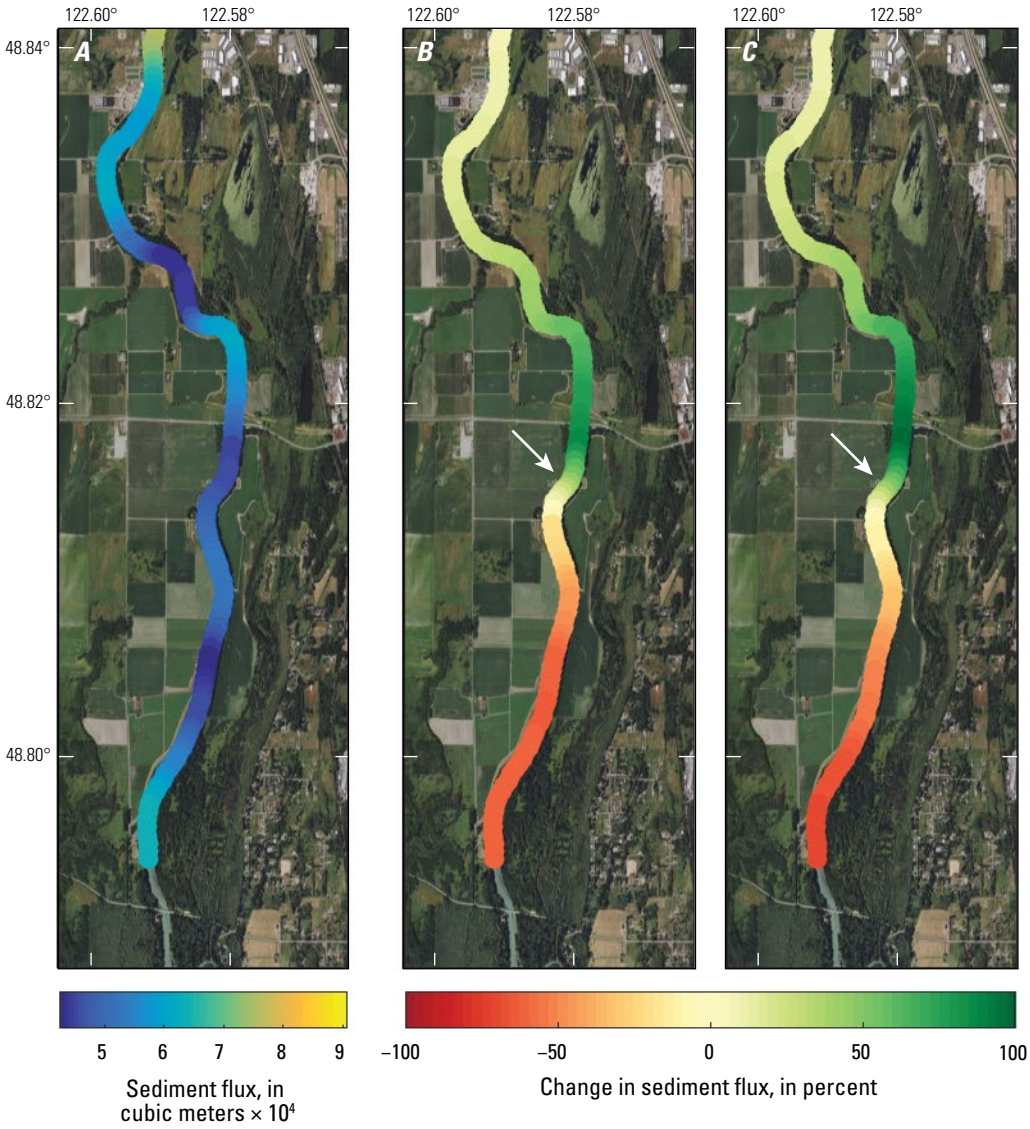


**Figure 22.** National Agricultural Imagery Program (NAIP) composite images showing (*A*) modeled sediment flux across Nooksack River Reach 1 during 10 percent annual exceedance probability (AEP) February 2020 Super Bowl flood and (*B*, *C*) computed change in sediment flux associated with (*B*) alternative 3B and (*C*) combined influences of alternatives 3B and 4C, indicating potential for sedimentation where flux decreases (locations shown by white arrows). NAIP images from U.S. Department of Agriculture National Agricultural Imagery Program.

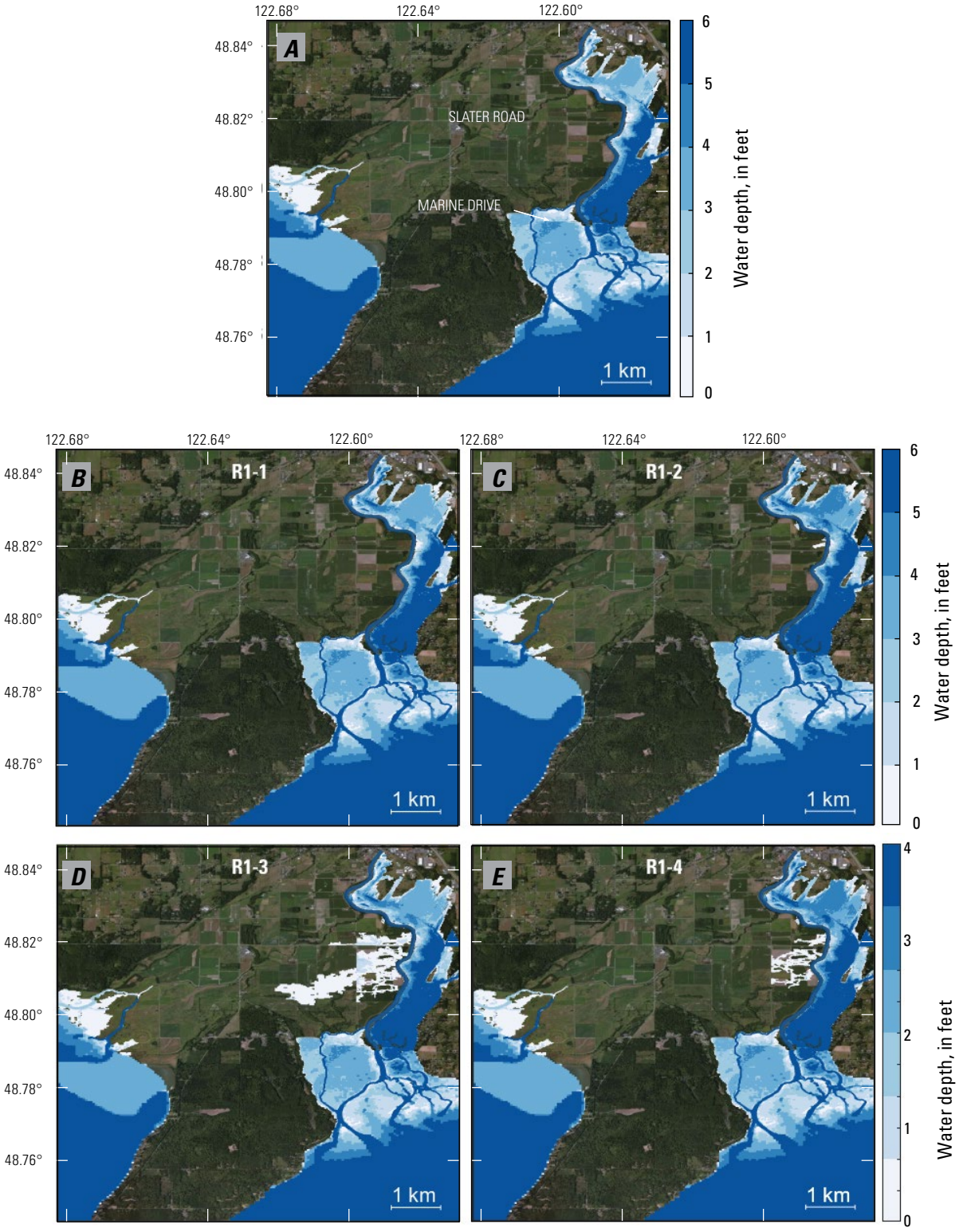


**Figure 23.** National Agricultural Imagery Program (NAIP) composite images showing modeled flood extents during 10 percent annual exceedance probability (AEP) stream flood, under (*A*) existing conditions and (*B–E*) with 3.3 feet (1.0 meter) of bed aggradation across Nooksack River subreaches (*B*) R1-1, (*C*) R1-2, (*D*) R1-3, and (*E*) R1-4 (which spans entire Nooksack River Reach 1). Extents of subreaches are shown in figure 4. NAIP images from U.S. Department of Agriculture National Agricultural Imagery Program.

R1-3 is projected to transform flooding of the western floodplain under a 10 percent AEP stream-flood event so that it is comparable to a 4 percent AEP stream-flood event such as the January 2009 flood (fig. 14*A*).

The additional sensitivity and exposure of the western floodplain to higher compound flooding under the 2040s and 2080s change scenarios was also evaluated with bed aggradation across the lower parts of subreaches R1-1 through R1-3 and the entire Reach 1. Modeled flooding of the western floodplain during a 10 percent AEP stream-flood event under the 2040s and 2080s mean-change scenarios was found to be much greater with the 3.3 ft (1.0 m) bed aggradation than without it (figs. 24*A*–24*D*), and it was also greater with aggradation lower in the system than with it across the entire Reach 1 (figs. 24*E*–24*H*). The greater influence of bed aggradation on 2040s and 2080s flood events of the western floodplain suggests that, in general, bed aggradation of the 3.3 ft (1.0 m) magnitude is more influential on flooding during higher flows when river stage is closer to or within flooding of the top of the levees. The greater amount of flooding of the western floodplain that is predicted with bed aggradation in only the lower parts of Reach 1 (for example, R1-3) rather than across the entire Reach 1 is consistent with greater flow being directed across the eastern floodplain in response to an elevated bed higher in the system, which would reduce flood stage lower in the main-stem channel (figs. 24*G*, 24*H*).

Modeled flooding of the western floodplain during a 4 percent AEP stream-flood event was found to be much more extensive with the 3.3 ft (1.0 m) of bed aggradation than without it (fig. 25), and it exposed the entire western floodplain to flooding in all future change scenarios, including the 2040s mean-change scenario, which showed only partial flooding under existing conditions (fig. 14*B*). Along with the entire western floodplain being affected, extreme flood depths that reach 3 to 4 ft in the 2040s change scenarios (figs. 25*A*–25*D*) and 5 to 6 ft in the 2080s change scenarios (figs. 25*E*–25*H*) were computed. Flooding during a 4 percent AEP stream flood is predicted to be equally as severe, or more severe, with bed aggradation across the entire Reach 1 (figs. 25*F*, 25*H*) rather than just subreach R1-3 (figs. 25*B*, 25*D*), unlike a 10 percent AEP flood, presumably because the difference between the 4 percent AEP stream-flood stage and the right-bank-levee elevation is generally less than the 3.3 ft (1.0 m) of the simulated bed increase. Improved understanding of the influence of sedimentation on this difference and ultimately the channel-flood conveyance is especially important in coastal settings such as Reach 1 of the Nooksack River, where these model results show that it will interact with, and be highly sensitive to, sea level, tides, and storm surge in complex ways.

### Effects of Alternatives

Modeled individual and cumulative effects of alternatives 3B and 4C, which are shown to reduce flood exposure projected in the 2040s and 2080s change scenarios (figs. 13, 17, 18, 19, 20), also have capacity to reduce additional flooding associated with potential bed aggradation (fig. 26; see also, appendix 1). Whereas 3.3 ft (1 m) of modeled bed aggradation caused flooding of the western floodplain under a 10 percent AEP stream-flood event, comparable to a 4 percent AEP stream-flood event (fig. 24), alternatives 3B and 4C had the effect of substantially reducing flood exposure across the western floodplain under a 10 percent AEP stream-flood event into the 2040s and 2080s (fig 26). The total area of the western floodplain that would be subject to flooding was computed to be 6.6 percent lower with the alternatives than without them when accounting for 3.3 ft of bed aggradation under existing conditions, as well as 20 to 27 percent in the 2040s change scenarios and 14 to 26 percent in the 2080s change scenarios (figs. 26, 27; see also, appendix 1). Areas that would be subject to more than 1 ft (0.3 m) of flood depth were reduced by 12 percent under the 2080s mean-change scenario (figs. 26*G*, 26*H*, 27; see also, appendix 1) and as much as 20 and 24 percent under the 2040s and 2080s high-change scenarios, respectively (appendix 1). These results show that potentially important opportunities to mitigate flood exposure associated with uncertain changes in sea-level position, storm surge, streamflow, and sedimentation exist. The results also suggest that the identified alternatives and the addition of others may provide cumulative benefits to help counter growing flood exposure. The model herein also provides a unique capacity to evaluate important metrics such as the severity of flood exposure in terms of specific depth thresholds of disturbance (for example, areas flooded more than 3 ft deep) to inform where and when in the future risk tolerance for specific land uses or community concerns may be exceeded.

## Direct Effects of Sea-Level Rise

### Tidal Effects on Extreme Water Levels and Stream Flooding

Inundation by tides and sea-level rise is constrained by the magnitude of stream discharge, as lower streamflows allow tidal waters to penetrate higher into the system. The modeling herein shows, for the first time, the extent to which sea-level rise will influence the Nooksack River Reach 1 spatially under varying levels of streamflows. Modeled effects of sea-level rise on the 50 percent AEP, 10 percent AEP, and 4 percent AEP streamflows indicate that Reach 1, the western floodplain, and the coastal plain along Lummi Bay will become systematically more vulnerable to flooding as sea-level rise progresses (fig. 28). Whereas a sea-level rise amount of 1.6 ft (0.5 m) that is associated with high risk by the 2060s or average risk by the 2090s (amounts are based on work by Miller and others [2018]) showed little influence on flood extent under the 50 percent AEP stream-flood event (fig. 28*A*), the sea-level rise of 3.3 ft (1.0 m) that is anticipated to occur between 2080 and 2100 is expected to lead to notably greater flooding of the western floodplain (fig. 29*B*). Under both scenarios, coastal flood extent reached across the Lummi Bay coastal plain to Haxton Road (see fig. 1 for location), a critical arterial

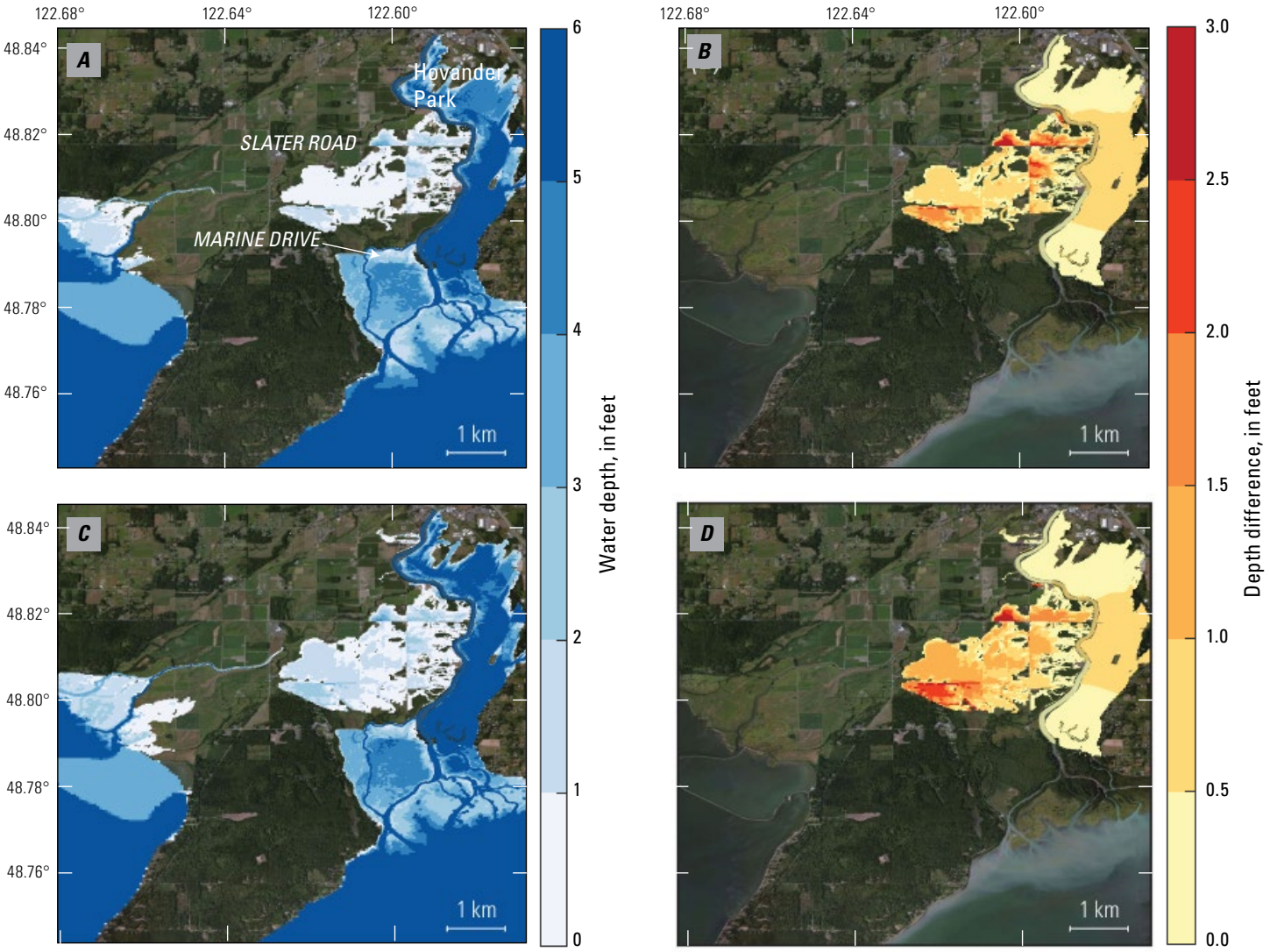


**Figure 24 (pages 36–37).** National Agricultural Imagery Program (NAIP) composite images showing modeled effects on flood extents (as water depths) and differences in water depths from existing conditions during 10 percent annual exceedance probability (AEP) stream flood. *A–D*, Flood extents (as water depths) and differences in water depths, respectively, with 3.3 feet (ft) (1.0 meter [m]) bed aggradation in lower part of Nooksack River Reach 1 for 2040s (*A*, *B*) and 2080s (*C*, *D*) mean-change scenarios. *E–H*, Flood extents (as water depths) and differences in water depths, respectively, with same bed aggradation as in *A–D* (3.3 ft [1.0 m]) across entire Nooksack River Reach 1 for 2040s (*E*, *F*) and 2080s (*G*, *H*) mean-change scenarios. NAIP images from U.S. Department of Agriculture National Agricultural Imagery Program.

accessway to the Lummi Reservation (figs. 28*A*, 28*B*). Under the 10 percent AEP stream-flood event with 1.6 ft of sea-level rise, flood extent and depth across the western floodplain are projected to increase only slightly above the 50 percent AEP streamflow effects, driven almost entirely by coastal flooding; flood depths across the eastern floodplain increase greatly (figure 28*C*). Sea-level rise of 3.3 ft and the 10 percent AEP stream flood have a much greater influence on flooding of the western floodplain, with flood extent reaching Slater Road west of Haxton Road, as well as east of, and presumably over, Haxton Road (fig. 28*D*). Flood exposure during a 4 percent AEP stream flood is greatly exacerbated by 1.6 ft of sea-level rise (fig. 28*E*) and 3.3 ft of sea-level rise (fig. 28*F*), with connected floodwaters over extensive areas of the western floodplain computed to reach 3 to 4 ft depths and, over the eastern floodplain, as deep as 7 to 8 ft.

Whereas maps of changing flood exposure owing to sea-level rise (fig. 28) help visualize the broader spatial and discrete locations of effects anticipated in the coming decades, modeled water-surface-elevation changes along the main-stem

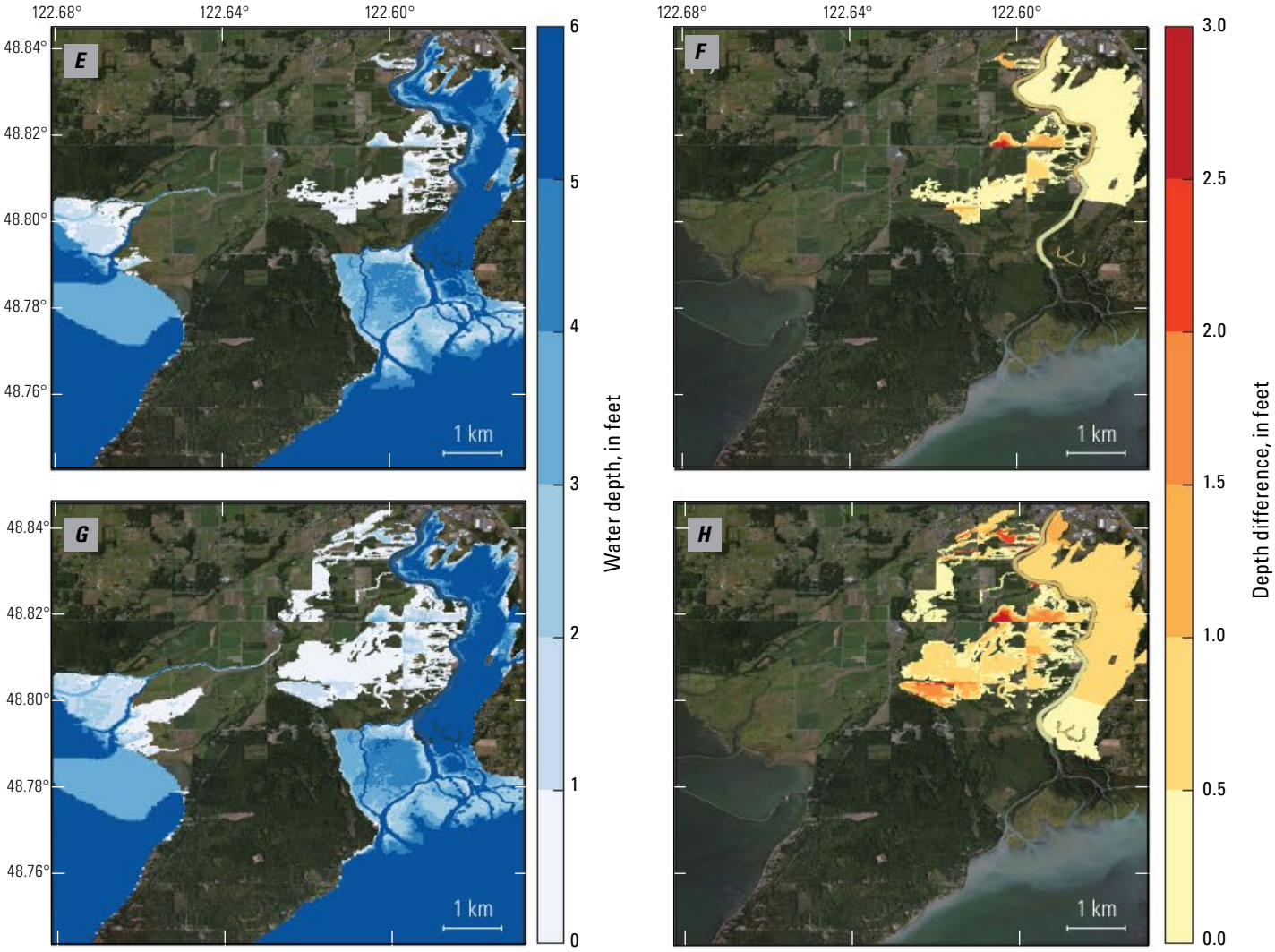


**Figure 24 (pages 36–37).**—Continued

river provide tools to identify opportunities for enhancing resilience and managing flow paths of floodwaters (fig. 29). Although sea-level rise through 2100 is not expected to cause the 50 percent AEP streamflow to flood the western floodplain, it is projected to push the boundary that tidal oscillations affect under 50 percent AEP water levels today (2023) from near the delta to upstream from Marine Drive and near Slater Road, depending on the rate of sea-level rise (fig. 29*A*). Daily tidal oscillations are computed to migrate to and upstream from Marine Drive by 2100 under today's (2023) 10 percent AEP streamflow (fig. 29*B*) and 4 percent AEP streamflow (fig. 29*C*). River stage under these 10 and 4 percent AEP streamflows is predicted to exceed the west-bank levee in several locations.

In addition to rising stream-flood exposure associated with sea-level rise, the upstream migrations of tidal backwatering and tidal oscillations are expected to increasingly affect groundwater and drainage processes. This is important in many Pacific Northwest estuaries and particularly for salmon habitat suitability and spring crop preparation in Nooksack River Reach 1 between Marine Drive and Ferndale. Modeled upstream tidal propagation of 0.5 to 1.0 mi for every foot of sea-level rise under 50 percent AEP streamflows (fig. 29*A*) represents a minimum migration distance for lower flows characteristic of March–May crop preparation when monthly mean flows range from 3,800 to 4,600 $ft^3/s$ (108–130 $m^3/s$). The higher water levels, and also their more frequent occurrence relative to today (2023) along

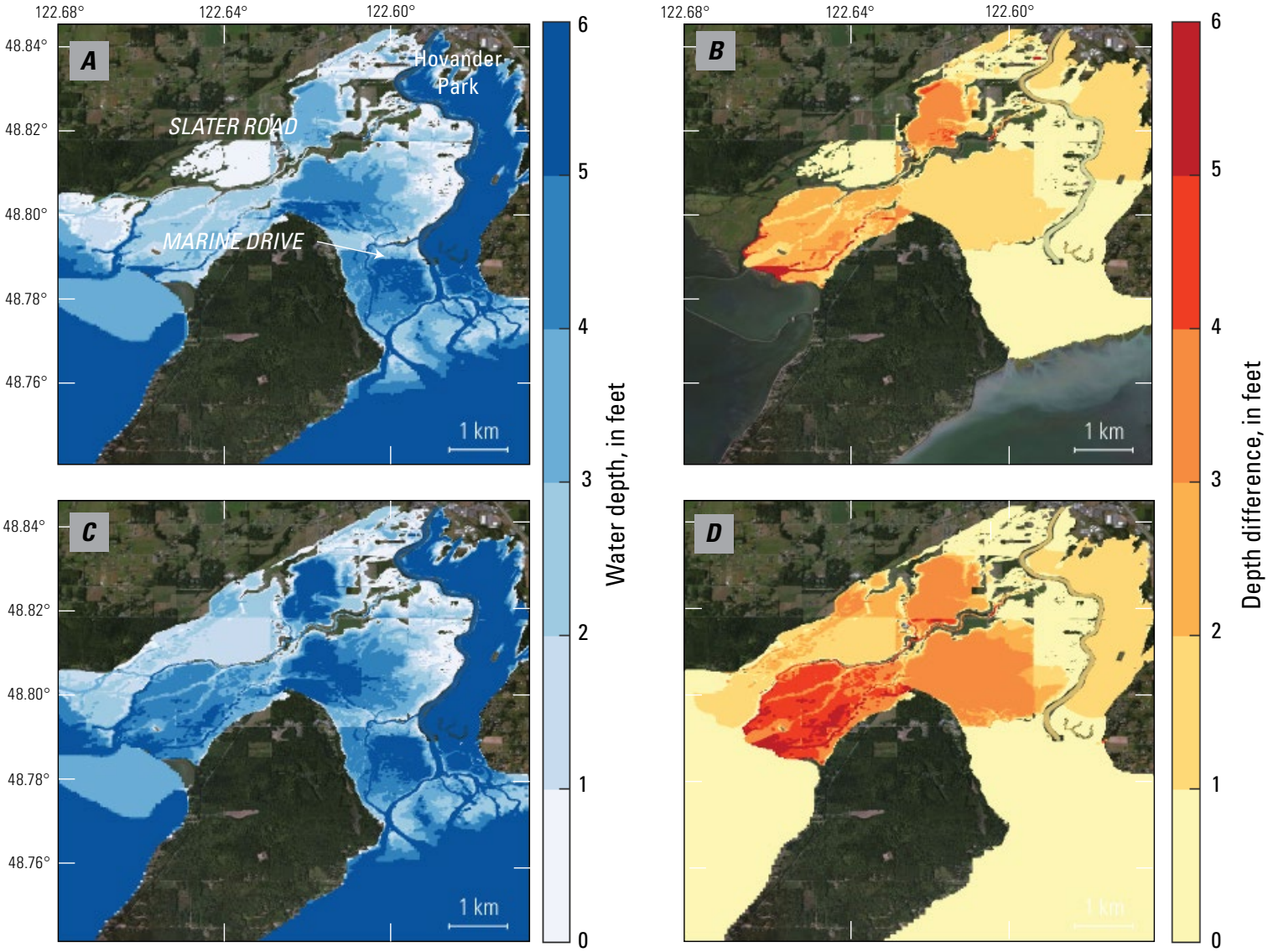


**Figure 25 (pages 38–39).** National Agricultural Imagery Program (NAIP) composite images showing modeled effects on flood extents (as water depths) and differences in water depths from existing conditions during 4 percent annual exceedance probability (AEP) stream flood. *A*–*D*, Flood extents (as water depths) and differences in water depths, respectively, with 3.3 feet (ft) (1.0 m) bed aggradation in lower part of Nooksack River Reach 1 for 2040s (*A*, *B*) and 2080s (*C*, *D*) mean-change scenarios. *E*–*H*, Flood extents (as water depths) and differences in water depths, respectively, with same bed aggradation as in *A*–*D* (3.3 ft [1 m]) across entire Nooksack River Reach 1 for 2040s (*E*, *F*) and 2080s (*G*, *H*) mean-change scenarios. NAIP images from U.S. Department of Agriculture National Agricultural Imagery Program.

Nooksack River Reach 1, are expected to reduce the efficacy of gravity-fed drainage efforts (Grossman and others, 2020) and exacerbate runoff associated with more intense rainfall not yet accounted for in the model. Lastly, the effects of more frequent high tides on backwatering streamflow and promoting sedimentation is expected to be a positive feedback to retard drainage, particularly when the channel bed elevation exceeds that of the subsided land elevation behind the levees.

## Summary

A hydrodynamic model constructed using Delft3D Flexible Mesh shows that the exposure of the lower Nooksack River and delta to compound flooding from the higher projected sea level and amount of stream runoff in the coming decades will increase substantially, and reach potential tipping points for community and ecosystem resilience. The model was used to

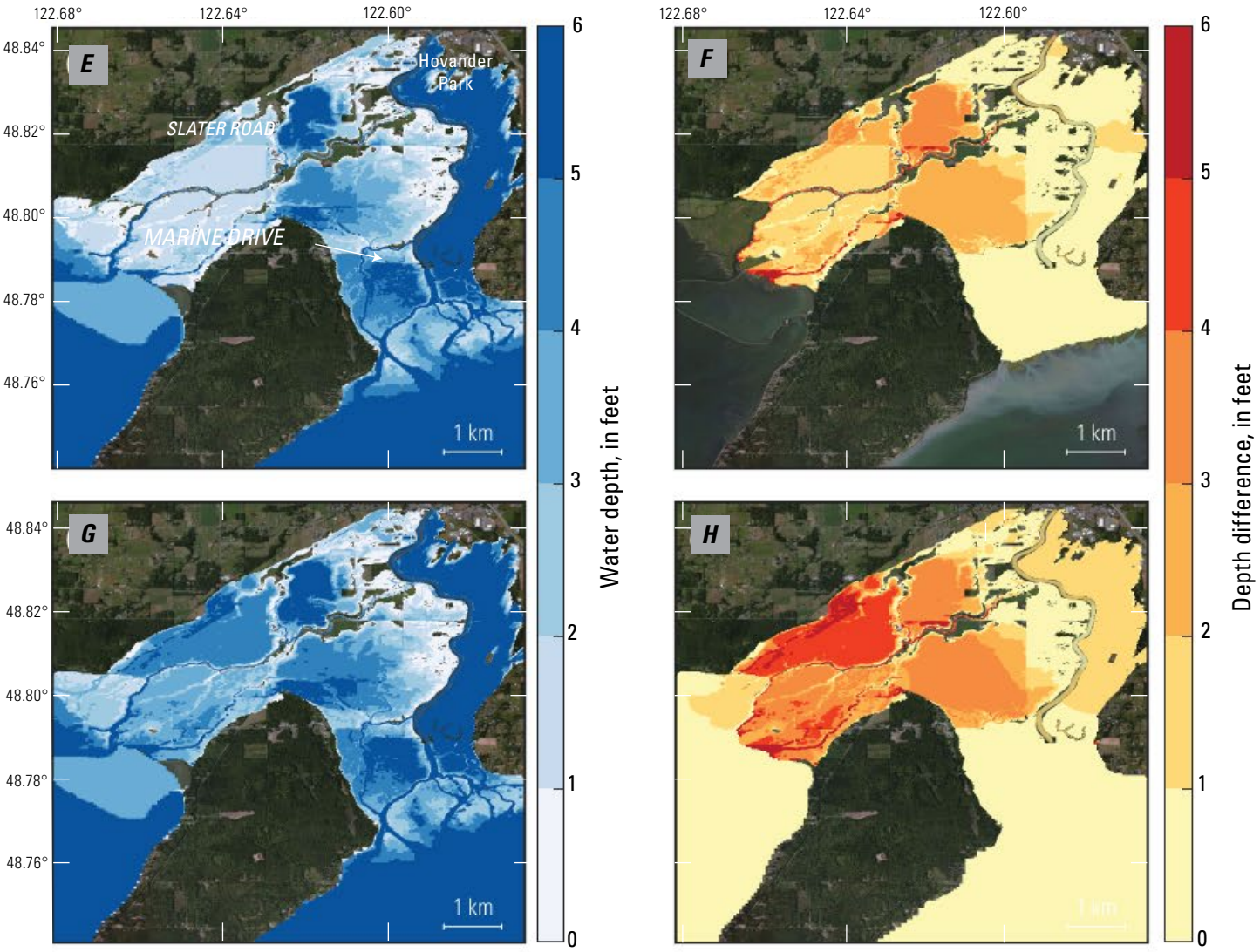


**Figure 25 (pages 38–39).**—Continued

evaluate how flood exposure will change by the 2040s and the 2080s, as well as to what extent flood mitigation alternatives with benefits to salmon habitat may offset flooding. This area of western Washington, including and downstream from Ferndale and Interstate Highway 5 (I–5) to Bellingham and Lummi Bays, referred to herein as Nooksack River Reach 1, is becoming increasingly vulnerable to extreme flooding, similar to what was observed in January 2009, February 2020, and twice again in November 2021. At stake are Ferndale and several smaller communities, the Lummi Reservation, Northwest Indian College, and Public Utility District No. 1 of Whatcom County and its water intakes, which supply two oil refineries and other customers, as well as nationally important agricultural areas, vital salmon habitat, and other industries. The model was used to examine how projected higher sea level and streamflows and flood-mitigation alternatives are likely to affect sedimentation of the Nooksack River watershed, which, in addition to large floods, has the highest sediment yield of all Puget Sound rivers. The model also examined the extent to which recently appreciated decadal-scale sedimentation that is progressing downstream through the study area may exacerbate flooding and be offset by flood-mitigation alternatives in the coming decades.

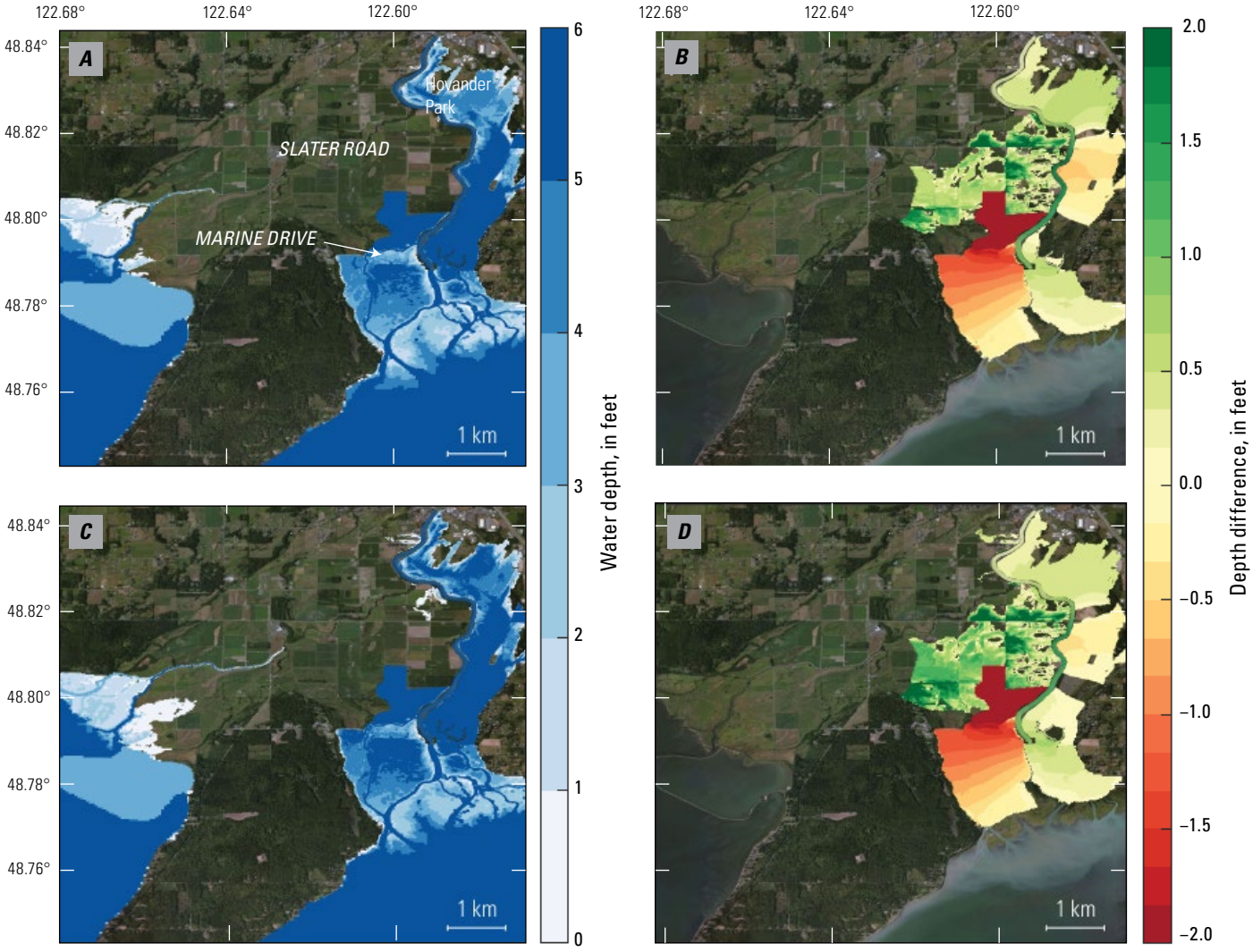


**Figure 26 (pages 40–41).** National Agricultural Imagery Program (NAIP) composite images showing modeled influences of combined alternatives 3B and 4C on flood extents (as water depths) and differences in water depths from existing conditions during 10 percent annual exceedance probability (AEP) stream flood. *A–D*, Flood extents (as water depths) and differences in water depths, respectively, with 3.3 feet (ft) (1.0 meter [m]) bed aggradation in lower part of Nooksack River Reach 1 for 2040s (*A*, *B*) and 2080s (*C*, *D*) mean-change scenarios. *E–H*, Flood extents (as water depths) and differences in water depths, respectively, with same bed aggradation as in *A–D* (3.3 ft [1 m]) across entire Nooksack River Reach 1 for 2040s (*E*, *F*) and 2080s (*G*, *H*) mean-change scenarios. NAIP images from U.S. Department of Agriculture National Agricultural Imagery Program.

The model accounted for the combined influences of tides, storm surge, and streamflow. Comparison of modeled and observed water levels during a two-year period and during two historical floods of record showed that the model is skillful, having a mean absolute error of less than 0.5 feet (ft) (0.15 meters [m]) in the river and less than 1 ft (0.3 m) across the floodplains. The model showed that tidal propagation reaches about 4.5 miles (7.5 kilometers) upstream from the river mouth, affecting flooding during events such as the February 2020 Super Bowl flood (a 10 percent annual exceedance probability [AEP] stream-flood event) and the January 2009 flood (a 4 percent AEP stream-flood event). The model captured the spatial extent and water depths associated with the February 2020 and January 2009 floods well, showing that recent efforts to fortify levees along the west bank (on the right side when traveling downstream) to protect valued agricultural lands and restore floodplain connectivity along the east bank (on the left side when traveling downstream) for fish and wildlife will mitigate some of the projected changes in flood exposure.

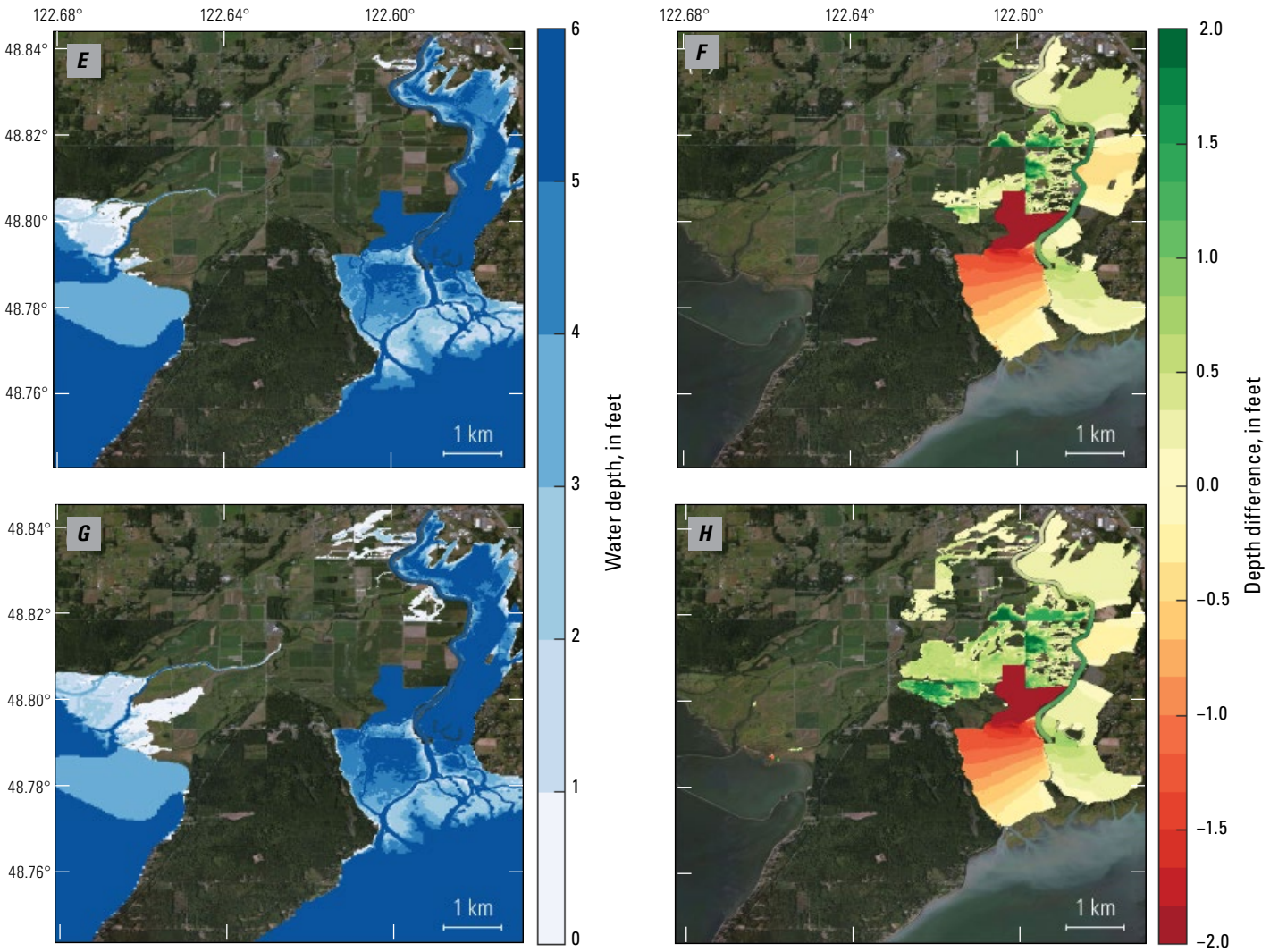


**Figure 26 (pages 40–41).**—Continued

During the coming decades, more intense rainfall and increased runoff is projected to drive substantial increases in stream-flood discharge of 20 to 32 percent by the 2040s and 52 to 72 percent by the 2080s. During the same time, sea-level rise of 0.4 to 3.1 ft (0.13–1.03 m) is expected to increasingly affect the capacity for the lower Nooksack River to convey floodwaters to Puget Sound. As a result, higher sea level and stream-flood levels are projected to cause more extreme and more frequent flooding across the Nooksack River Reach 1 floodplain, with steadily expanding flood extents and flood depths over land. By the 2040s, flood exposure during today's (2023) 10 percent AEP stream-flood event is expected to exceed that of the observed 4 percent AEP stream-flood event and what occurred during the recent November 2021 flood under the 2040s high-change scenario. By the 2080s, today's (2023) 4 percent AEP stream-flood event under the 2080s mean- and high-change scenarios is projected to be 121 and 158 percent larger, respectively, than the recent November 2021 flood. Modeled flood extent suggests that, whereas the 10 percent AEP stream flood such as the February 2020 Super Bowl flood (SBF) affected only 1 percent of the western floodplain, by the 2040s it will cause flooding of as much as 33 percent and, by the 2080s, as much as 58 percent of the western floodplain. The model indicates that flooding associated with the 4 percent AEP stream flood will expand from affecting 23 percent of the western floodplain to 50 to 94 percent in the 2040s and 84 to 94 percent in the 2080s, depending on if the mean- or high-change scenario

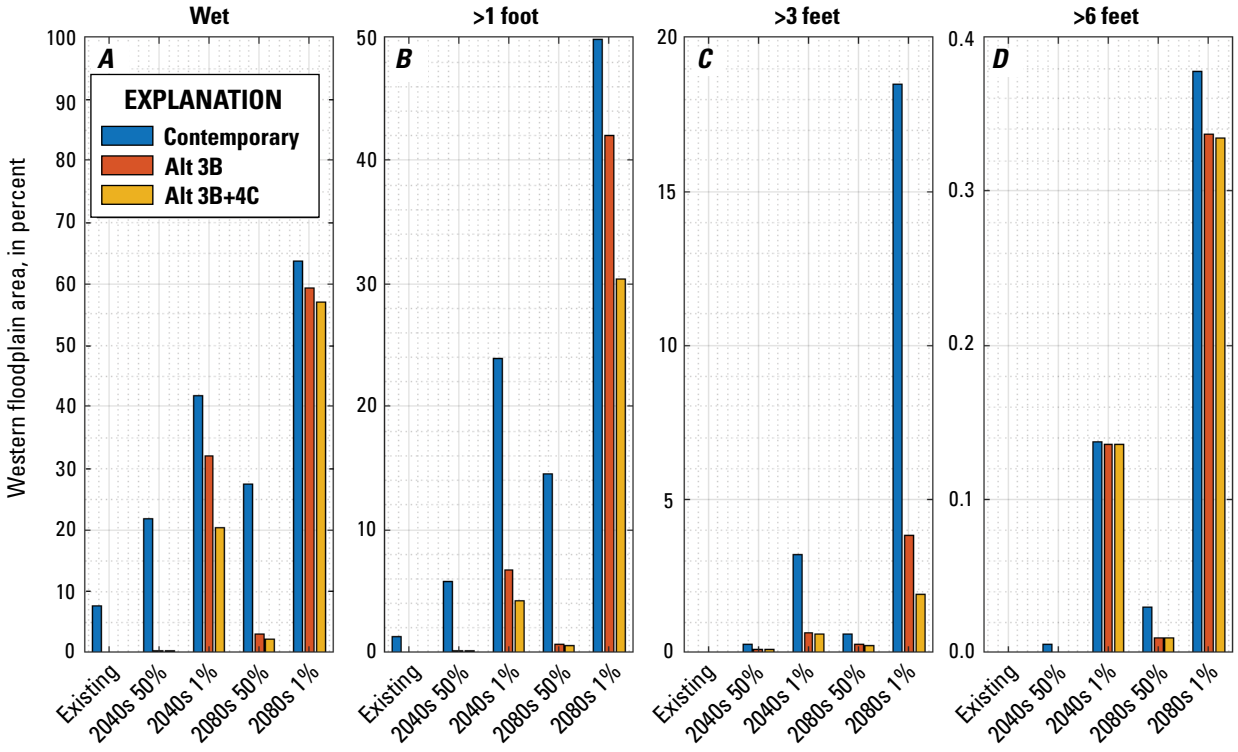


**Figure 27.** Bar plots showing percentages of area in western floodplain under 10 percent annual exceedance probability (AEP) stream flood, computed to experience flooding of (*A*) about 1 inch (wet), (*B*) >1 foot (ft), (*C*) >3 feet, and (*D*) >6 feet, after no action (contemporary; blue bars) compared to after alternatives 3B (alt 3B; red bars) and 3B and 4C combined (alt 3B+4C; gold bars), under existing conditions and with 3.3 feet (1.0 meter) of bed aggradation in Nooksack River subreach R1-3 under 2040s and 2080s mean- and high-change scenarios (50 and 1 percent probabilities, respectively). Extent of subreach R1-1 is shown in figure 4.

occurs. These projections intend to help communities evaluate impending hazards, community tolerance for disturbance, and define tipping points that may help inform planning.

An important strength of the model is its ability to evaluate a range of potential outcomes of mitigation efforts in addition to vulnerability to natural land-surface processes. Modeled flood extents that account for flood-mitigation alternatives that have benefits for recovering important fish habitats indicate that the severity of floods today (2023) and into the future may be offset by reconnecting floodplain side channels that can route floodwaters away from areas of vulnerability. Modeling of the Lower Nooksack River Project alternatives 3B and 4C, two of many identified potential actions to reduce flood exposure, shows that these alternatives can reduce main-stem river flood stage by about 2 ft during floods equivalent to a 10 percent AEP stream-flood event, in addition to reducing flood exposure. The individual and cumulative benefits of the two identified alternatives evaluated in this study, which would reduce flood exposure during higher projected floods in the 2040s and 2080s, suggest that additional mitigation opportunities may exist with the many other strategies being considered.

Noteworthy uncertainty and concern surround the extent to which higher streamflows, sea-level rise, and flood-mitigation alternatives may increase sedimentation in Reach 1 and the Nooksack River delta. The combination of a higher flux of fluvial sediment and the retarding of flow by higher sea level is expected to reduce flow conveyance, raising flood risk and adversely affecting navigation, fishing access, and other valued aspects of the system. The sediment-transport modeling results in this study show that much more sediment is likely to be delivered to and through Nooksack River Reach 1 under the projected 2040s and 2080s change scenarios and that mitigation alternatives may lead to additional sedimentation by rerouting the high-velocity floodwaters that generally move sediment. An additional complexity facing efforts to manage and balance flood protection with habitat restoration is the recent finding of decadal-scale river-channel aggradation that may be progressing downstream through the study area in the coming years. Modeled flood extents that account for bed aggradation in Reach 1 show that streamflows such as the 10 percent AEP stream-flood event, which had little effect across the western floodplain in the past, will become much more severe by the 2040s and 2080s. Lastly, the model showed

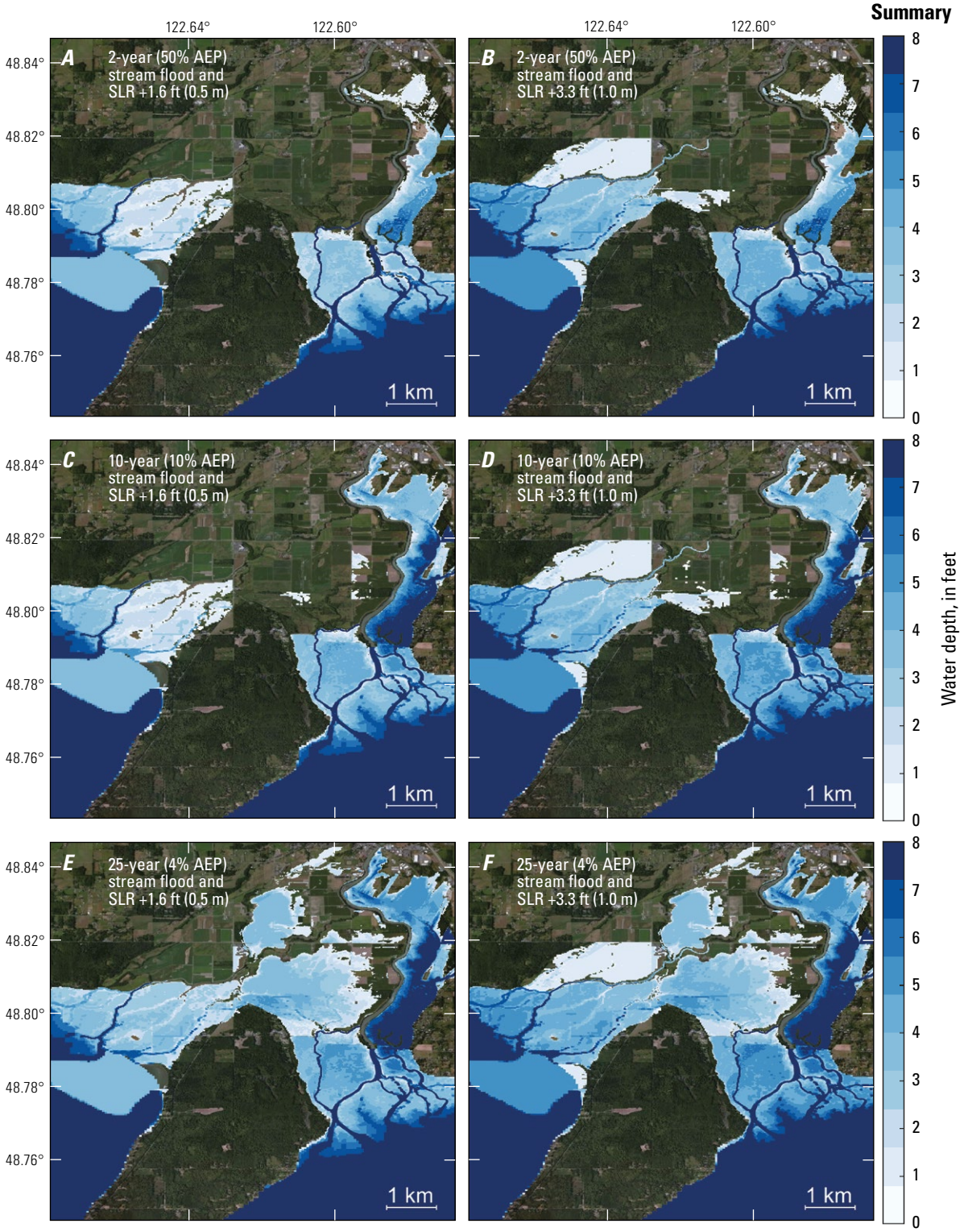


**Figure 28.** National Agricultural Imagery Program (NAIP) composite images showing water depth after 1.6 feet (ft) (0.5 meter [m]) and 3.3 feet (1.0 m) of sea-level rise (SLR) for 50 percent, 10 percent, and 4 percent annual exceedance probability (AEP) stream floods, which are expected in coming decades and which will increasingly affect groundwater, drainage issues, and frequencies of tidal and storm surges. *A*, *B*, Water depths after 1.6 ft (0.5 m) and 3.3 ft (1.0 m) SLR, respectively, for 50 percent (2 year) AEP stream flood. *C*, *D*, Water depths after 1.6 ft (0.5 m) and 3.3 ft (1.0 m) SLR, respectively, for 10 percent (10 year) AEP stream flood. *E*, *F*, Water depths after 1.6 ft (0.5 m) and 3.3 ft (1.0 m) SLR, respectively, for 4 percent AEP (25 year) stream flood. NAIP images from U.S. Department of Agriculture National Agricultural Imagery Program.

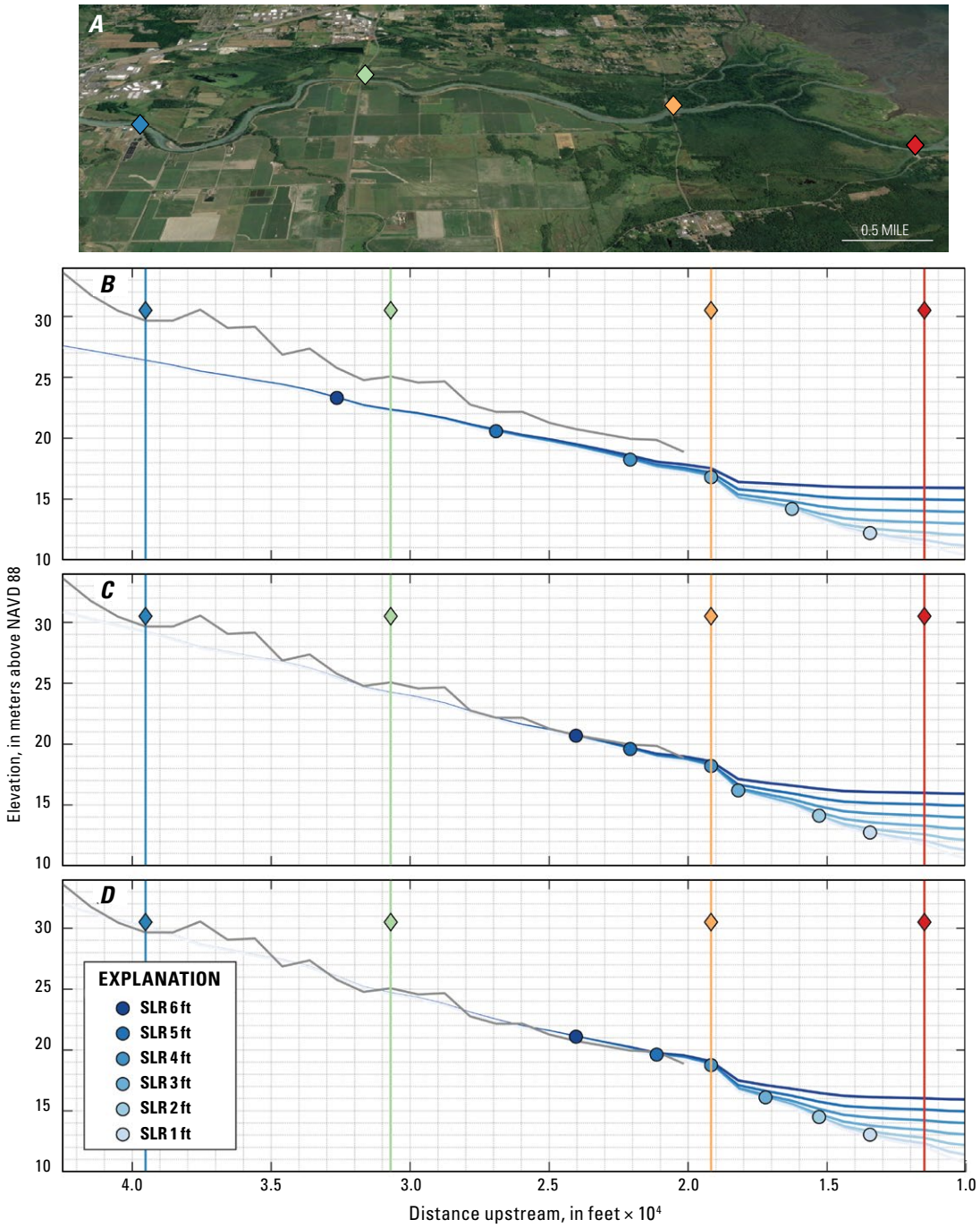


**Figure 29.** *A*, Oblique-view National Agricultural Imagery Program (NAIP) composite image showing locations of validation sites (colored diamonds): blue, Ferndale Wastewater Treatment Plant; green, Slater Road; orange, Marine Drive; red, Nooksack River delta. NAIP image from U.S. Department of Agriculture National Agricultural Imagery Program. *B*–*D*, Plots showing modeled influence of sea-level rise (SLR) in 1 foot (ft) (0.3 meter [m]) increments on water surface elevations along main-stem Nooksack River with respect to west-bank-levee elevation (gray line) for (*A*) 50 percent annual exceedance probability (AEP), (*B*) 10 percent AEP, and (*C*) and 4 percent AEP stream floods. Colored dots show upstream locations of landwardmost inundation, where water line meets land elevation, for several increments of sea-level rise. Colored diamonds showing validation sites plotted for reference. NAVD 88, North American Vertical Datum of 1988.

that identified flood-mitigation alternatives could help offset additional flooding caused by bed aggradation, suggesting that opportunities are likely to exist but will require strategic planning. The model herein helps to identify vulnerable areas within Reach 1, important sediment-transport processes, and sediment-transport characteristics (for example, bed and suspended-sediment grain sizes, settling velocities, and critical shear amounts for erosion) needed to advance a more robust sediment-transport model that can resolve individual and cumulative project alternative outcomes and account for the geomorphic changes that contribute strongly to flood exposure.

The compound flood modeling described herein showed that impending flood risk is expected to increase and that it is sensitive to a complex and uncertain mix of future tides, storm surge, sea-level rise, stream flooding, and sediment dynamics. Whereas the present findings accounted for the combination of these important, dynamic processes, they were based on scenarios in the form of discrete hydrographs that are representative of observed stream floods. The modeled changes, therefore, help evaluate the extent to which flood exposure may change in response to higher sea level and specific extreme stream-flood events, but they do not cover the entire variability of potential flooding likely to occur. Although we can infer from this study that the magnitude of a 10 percent AEP stream-flood event will be equal to or exceed that of a 4 percent AEP stream-flood event in response to higher streamflows, the results do not inform how the many less severe recurrence events (for example, the 2-year [50 percent AEP] and 5-year [20 percent AEP] floods, which are expected to increase in magnitude with sea-level rise) will add to cumulative exposure.

The model constructed is computationally efficient and able to simulate continuous decades-long time periods (for example, 30–100 years) that represent the region's climatology and derive flood metrics—cell by cell—across the model domain. A suggested next step for the comprehensive evaluation of flood risk across the Nooksack River Reach 1 is to apply the model to simulate various scenarios across the decadal-scale time periods, so that, for the first time, flood statistics that reflect the joint probabilities of tides, storm surge, sea-level rise, and stream floods, which affect total water levels, can be fully determined. The joint probabilities of extreme water levels that cause flooding provide a more comprehensive assessment of exposure, including the added capacity to define the magnitude and timing of discrete tipping points that may exceed community thresholds for disturbance. The compound flooding evaluated in this study is expected to be further exacerbated by pluvial, groundwater, and additional sediment-transport dynamics, which are planned for integration in future versions of the model. An improved model that accounts for these processes will enable flood managers to better evaluate the relative contributions of individual flood-forcing mechanisms in a probabilistic, risk-based framework. Relating the magnitude, timing, frequency, and probability of flooding to individual and cumulative factors will help identify solutions and inform complex trade-off decisions, adaptive-management opportunities, and coordinated investments in resilient flood-management, human-safety, transportation, and ecosystem-restoration efforts.

# References Cited

Anderson, S.W., and Grossman, E.E., 2017, Topographic and bathymetric data on the mainstem Nooksack River, fall 2015: U.S. Geological Survey data release, https://doi.org/10.5066/F72B8W7M.

Anderson, S.W., Konrad, C.P., Grossman, E.E., and Curran, C.A., 2019, Sediment storage and transport in the Nooksack River basin, northwestern Washington, 2006–15: U.S. Geological Survey Scientific Investigations Report 2019–5008, 43 p., https://doi.org/10.3133/sir20195008.

Barnosky, A.D., Hadly, E.A., Bascompte, J., Berlow, E.L., Brown, J.H., Fortelius, M., Getz, W.M., Harte, J., Hastings, A., Marquet, P.A., Martinez, N.D., Mooers, A., Roopnarine, P., Vermeij, G., Williams, J.W., Gillespie, R., Kitzes, J., Marshall, C., Matzke, N., Mindell, D.P., Revilla, E., and Smith, A.B., 2012, Approaching a state shift in Earth's biosphere: Nature, v. 486, p. 52–58, https://doi.org/10.1038/nature11018.

Boyd, K., Pittman, P., Nelson, A., and Thatcher, T., 2019, Lower Nooksack River geomorphic assessment—Final report: Bozeman, Mont., and Bellingham, Wash., Applied Geomorphology, Inc., Element Solutions, Northwest Hydraulic Consultants, and DTM Consulting, report prepared for the Whatcom County Flood Control Zone District, 153 p., last accessed December 20, 2021, at https://www.whatcomcounty.us/DocumentCenter/View/39545/Lower-Nooksack-Geomorphic-Assessment-Final-Report-02112019.

Brunner, G.W., 2021, HEC-RAS 2D User's Manual: U.S. Army Corps of Engineers website, https://www.hec.usace.army.mil/confluence/rasdocs/r2dum/latest.

Chow, V.T., 1959, Open-Channel Hydraulics: New York, McGraw-Hill, 700 p.

Collins, B.D., Montgomery, D.R., and Haas, A.D., 2002, Historical changes in the distribution and functions of large wood in Puget Lowland rivers: Canadian Journal of Fisheries and Aquatic Sciences, v. 59, no. 1, p. 66–76.

Collins, B.D., Montgomery, D.R., and Sheikh, A.J., 2003, 4. Reconstructing the historical riverine landscape of the Puget Lowland, *in* Montgomery, D.R., Bolton, S.M., Booth, D.B., and Wall, L., eds., Reconstruction of Puget Sound Rivers: Seattle, Wash., University of Washington Press, p. 79–128.

Curran, C.A., Grossman, E.E., Mastin, M.C., and Huffman, R.L., 2016, Sediment load and distribution in the lower Skagit River, Skagit County, Washington: U.S. Geological Survey Scientific Investigations Report 2016–5106, 24 p., https://doi.org/10.3133/sir20165106.

Czuba, J.A., Magirl, C.S., Czuba, C.R., Grossman, E.E., Curran, C.A., Gendaszek, A.S., and Dinicola, R.S., 2011, Sediment load from major rivers into Puget Sound and its adjacent waters: U.S. Geological Survey Fact Sheet 2011–3083, 4 p., https://doi.org/10.3133/fs20113083.

Grossman, E.E., Crosby, S.C., Stevens, A.W., Nowacki, D.J., vanArendonk, N.R., and Curran, C.A., 2022, Assessment of vulnerabilities and opportunities to restore marsh sediment supply at Nisqually River Delta, west-central Washington: U.S. Geological Survey Open-File Report 2022–1088, 50 p., https://doi.org/10.3133/ofr20221088.

Grossman, E.E., Stevens, A.W., Dartnell, P., George, D., and Finlayson, D., 2020, Sediment export and impacts associated with river delta channelization compound estuary vulnerability to sea-level rise, Skagit River Delta, Washington, USA: Marine Geology, v. 430, https://doi.org/10.1016/j.margeo.2020.106336.

Grossman, E.E., vanArendonk, N.R., Nederhoff, K., and Parker, K.A., 2023, Model input and projections of compound floodwater depths for the lower Nooksack River and delta, western Washington State: U.S. Geological Survey data release, https://doi.org/10.5066/P9DJM7X2.

Hamlet, A.F., Elsner, M.M., Mauger, G.S., Lee, S.-Y., Tohver, I., and Norheim, R.A., 2013, An overview of the Columbia Basin Climate Change Scenarios Project—Approach, methods, and summary of key results: Atmosphere-Ocean, v. 51, no. 4, p. 392–415, https://doi.org/10.1080/07055900.2013.819555.

Hamman, J.J., Hamlet, A.F., Lee, S.-Y., Fuller, R., and Grossman, E.E., 2016, Combined effects of projected sea level rise, storm surge, and peak river flows on water levels in the Skagit floodplain: Northwest Science, v. 90, no. 1, p. 57–78, https://doi.org/10.3955/046.090.0106.

Herdman, L., Erikson, L. and Barnard, P., 2018, Storm surge propagation and flooding in small tidal rivers during events of mixed coastal and fluvial influence: Journal of Marine Science and Engineering, v. 6, no. 4, p. 158.

KCM, Inc., 1995, Whatcom County, Lower Nooksack River Comprehensive Flood Hazard Management Plan—Nooksack River Flood History: Seattle, Wash., KCM, Inc., report prepared for Whatcom County Transportation Services Department, Division of Engineering, River and Flood Control Section, 47 p., https://www.whatcomcounty.us/DocumentCenter/View/25545.

Kernkamp, H.W.J., Van Dam, A., Stelling, G.S., and de Goede, E.D., 2011, Efficient scheme for the shallow water equations on unstructured grids with application to the Continental Shelf: Ocean Dynamics, v. 61, p. 1175–1188, https://doi.org/10.1007/s10236-011-0423-6.

Lee, S.-Y., Hamlet, A.F., and Grossman, E.E., 2016, Impacts of climate change on regulated streamflow, hydrologic extremes, hydropower production, and sediment discharge in the Skagit River Basin: Northwest Science. v. 90, no. 1, p. 23–43, https://doi.org/10.3955/046.090.0104.

Mattocks, C., and Forbes, C., 2008, A real-time, event-triggered storm surge forecasting system for the state of North Carolina: Ocean Modelling, v. 25, nos. 3–4, p. 95–119, https://doi.org/10.1016/j.ocemod.2008.06.008.

Mauger, G.S., Casola, J.H., Morgan, H.A., Strauch, R.L., Jones, B., Curry, B., Busch Isaksen, T.M., Whitely Binder, L., Krosby, M.B., and Snover, A.K., 2015, State of knowledge—Climate change in Puget Sound: Seattle, University of Washington, Climate Impacts Group, report prepared for the Puget Sound Partnership and the National Oceanic and Atmospheric Administration, 299 p., https://doi.org/10.7915/CIG93777D.

Miller, I., Morgan, H., Mauger, G., Newton, T., Weldon, R., Schmidt, D., Welch, M., and Grossman, E., 2018, Projected sea level rise for Washington State—A 2018 assessment: University of Washington, University of Oregon, Washington Sea Grant, and U.S. Geological Survey, report prepared for the Washington Coastal Resilience Project, https://cig.uw.edu/projects/projected-sea-level-rise-for-washington-state-a-2018-assessment/.

Moore, J.C., 2018, Predicting tipping points in complex environmental systems: PNAS [Proceedings of the National Academy of Sciences], v. 115, no. 4, p. 635–636, https://doi.org/10.1073/pnas.1721206115.

Nederhoff, K., Saleh, R., Tehranirad, B., Herdman, L., Erikson, L., Barnard, P.L., and van der Wegen, M., 2021, Drivers of extreme water levels in a large, urban, high-energy coastal estuary—A case study of the San Francisco Bay: Coastal Engineering, v. 170, 12 p., https://doi.org/10.1016/j.coastaleng.2021.103984.

Northwest Hydraulic Consultants, 2015, Geomorphic characterization, appendix C *of* Lower Nooksack River project—Alternatives analysis: Seattle, Wash., Northwest Hydraulic Consultants, final report prepared for The Watershed Company, on behalf of Whatcom County Flood Control Zone District, 59 p., last accessed April 4, 2023, at https://www.whatcomcounty.us/DocumentCenter/View/13334.

Santiago-Collazo, F.L., Bilskie, M.V., and Hagen, S.C., 2019, A comprehensive review of compound inundation models in low-gradient coastal watersheds: Environmental Modelling & Software, v. 119, p. 166–181, https://doi.org/10.1016/j.envsoft.2019.06.002.

Sweet, W.V., Hamlington, B.D., Kopp, R.E., Weaver, C.P., Barnard, P.L., Bekaert, D., Brooks, W., Craghan, M., Dusek, G., Frederikse, T., Garner, G., Genz, A.S., Krasting, J.P., Larour, E., Marcy, D., Marra, J.J., Obeysekera, J., Osler, M., Pendleton, M., Roman, D., Schmied, L., Veatch, W., White, K.D., and Zuzak, C., 2022, Global and regional sea level rise scenarios for the United States—Updated mean projections and extreme water level probabilities along U.S. coastlines: National Oceanic and Atmospheric Administration, National Ocean Service, NOAA Technical Report NOS 01, 96 p., https://oceanservice.noaa.gov/hazards/sealevelrise/sealevelrise-tech-report-sections.html.

Tyler, D.J., Danielson, J.J., Grossman, E.E., and Hockenberry, R.J., 2020, Topobathymetric model of Puget Sound, Washington, 1887 to 2017: U.S. Geological Survey data release, https://doi.org/10.5066/P95N6CIT.

U.S. Geological Survey [USGS], 2022, National Water Information System: U.S. Geological Survey website, last accessed May 2022 at https://nwis.waterdata.usgs.gov/nwis. [Also available at https://doi.org/10.5066/F7P55KJN.]

Wahl, T., Jain, S., Bender, J., Meyers, S.D., and Luther, M.E., 2015, Increasing risk of compound flooding from storm surge and rainfall for major US cities: Nature Climate Change, v. 5, p. 1093–1097, https://doi.org/10.1038/nclimate2736.

Wang, S., Najafi, M.R., Cannon, A.J., and Khan, A.A., 2021, Uncertainties in riverine and coastal flood impacts under climate change: Water, v. 13, no. 13, 26 p., https://doi.org/10.3390/w13131774.

Whatcom County, 2017, Nooksack River system-wide improvement framework—Whatcom County, Washington: Bellingham, Wash., Whatcom County, report prepared for Whatcom County Flood Control Zone District, 61 p., last accessed June 15, 2022, at https://www.whatcomcounty.us/DocumentCenter/View/26159.

Whatcom County Department of Public Works, 1999, Lower Nooksack River Comprehensive Flood Hazard Management Plan: Bellingham, Wash., Whatcom County Department of Public Works, report prepared for Whatcom County Flood Control Zone District, 177 p., last accessed June 15, 2022, at https://www.whatcomcounty.us/DocumentCenter/View/1400.

# Appendix 1. Computed Flood Extents of the Western Nooksack River Reach 1 Floodplain

**Table 1.1.** Computed flood extents of the western Nooksack River Reach 1 floodplain.

[Flood extents, as areal percentages, under contemporary (present day [2023]) conditions and under projected conditions in 2040s and 2080s mean- and high-change scenarios (that is, 50 and 1 percent probabilities, respectively), for 10 and 4 percent annual exceedance probability (AEP) stream floods, using flood-depth thresholds of 1 inch (in.), >1 foot (ft), >3 ft, and >6 ft, with and without bed aggradation and mitigation alternatives. See figure 4 for extent of Nooksack River subreach R1-3. cm, centimeter]

| Event | Bed aggradation | Mitigation alternative | Depth threshold | Flood extent (areal percentage) | | | | |
|---|---|---|---|---|---|---|---|---|
| | | | | Contemporary | 2040 50% | 2040 1% | 2080 50% | 2080 1% |
| 10% AEP stream flood | None (existing bed) | None (existing conditions) | 1 in. (2.5 cm) | 0.0 | 0.8 | 32.7 | 6.3 | 58.5 |
| | | | >1 ft (30 cm) | 0.0 | 0.2 | 7.2 | 1.0 | 41.8 |
| | | | >3 ft (91 cm) | 0.0 | 0.1 | 0.6 | 0.3 | 3.3 |
| | | | >6 ft (182 cm) | 0.0 | 0.0 | 0.1 | 0.0 | 0.3 |
| | | Alternative 3B | 1 in. (2.5 cm) | 0.0 | 0.2 | 11.3 | 2.0 | 52.6 |
| | | | >1 ft (30 cm) | 0.0 | 0.2 | 2.1 | 0.5 | 29.2 |
| | | | >3 ft (91 cm) | 0.0 | 0.1 | 0.4 | 0.2 | 1.7 |
| | | | >6 ft (182 cm) | 0.0 | 0.0 | 0.1 | 0.0 | 0.3 |
| | | Alternatives 3B and 4C | 1 in. (2.5 cm) | 0.0 | 0.2 | 9.1 | 1.9 | 42.9 |
| | | | >1 ft (30 cm) | 0.0 | 0.2 | 1.8 | 0.5 | 24.1 |
| | | | >3 ft (91 cm) | 0.0 | 0.1 | 0.4 | 0.2 | 1.7 |
| | | | >6 ft (182 cm) | 0.0 | 0.0 | 0.1 | 0.0 | 0.3 |
| | Bed aggradation in subreach R1-3 | None (existing conditions) | 1 in. (2.5 cm) | 7.6 | 21.8 | 41.8 | 27.5 | 63.7 |
| | | | >1 ft (30 cm) | 1.3 | 5.8 | 23.9 | 14.5 | 49.8 |
| | | | >3 ft (91 cm) | 0.0 | 0.3 | 3.2 | 0.6 | 18.5 |
| | | | >6 ft (182 cm) | 0.0 | 0.0 | 0.1 | 0.0 | 0.4 |
| | | Alternative 3B | 1 in. (2.5 cm) | 0.0 | 0.3 | 32.0 | 3.0 | 59.3 |
| | | | >1 ft (30 cm) | 0.0 | 0.2 | 6.7 | 0.6 | 42.0 |
| | | | >3 ft (91 cm) | 0.0 | 0.1 | 0.7 | 0.3 | 3.8 |
| | | | >6 ft (182 cm) | 0.0 | 0.0 | 0.1 | 0.0 | 0.3 |
| | | Alternatives 3B and 4C | 1 in. (2.5 cm) | 0.0 | 0.2 | 20.3 | 2.2 | 56.9 |
| | | | >1 ft (30 cm) | 0.0 | 0.1 | 4.2 | 0.6 | 30.4 |
| | | | >3 ft (91 cm) | 0.0 | 0.1 | 0.6 | 0.2 | 1.9 |
| | | | >6 ft (182 cm) | 0.0 | 0.0 | 0.1 | 0.0 | 0.3 |

**Table 1.1.** Computed flood extents of the western Nooksack River Reach 1 floodplain.—Continued

| Event | Bed aggradation | Mitigation alternative | Depth threshold | Flood extent (areal percentage) | | | | |
|---|---|---|---|---|---|---|---|---|
| | | | | Contemporary | 2040 50% | 2040 1% | 2080 50% | 2080 1% |
| 4% AEP stream flood | None (existing bed) | None (existing conditions) | 1 in. (2.5 cm) | 21.5 | 48.8 | 92.0 | 85.7 | 95.1 |
| | | | >1 ft (30 cm) | 4.5 | 34.5 | 81.2 | 70.2 | 87.2 |
| | | | >3 ft (91 cm) | 0.3 | 9.5 | 62.5 | 25.8 | 69.9 |
| | | | >6 ft (182 cm) | 0.1 | 0.2 | 4.4 | 0.3 | 48.0 |
| | | Alternative 3B | 1 in. (2.5 cm) | 0.0 | 42.1 | 91.5 | 75.7 | 94.8 |
| | | | >1 ft (30 cm) | 0.0 | 25.7 | 80.2 | 55.5 | 86.9 |
| | | | >3 ft (91 cm) | 0.0 | 6.1 | 61.3 | 20.6 | 69.4 |
| | | | >6 ft (182 cm) | 0.0 | 0.2 | 3.6 | 0.2 | 46.9 |
| | | Alternatives 3B and 4C | 1 in. (2.5 cm) | 1.9 | 35.1 | 89.5 | 66.6 | 93.9 |
| | | | >1 ft (30 cm) | 0.6 | 14.4 | 75.6 | 42.8 | 84.5 |
| | | | >3 ft (91 cm) | 0.0 | 5.2 | 46.4 | 9.9 | 66.1 |
| | | | >6 ft (182 cm) | 0.0 | 0.2 | 1.7 | 0.2 | 25.1 |
| | Bed aggradation in subreach R1-3 | None (existing conditions) | 1 in. (2.5 cm) | 35 | 73 | 94 | 89 | 96 |
| | | | >1 ft (30 cm) | 22 | 53 | 84 | 76 | 89 |
| | | | >3 ft (91 cm) | 3 | 25 | 67 | 42 | 73 |
| | | | >6 ft (182 cm) | 0 | 0 | 28 | 2 | 53 |
| | | Alternative 3B | 1 in. (2.5 cm) | 12 | 50 | 93 | 87 | 96 |
| | | | >1 ft (30 cm) | 3 | 37 | 83 | 73 | 89 |
| | | | >3 ft (91 cm) | 0 | 16 | 65 | 30 | 72 |
| | | | >6 ft (182 cm) | 0 | 0 | 12 | 1 | 53 |
| | | Alternatives 3B and 4C | 1 in. (2.5 cm) | 6 | 46 | 92 | 72 | 95 |
| | | | >1 ft (30 cm) | 2 | 28 | 81 | 57 | 87 |
| | | | >3 ft (91 cm) | 0 | 7 | 59 | 19 | 69 |
| | | | >6 ft (182 cm) | 0 | 0 | 4 | 0 | 45 |

Moffett Field Service Center, California
Manuscript approved for publication April 14, 2023
Edited by Taryn A. Lindquist
Illustration support by Cory Hurd
Layout by Kimber Petersen

ISSN 2328-0328 (online)
https://doi.org/10.3133/sir20235047.